New insights into hydraulic processes and water quality dynamics of alpine karst systems

zur Erlangung des akademischen Grades eines

Doktors der Naturwissenschaften

von der KIT-Fakultät für Bauingenieur-, Geo- und Umweltwissenschaften

des Karlsruher Instituts für Technologie (KIT)

genehmigte

Dissertation

von

M. Sc. Simon Frank

aus Altötting

Tag der mündlichen Prüfung:

15. Mai 2020

Referent: Prof. Dr. Nico Goldscheider

Korreferent: Prof. Dr. Thomas Neumann

Karlsruhe 2020

Abstract

Karst aquifers are important water resources for drinking water supply, especially in alpine regions. Recent studies estimate that over 800 Mio. people worldwide rely on drinking water from karst areas. In view of the increasing water demand in many parts of the world, karst aquifers offer an enormous potential for future water supply. Karst springs often show a high variability in water quantity and quality because of the special characteristics of karst aquifers. Karst aquifers reveal a strong hydraulic anisotropy and heterogeneity and are therefore highly vulnerable to contamination. To use these kind of water resources, adapted management strategies and especially a detailed knowledge of the functioning of the respective aquifer is of special importance. In view of the increasing water demand and climate change, a profound understanding of the hydrogeological conditions is essential.

Within this thesis, alpine karst aquifers were investigated in order to develop conceptual models for the different aquifers to gain a better knowledge of the functioning of these aquifers for their use for water supply.

Extensive field studies and hydrochemical analysis were carried out and resulted in a hydrogeological conceptual model for the karst aquifer system drained by the Marulbachquelle (MBQ), which is presented in chapter 2. In this study, hydrogeochemical investigations characterized the water of a spring draining a complex carbonate-gypsum karst system. The reaction of the spring to a rainfall event was examined to identify the relevant hydrological processes controlling the hydrochemistry of the spring, and to understand water-rock interactions and conduit-matrix exchange. Comparisons of ion ratios show that both carbonate and gypsum rocks influence the water chemistry of the spring. A conceptual model of the spring behavior during low-flow and high-flow conditions, including conduit-matrix interaction, was developed which can explain the observations. Results of this study demonstrated that 1) during low-flow conditions, the spring is characterized by high sulfate content, while after rainfall events, the water chemistry is dominated by bicarbonate; 2) a change in water chemistry is associated with a significant shift from low-flow to high-flow conditions; and 3) conduit-matrix exchange is an important factor as shown by the discharge-sulfate relationship and clearly influences the behavior of the spring and the matrix acts as water storage.

The study in chapter 2 gives general information about the functioning of the aquifer but no information about the contamination dynamics. Therefore, the second study of this thesis (chapter 3) focuses on the characterization of the contamination dynamics and the development of a real-time warning system for organic and bacterial contamination.

A fluorescence-based multi-parameter approach was used to characterize the dynamics of organic carbon, faecal bacteria, and particles at three alpine karst springs. At the first system, peak A fluorescence and total organic carbon (TOC) were strongly correlated, indicating that a large part of the organic matter is related to humic-like substances. Protein-like fluorescence and cultivation-based determinations of coliform bacteria also had a significant correlation, indicating that protein-like fluorescence is directly related to faecal pollution. Additionally, there was a strong correlation between small particle fractions, a secondary turbidity peak and bacteria. At one of these springs, discharge was constant despite the reaction of all other parameters to a rainfall event. The results of this study demonstrated that 1) all three springs showed fast and marked responses of all investigated water-quality parameters after rain events; 2) a constant discharge does not necessarily mean constant water quality; 3) at high contamination levels, protein-like fluorescence is a good indicator of bacterial contamination, while at low contamination levels no correlation between protein-like fluorescence and bacterial values was detected; and 4) a combination of fluorescence measurements and particle-size analysis is a promising approach for a rapid assessment of organic contamination, especially relative to time-consuming conventional bacterial determination methods.

The study described in chapter 3 showed that protein-like fluorescence is a promising tool for a real-time contamination indication system. As the transport properties and transport behaviour of tryptophan and humic substances are still insufficiently known, chapter 4 focuses on the transport behaviour of tryptophan and humic-like substances.

In the study described in chapter 4, a comparative tracer test in a karst experimental site was conducted to investigate the transport properties and behavior of tryptophan and humic acid. These two tracers were compared with the conservative tracer uranine. Fluorescence measurements were conducted with an online field fluorometer and in the laboratory. The obtained breakthrough curves (BTCs) and the modeling results demonstrate that 1) the online field fluorometer is suitable for real-time fluorescence measurements of all three tracers; 2) the transport parameters obtained for uranine, tryptophan and humic acid are comparable in the fast flow areas of the karst system 3) the transport velocities of humic acid are slower and the resulting residence times are accordingly higher, compared to uranine and tryptophan in the slower and longer flow paths; 4) the obtained BTCs reveal additional information about the investigated karst system. As a conclusion, the experiments show that the transport properties of tryptophan are similar to those of uranine while humic acid is partly transported slower and with retardation. These findings allow a better and quantitative interpretation of the results when these substances are used as a natural faecal and contamination indicators.

Climate change and heavy rainfall events are special challenges in managing alpine karst aquifers which possess an enormous potential for future drinking water supply. In the study described in chapter 5, we present the results of investigations of a high alpine karst system in the UNESCO Biosphere Reserve Großes Walsertal in Austria, which has a clearly defined catchment and is drained by only one spring system. The results show that 1) the investigated system is a highly dynamic karst aquifer with distinct reactions to rainfall events in discharge and electrical conductivity; 2) the estimated transient atmospheric CO_2 sink for the investigated karst system is about 270 t/a; 3) the calculated denudation rate for the outcropping carbonate rocks in the investigation area is between 23 and 47 mm/1000a and 4) the rainfall discharge behavior and the internal flow dynamics can be successfully simulated using the modelling package KarstMod. The modelling results indicate the importance of matrix storage in determining the discharge behavior of the spring, especially during low-flow periods. Especially with regard to climate change, this research can contribute and initiate a better understanding and management of alpine karst aquifers.

This thesis presents different water quality and water quantity aspects related to karst aquifers in the Lechquellen Mountains in Vorarlberg, Austria. The investigation approach and the obtained results lead to a better understanding of the karst systems and deliver a valuable base for the use of these aquifers for drinking water supply.

Kurzfassung

Karstaquifere sind wichtige Wasserressourcen für die Trinkwasserversorgung, vor allem in alpinen Regionen. Neue Studien schätzen, dass weltweit über 800 Mio. Menschen auf Trinkwasser aus Karstgebieten angewiesen sind. Angesichts des steigenden Wasserbedarfs in vielen Teilen der Welt bieten Karst-Aquifere ein enormes Potenzial für die zukünftige Wasserversorgung. Karstquellen weisen aufgrund der besonderen Eigenschaften der Karst-Aquifere oft eine hohe Variabilität der Wassermenge und -qualität auf. Karst-Aquifere weisen eine starke hydraulische Anisotropie und Heterogenität auf und sind daher sehr anfällig für Verunreinigungen. Um diese Art von Wasserressourcen nutzen zu können, sind angepasste Managementstrategien und vor allem eine detaillierte Kenntnis der Funktionsweise des jeweiligen Aquifers von besonderer Bedeutung. Angesichts des steigenden Wasserbedarfs und des Klimawandels ist ein tiefgreifendes Verständnis der hydrogeologischen Verhältnisse unerlässlich.

Im Rahmen dieser Arbeit wurden alpine Karst-Aquifere untersucht, um konzeptionelle Modelle für die verschiedenen Aquifere zu entwickeln, um ein besseres Wissen über die Funktionsweise für ihre zukünftige Nutzung für die Wasserversorgung zu erhalten.

Umfangreiche Felduntersuchungen und hydrochemische Analysen wurden durchgeführt und führten zu einem hydrogeologischen Konzeptmodell für das von der Marulbachquelle entwässerte Karstaquifersystem, das in Kapitel 2 vorgestellt wird. In dieser Studie wurde das Wasser einer Quelle, die ein komplexes Karbonat-Gipskarst-System entwässert, hydrogeochemisch untersucht. Die Reaktion der Quelle auf ein Niederschlagsereignis wurde untersucht, um die relevanten hydrologischen Prozesse zu identifizieren, die die Hydrochemie der Quelle beeinflussen, und um die Wasser-Gesteins-Wechselwirkungen und den Conduit-Matrix-Austausch zu verstehen. Vergleiche von Ionenverhältnissen zeigen, dass sowohl Karbonat- als auch Gipsgesteine die Wasserchemie der Quelle beeinflussen. Es wurde ein konzeptionelles Modell des Quellverhaltens unter Niedrig- und Hochwasserbedingungen, einschließlich der Conduit-Matrix-Wechselwirkung, entwickelt, das die Beobachtungen erklären kann. Die Ergebnisse dieser Studie zeigen, dass 1) die Quelle unter Niedrigwasserbedingungen durch einen hohen Sulfatgehalt gekennzeichnet ist, während nach Niederschlagsereignissen die Wasserchemie von Hydrogenkarbonat dominiert wird; 2) eine Änderung der Wasserchemie mit einer signifikanten Verschiebung von Niedrigwasser- zu Hochwasserbedingungen verbunden ist und 3) wie die Abfluss-Sulfat-Beziehung zeigt, ist die Conduit-Matrix-Wechselwirkung ein wichtiger Faktor, der das Verhalten der Quelle deutlich beeinflusst.

Die Studie in Kapitel 2 gibt allgemeine Informationen über die Funktionsweise des Aquifers, aber keine Informationen über die Dynamik der Kontamination. Daher konzentriert sich die zweite

Studie dieser Arbeit (Kapitel 3) auf die Charakterisierung der Kontaminationsdynamik und die Entwicklung eines Echtzeit-Warnsystems für organische und bakterielle Kontaminationen.

Mit Hilfe eines fluoreszenzbasierten Multiparameter-Ansatzes wurde die Dynamik von organischem Kohlenstoff, Fäkalbakterien und Partikeln an drei alpinen Karstquellen charakterisiert. Beim ersten System waren die Peak A-Fluoreszenz und der gesamte organische Kohlenstoff (TOC) stark korreliert, was darauf hindeutet, dass ein großer Teil der organischen Substanz mit huminstoffähnlichen Substanzen in Verbindung steht. Proteinähnliche Fluoreszenz und kultivierungsbasierte Bestimmungen von coliformen Bakterien wiesen ebenfalls eine signifikante Korrelation auf, was darauf hinweist, dass die proteinähnliche Fluoreszenz direkt mit fäkalen Verunreinigungen zusammenhängt. Zusätzlich gab es eine starke Korrelation zwischen kleinen Partikelfraktionen, einem sekundären Trübepeak und Bakterien. An einer dieser Quellen war der Abfluss trotz der Reaktion aller anderen Parameter auf das Niederschlagsereignis konstant. Die Ergebnisse dieser Studie zeigten, dass 1) alle drei Quellen nach Regenereignissen schnelle und deutliche Reaktionen aller untersuchten Wasserqualitätsparameter aufwiesen; 2) ein konstanter Abfluss nicht unbedingt eine konstante Wasserqualität bedeutet; 3) bei hohen Verschmutzungsgraden die proteinähnliche Fluoreszenz ein guter Indikator für bakterielle Verunreinigungen ist, während bei niedrigen Verschmutzungsgraden keine Korrelation zwischen proteinähnlicher Fluoreszenz und bakteriellen Werten festgestellt wurde; und 4) eine Kombination aus Fluoreszenzmessungen und Partikelgrößenanalyse ein vielversprechender Ansatz für eine schnelle Beurteilung der organischen Verschmutzung ist, insbesondere im Vergleich zu zeitaufwendigen konventionellen bakteriellen Bestimmungsmethoden.

Die in Kapitel 3 beschriebene Studie zeigte, dass die proteinähnliche Fluoreszenz ein vielversprechendes Werkzeug für ein Echtzeit-Kontaminationsanzeigesystem ist. Da die Transporteigenschaften und das Transportverhalten von Tryptophan und Huminstoffen noch unzureichend bekannt sind, konzentriert sich Kapitel 4 auf das Transportverhalten von Tryptophan und huminstoffähnlichen Stoffen.

In der in Kapitel 4 beschriebenen Studie wurde ein vergleichender Tracerversuch in einem Epikarstsystem durchgeführt, um die Transporteigenschaften und das Verhalten von Tryptophan und Huminsäuren zu untersuchen. Diese beiden Tracer wurden mit dem konservativen Tracer Uranin verglichen. Die Fluoreszenzmessungen wurden mit einem Online-Feldfluorimeter und im Labor durchgeführt. Die erhaltenen Durchgangskurven und die Modellierungsergebnisse zeigen, dass 1) das Online-Feldfluorimeter für Echtzeit-Fluoreszenzmessungen aller drei Tracer geeignet ist; 2) die Transportparameter von Uranin, Tryptophan und Huminsäuren in den schnellen Fließwegen des Karstsystems vergleichbar sind; 3) dass in den langsameren und längeren Fließpfaden, im Vergleich zu Uranin und Tryptophan, die Transportgeschwindigkeiten von

Huminsäuren langsamer und die Verweilzeiten entsprechend höher sind; 4) die erhaltenen Durchgangskurven zusätzliche Informationen über das untersuchte Karstsystem liefern. Zusammenfassend zeigen diese Experimente, dass das Transportverhalten von Uranin und Tryptophan vergleichbar ist während Huminsäuren langsamer und verzögert transportiert werden. Diese Erkenntnisse erlauben eine bessere und quantitative Interpretation von Ergebnissen wenn diese Substanzen als natürliche Fäkal- und Kontaminationsanzeiger verwendet werden.

Klimawandel und Starkregenereignisse sind besondere Herausforderungen bei der Bewirtschaftung alpiner Karstgrundwasserleiter. In der in Kapitel 5 beschriebenen Studie werden die Ergebnisse von Untersuchungen eines hochalpinen Karstsystems im UNESCO-Biosphärenreservat Großes Walsertal in Österreich vorgestellt, das über ein klar definiertes hydrogeologisches Einzugsgebiet verfügt und von nur einem Quellsystem entwässert wird. Die Ergebnisse zeigen, dass 1) das untersuchte System ein hochdynamischer Karst-Aquifer mit ausgeprägten Reaktionen auf Niederschlagsereignisse von Schüttung und elektrischer Leitfähigkeit ist; 2) die geschätzte transiente atmosphärische CO_2-Senke für das untersuchte Karstsystem ca. 270 t/a beträgt; 3) die berechnete Denudationsrate für die auftretenden Karbonatgesteine im Untersuchungsgebiet zwischen 23 und 47 mm/1000a beträgt und 4) das Niederschlags- Abflussverhalten und die innere Strömungsdynamik des untersuchten Karstsystems erfolgreich mit dem Softwarepaket KarstMod simuliert werden kann. Die Modellierungsergebnisse zeigen die Bedeutung der Matrix als Speicher, insbesondere in Niedrigwasserperioden. Gerade im Hinblick auf den Klimawandel kann diese Forschung einen Beitrag zum besseren Verständnis und Management der alpinen Karstaquifere leisten und initiieren.

In dieser Arbeit werden verschiedene Aspekte der Wasserqualität und Wasserquantität im Zusammenhang mit Karstaquiferen im Lechquellengebirge in Vorarlberg, Österreich, vorgestellt. Der Untersuchungsansatz und die erzielten Ergebnisse führen zu einem besseren Verständnis der jeweiligen Karstsysteme und liefern eine wertvolle Grundlage für die zukünftige Nutzung dieser Aquifere für die Trinkwasserversorgung.

Table of Contents

List of Figures

List of Tables

Chapter 1

1 Introduction

1.1 General Motivation and Background

Karst describes a comprising terrain with a distinctive hydrology and landforms that are formed by a combination of high rock solubility and well developed secondary (fracture) porosity. Generally karst areas are characterized by sinking streams, swallow holes, caves, depressions and (large) springs (Ford and Williams, 2007). Karst aquifers are developed especially in soluble rocks such as limestone and dolomite (Ford and Williams, 2007). Karst can also occur in other rock types with a predominantly carbonatic composition, including carbonatic conglomerates (Goeppert et al., 2011) and carbonatic metamorphic rocks such as marble, calcite or schist (Skoglund and Lauritzen, 2011). Gypsum, anhydrite and other evaporitic formations are also highly karstifiable (Goldscheider and Drew, 2007).

A schematic overview of typical karst features occurring in alpine areas is given in Figure 1.
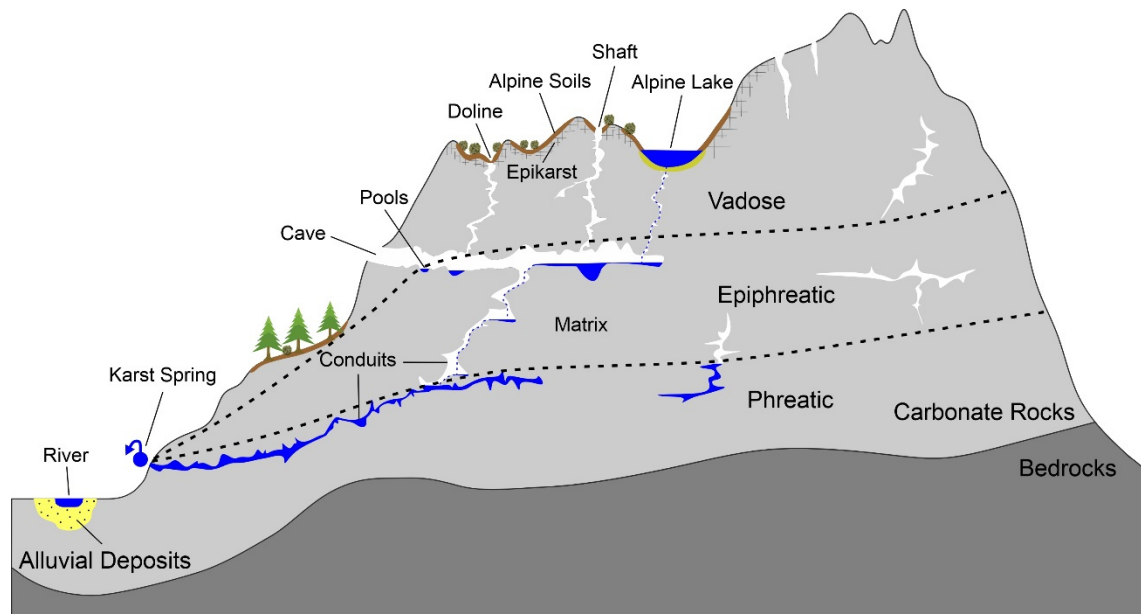
Figure 1: Schematic overview of typical karst features in an alpine karst aquifer.

Generally, karst aquifers are formed by chemical dissolution of soluble rocks. In the case of carbonate rocks, CO_2 from the atmosphere and/or soil zone plays a critical role in karstification (Ford and Williams, 2007). Karstification is caused by water (containing CO_2) from the atmosphere or from the soil entering the geological underground and circulating in small fissures and fractures of carbonate rocks (Goldscheider et al., 2020), and enhances the primary low porosity of the rock matrix. The process of karstification is a self-amplifying process (Fig. 2):

higher through-flow and chemical dissolution occurs along the fractures, leading to a fissured network, which causes a secondary porosity. The accelerated growth of their apertures than leads to the formation of a hierarchically-connected network of fractures, conduits and caves, often converging into one master conduit drained by a large spring (Dreybrodt, 1990). Therefore, karst aquifers are often described as having a triple porosity structure.
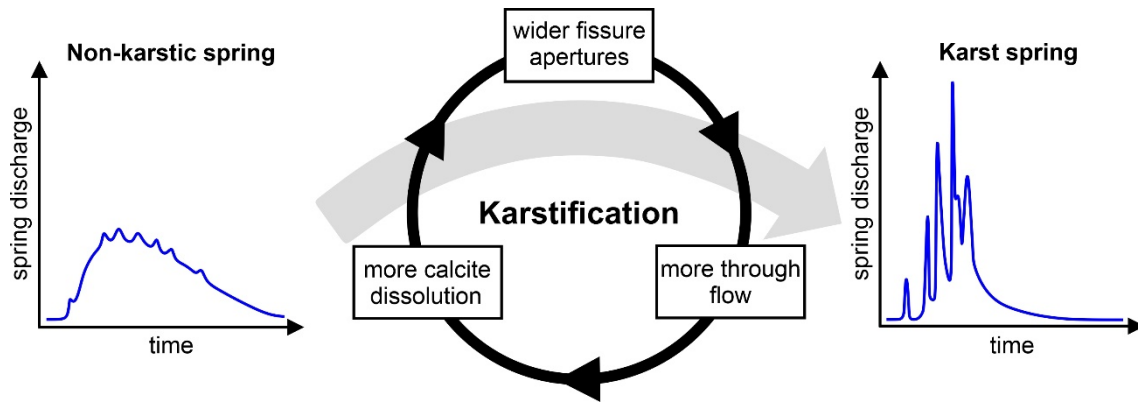
Figure 2: Schematic description of the karstification process and its influence on the hydrodynamic behavior of spring discharge (Hartmann et al., 2014).

While flow in karst conduits is rapid and often turbulent, flow in the surrounding matrix is much slower and laminar. However, water storage in conduits is often limited, while the majority of water storage occurs in the surrounding matrix (Ford and Williams, 2007). The interaction between karst conduits and the matrix is an often described process in the literature (e.g. Ford and Williams, 2007) but quantitative descriptions of this process are rare because the exchange process itself is hard to observe directly. The following figure shows a general conceptual description of this process.
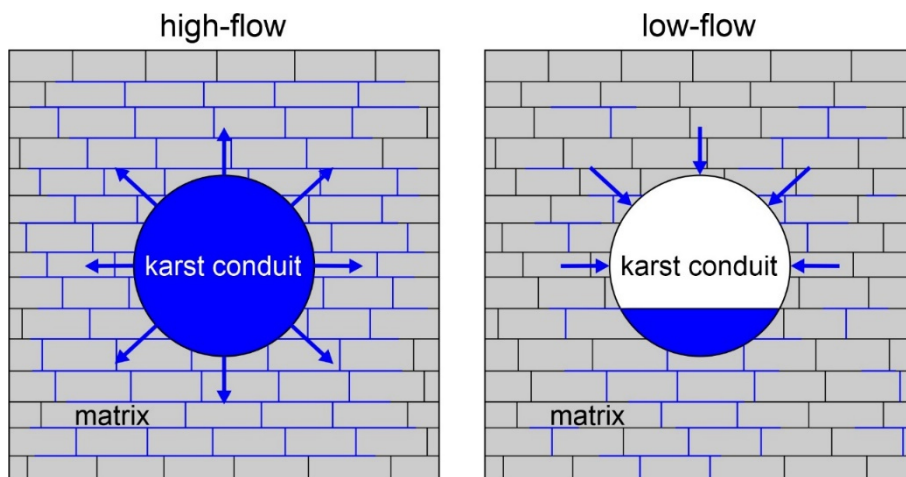
Figure 3: Conceptual description of the interaction between karst conduits and the surrounding rock matrix for different hydrological conditions (modified after Goldscheider, 2005a).

Furthermore, there is a duality of recharge and infiltration in karst areas. Recharge can either be autogenic (from the karst area itself) or allogenic (from adjacent non-karst areas). The infiltration into the aquifer occurs either concentrated via swallow holes (e.g. shafts or dolines, Fig. 1) or

diffuse into small fissures or through the overlying soil (Goldscheider and Drew, 2007). Within the vadose zone, the water flow is vertically down to the phreatic zone (Fig. 1), either concentrated and rapid via vertical shafts or diffuse and slow through the matrix. The groundwater flow in the phreatic zone is mostly concentrated in often highly conductive conduits (Chen, 2017). Depending on the distribution of the hydraulic heads within the karst aquifer, the conduits exchange water with the adjacent matrix (e.g. Frank et al., 2019).

Compared to other groundwater systems, karst aquifers are considered as highly vulnerable because contaminants can easily reach the groundwater. This is due to the high permeability in the solutionally enlarged fissures and channels and to the lack of effective attenuation mechanisms (Ford and Williams, 2007). In many karst regions, the soil cover is thin or even completely absent. Consequently, the breakdown of contaminants by microorganisms and by physical and chemical processes, which normally occur effectively in the soil zone, is weak. Where streams directly sink underground, the soil-zone is completely bypassed. Furthermore, the recharge water can pass quickly through the unsaturated zone via shafts and fissures (Fig. 1). In consequence, the unsaturated zone looses its filtration function, which normally delays the arrival of contaminants and further attenuates them by physical and chemical processes (Leibundgut, 1998). In the saturated zone, mainly dilution and dispersion take place.

Hence, karst aquifers show a large heterogeneity of groundwater flow, which often is completely independent of topography. Therefore, conventional hydrogeological methods like pumping tests and potentiometric surface mapping are often not suitable for karst aquifers. Karst aquifers often require special techniques for investigation, like natural and artificial tracer tests (Maliva, 2016). Nevertheless, karst areas and karst aquifers are of special importance, especially for drinking water supply.

Recent studies estimate that continuous carbonate rocks cover about 9 % of the planet's dry and ice-free land surface and about 6 % are covered by discontinuous carbonate rocks or mixed with evaporites (Goldscheider et al., 2020). In whole Europe, about 14 % of the land surface is covered by carbonate outcrops (Chen et al., 2017). Figure 4 shows an extract of the World Karst Aquifer Map (WOKAM) of the alpine region with the study area of this thesis.

Stevanović (2018) estimated that in total, about 800 Mio. people worldwide rely on drinking water from karst aquifers. For example in Austria, while only 25 % of the land surface is covered by karstifiable carbonate rocks (Chen et al., 2017), over 50 % of the population depends on drinking water from karst aquifers, including large cities like Vienna, Salzburg and Innsbruck (Kralik, 2001).

In view of climate change and increasing water demand in many parts of the world the importance of karst aquifers will rise and especially such high alpine karst aquifers offer an enormous

potential for future water supply. On the other hand, especially in the alpine region, the climate change will have a direct impact on the water cycle and therefore, the quantity and quality of water resources. Such impacts can include floods, droughts, higher frequency of extreme weather (again especially in alpine regions), higher water levels, and water temperatures.
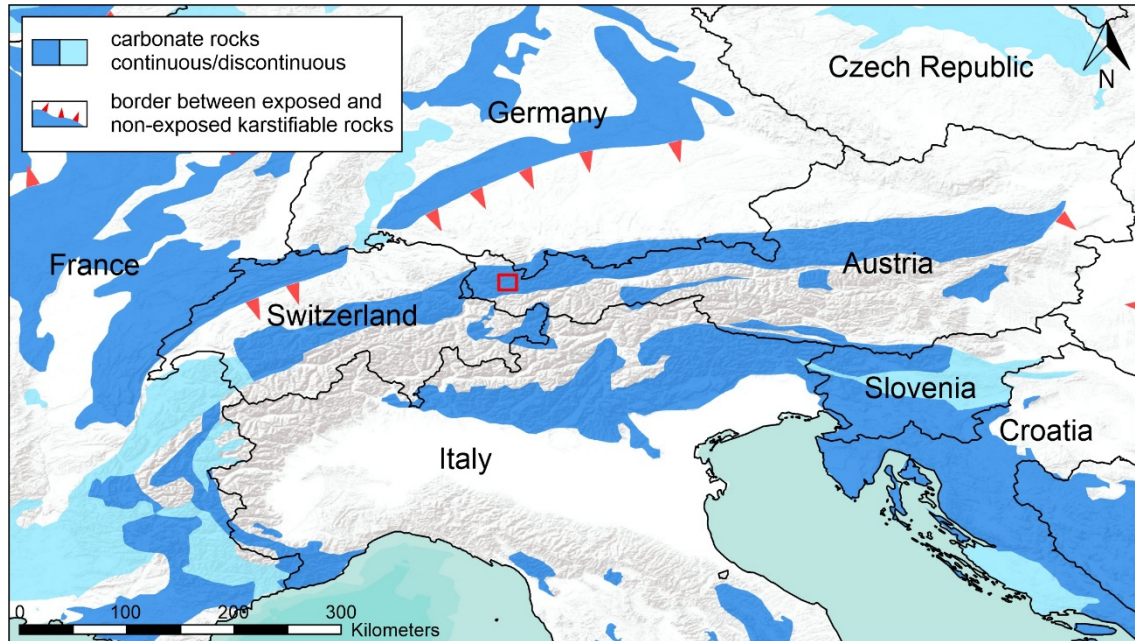
Figure 4: Extract of the World Karst Aquifer Map (WOKAM, Chen et al., 2017) to illustrate the appearance of karst areas in the European Alps. Red rectangle = study area.

Such alpine karst systems are especially vulnerable under changing climatic conditions because snowmelt in mountainous environments (itself highly sensitive to changing climate conditions) is an important factor for aquifer recharge (Finger et al., 2012; Gremaud et al., 2009). The discharge regime of mountainous karst aquifers and the future water availability in their forelands will be significantly affected by the changing precipitation and temperature (Finger et al., 2013).

Especially the increased frequency of extreme events due to climate change will lead to many challenges in karst water management. The high variability in water availability and water quality requires rapid estimation strategies of contamination parameters and adapted management and protection strategies to ensure a sustainable water supply.

1.2   Objectives and Approaches

The aim of this thesis is a contribution to a better understanding of alpine karst systems and their hydraulic functioning, particularly regarding the high variability of water quality. Since many people in alpine areas are depending on drinking water from karst springs, an exemplary investigation of alpine karst aquifers in the Lechquellen Mountains in Austria (Fig. 5) is presented in this thesis. In the whole investigation area, 185 sampling locations (springs and streams) were investigated (Fig. 5).
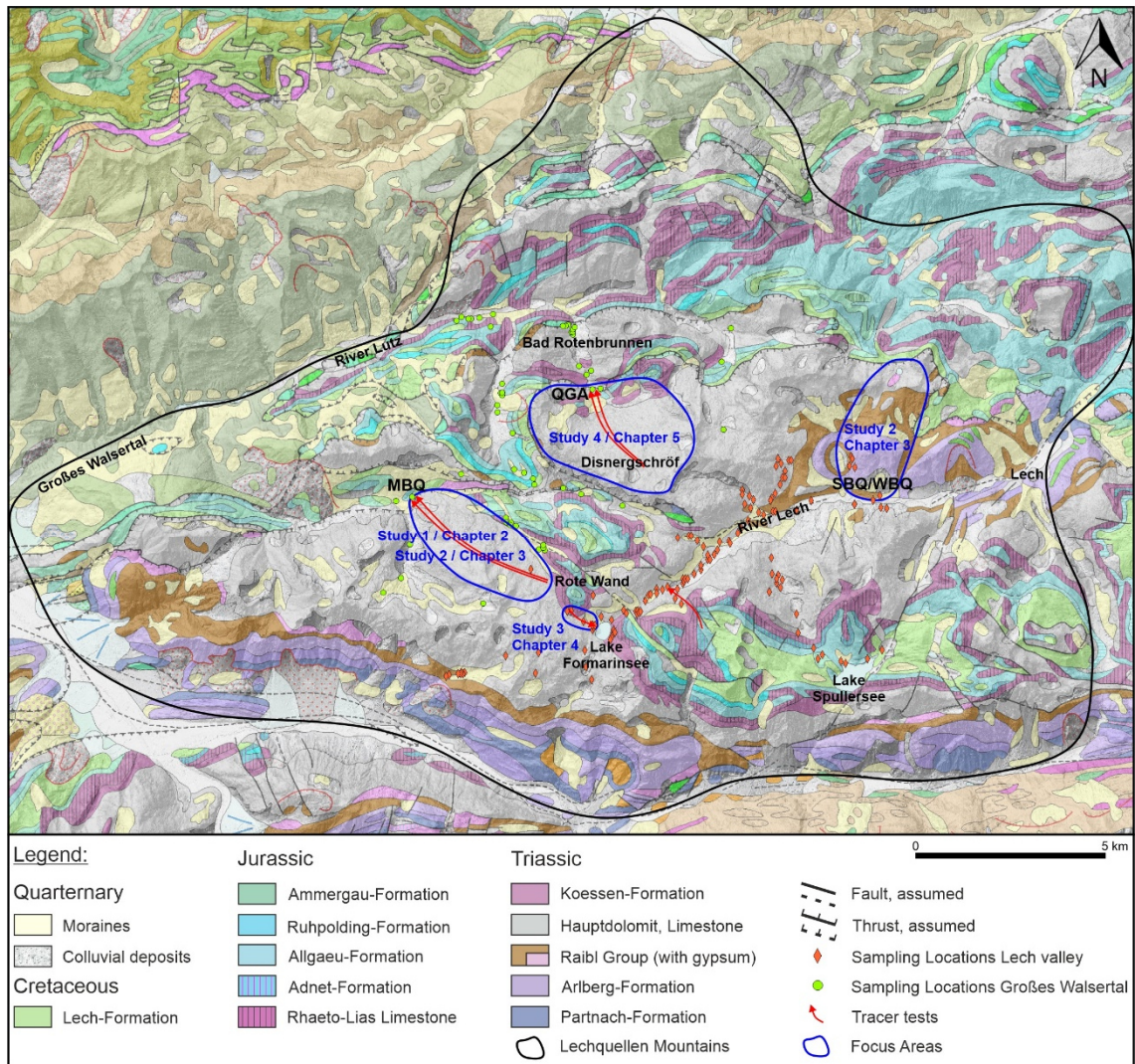
Figure 5: Geological map of the investigation area Lechquellen Mountains with the most important geological units in the respective focus areas, together with all sampling and measuring locations in the upper Lech Valley and in the Großes Walsertal. Blue borders indicate the karst aquifers investigated in detail and described in chapters 2, 3, 4 and 5.

The Lechquellen Mountains are formed by two geological units, the Penninic and Austroalpine nappes. The Triassic Arlberg and Partnach formations are the oldest formations in the study area. These are overlain by the Raibl Group, which consist of dark, indurated limestone and slatey, impermeable marls, as well as gypsum and rauhwackes. The Hauptdolomit-Plattenkalk Fm. lies above the Raibl Group and covers most of the study area. Above this formation follow Jurassic limestone formations.

The thesis focuses on four areas with special characteristics. Study 1 and 2 focus on a karst aquifer (Marulbachquelle, MBQ) with special geological features, namely gypsum layers underlying carbonatic layers. The Marulbachquelle is intended to be used for drinking water supply in the future while the other spring investigated in study 2 (chapter 3), the Schwarzbachquelle (SBQ) is already used for drinking water supply for the village Lech. Study 3 (chapter 4) focuses on a small epikarst system with typical karst features, like fractures and karren. This system is characterised

by high flow velocities and is the only permanent inflow into Lake Formarinsee. Study 4 (chapter 5) focuses on a karst aquifer with a clearly defined catchment that is only drained by one single spring system. This aquifer is characterised by a thick main dolomite/limestone complex.

The investigation approach includes the development of conceptual hydrogeological models by using different hydrological and hydrogeological methods, e.g. tracer tests and hydrochemical analysis. Based on the conceptual models, the investigated karst systems could be described in more detail.

The first investigated aquifer is a complex carbonate-gypsum karst aquifer with gypsum layers underlying the karstified limestone-dolomite formation. In this context, the following research questions have arisen:

- How does the spring water chemistry react during a stable period interrupted by a heavy rain event?
- Can major ion concentrations be used to describe the relevant hydrological processes and the main factors controlling the hydrogeochemical characteristics of the investigated spring?
- Can natural tracers be used to verify and to quantify possible water exchange between conduits and the surrounding matrix during low-flow and during high-flow conditions?

Such hydrochemical analysis can contribute to a better understanding of the functioning of a karst aquifer. Because karst aquifers are also very vulnerable to contamination, the development of rapid determination methods of contamination parameters are essential. A fluorescence-based multi-parameter approach is a promising tool to characterize the dynamics of organic carbon, faecal bacteria and particles. Two large karst springs were investigated and compared. The main research questions therefore are:

- How do the measured parameters react to hydrological events and are there any differences between the investigated springs and catchments?
- What information about the contamination dynamics can be obtained from turbidity and particle-size distribution?
- Is there any relation between fluorescence values and other water quality parameters, especially TOC and fluorescence and between protein-like fluorescence and cultivation-based determinations of bacteria?
- Is fluorescence spectroscopy a valuable tool to measure organic and faecal contamination? Can a certain combination of these techniques be used as a real-time indication system?

Tryptophan-like fluorescence is a promising indicator for bacterial contamination and is used by other studies as a real-time water quality indicator. Because the transport behaviour of tryptophan and also of humic substances is still insufficiently known, a tracer test in a well-studied model (epi)karst aquifer was conducted where tryptophan and humic acid (as humic acid sodium salt) were used as artificial tracers and compared to the conservative tracer uranine. The main research questions were:

- Are there any differences in the transport properties between the ideal conservative tracer and the two natural tracers that were here used as artificial tracers?
- Can online field measurements (field fluorometer) be used to measure tryptophan and humic-acid in near real-time?
- Do the results of the tracer test deliver any additional information about the investigated karst system?

With regard to climate change, high alpine karst aquifers will become more important for future water supply. We investigated a high alpine karst system with a clearly defined catchment, which has only one spring as outlet. Such karst systems are quite rare but scientifically valuable, especially for water- and mass balance calculations. This study focuses on the following research questions:

- How much does the investigated karst system contribute to the atmospheric CO_2 sink?
- What is the denudation rate for carbonate rocks in the investigated system and can it be compared to other studies of alpine karst systems?
- Can the internal flows within the karst aquifer (conduit – matrix) be assessed by modelling the rainfall-discharge behaviour?

By addressing these specific research questions, a profound understanding of the investigated karst systems could be developed. The carried out investigation procedure allows new insights into the hydraulic processes and water quality dynamics of alpine karst systems and can therefore also contribute to a better protection and utilization of alpine karst aquifers.

1.3   Structure of the Thesis

The structure of the present thesis is of a cumulative type, consisting of four studies (chapters 2, 3, 4 and 5) that cover different aspects of karst hydrogeology and a section with summarized conclusion and outlook (chapter 6). The studies in the chapters 2, 3 and 4 are published in ISI-listed journals, the study in chapter 5 is submitted.

Chapter 2 presents the results of hydrogeochemical investigations, which were used to characterize the water of a spring draining a complex carbonate-gypsum karst system. The spring

reaction to a rainfall event was examined to identify the relevant hydrological processes controlling the hydrochemistry and further to understand water-rock interactions and conduit-matrix exchange.

Chapter 3 shows the results of a fluorescence-based multi-parameter approach to characterize dynamics of organic carbon, faecal bacteria and particles at alpine karst springs. The correlation between the investigated parameters were presented and it was demonstrated that a combined measurement of tryptophan-like fluorescence and particle-size distribution is a promising approach for the rapid assessment of organic contamination, especially relative to time-consuming conventional bacterial determination methods.

As fluorescence measurements (especially of tryptophan-like fluorescence) become more and more popular to determine faecal contamination in real time, it was of special need to enhance the knowledge about the transport properties of tryptophan and also of humic-like substances. **Chapter 4** presents the results of a comparative field tracer test to evaluate these transport properties in comparison with the conservative tracer uranine. Laboratory measurements were compared with online field fluorometer measurements in order to demonstrate the suitability of these instruments for real-time measurements.

Chapter 5 presents the results of the investigations of a high alpine karst system, which has only one spring as major outlet. For this system, the contribution to the CO_2 sink and the denudation rate for the carbonate rocks were determined and compared to other studies of alpine karst systems. Furthermore, the applicability of the modelling package KarstMod was tested and the modelling results were used to assess the internal flows within the aquifer.

In **chapter 6**, a summary and conclusion of the major results and highlights are given, to understand the meaning of the findings for the research regarding hydraulic processes and water quality dynamics especially of alpine karst system.

Chapter 2

2   Sulfate variations as a natural tracer for conduit-matrix interaction in a complex karst aquifer

Abstract

Large areas of Europe, especially in the Alps, are covered by carbonate rocks, and karst springs are an important source for drinking water supply. Because of their high variability and heterogeneity, understanding the hydrogeological functioning is of particular importance for protection of karst aquifers. In this study, hydrogeochemical investigations characterized the water of a spring draining a complex carbonate-gypsum karst system in the Alps. The reaction of the spring to a rainfall event was examined to identify the relevant hydrological processes controlling the hydrochemistry of the spring, and to understand water-rock interactions and conduit-matrix exchange. A fast and marked reaction of discharge and electrical conductivity was observed. The main cations are Ca^{2+} and Mg^{2+} which showed a distinct decrease after the rainfall. Bicarbonate and sulfate were identified as major anions. While HCO_3^- showed only minor fluctuations, SO_4^{2-} decreased by 72 % after the rain event. Comparisons of ion ratios show that both carbonate and gypsum rocks influence the water chemistry of the spring. The rainfall event caused a dilution effect, but dilution alone cannot explain the observed water chemistry. A conceptual model of the spring behavior during low-flow and high-flow conditions, including conduit-matrix interaction, was developed which can explain the observations. This study aims to give new insights into the highly dynamic exchange processes between karst conduits and the surrounding matrix and the results demonstrated that 1) during low-flow conditions, the spring is characterized by high sulfate content, while after rainfall events, the water chemistry is dominated by bicarbonate. These findings show the dependency of water chemistry from the lithology; 2) a change in water chemistry is associated with a significant shift from low-flow to high-flow conditions; 3) conduit-matrix exchange is an important factor as shown by the discharge-sulfate relationship and clearly influences the behavior of the spring.

2.1   Introduction

About 14 % of Europe is covered by carbonate rocks. Water from these karst areas contributes significantly to the water supply of many countries. In Austria, 25 % of the land surface is covered by carbonate rocks (Chen et al., 2017), and over 50 % of the population, including large cities, such as Vienna, Salzburg and Innsbruck, depend on drinking water from karst aquifers (Kralik, 2001). In view of increasing water demand, high alpine karst aquifers in particular offer an enormous potential for future water supply. At the same time, such karst aquifers are vulnerable to contamination, because contaminants can easily enter the subsurface and spread all over the conduit system with little to no natural degradation. Therefore, the hydrogeological investigations and protection of karst aquifers are of particular importance (Zwahlen, 2004).

Understanding of alpine hydrogeology must continuously advance, since recharge processes, drainage structures and potentially available water resources are generally insufficiently known, especially in alpine karst aquifer systems (Goldscheider, 2011).

The main complications in karst areas are variability and heterogeneity. Karst aquifers can be described as having triple porosity; intergranular porosity within the matrix rock and small fracture porosity which are usually generalized as matrix, and large conduit porosity (e.g. Smart and Hobbs, 1986; White, 2003). Many karst simulation models, like the double continuum approach (DC) or the combined discrete-continuum approach (CDC) only use dual porosity, i.e. conduit and matrix (Hartmann et al., 2014).

Most karst aquifers cannot be separated into purely diffuse or conduit flow but rather a combination of these two flow types (e.g. Atkinson, 1977; Ford and Williams, 2007.). This view of karst aquifers suggests that they constitute a two-component system, in which a majority of the storage occurs within the matrix porosity and in fractures, while the majority of flow and transport occurs in the conduits.

Conduits can be connected to surface water through swallow holes. This allows extensive mixing of groundwater and surface water which results in natural changes in the chemical composition of the groundwater and also increases the vulnerability to contamination (Field, 1988; Martin and Dean, 2001; White et al., 1995).

When contaminants directly enter a vadose or non-pressurized conduit system, there is little impact on water quality within the intergranular porosity because the tainted waters are rapidly transported and discharged at springs (Mahler and Lynch, 1999; Meiman et al., 1988). Thus, only the water quality of springs is affected and there is only little long-term impact on the stored groundwater reservoir (Martin and Screaton, 2001). However, if conduit water and matrix water

do mix, contaminants can reside in the matrix porosity, resulting in long residence times in the groundwater reservoir (Katz et al., 1999) and therefore long-term impacts on water quality.

Conduit-matrix interaction can be described as a gradient inversion within the karst system between low-flow and high-flow conditions and vice versa. Due to an increase of hydraulic pressure in the conduits and the rise of the water table, water is pressed into the matrix and the unsaturated zone. Later on, during low-flow conditions, the conduits drain these zones again. However, this phenomenon is difficult to observe directly.

Understanding and quantification of the extent of exchange between the different porosity systems within karst aquifers is therefore critical to determine the sources of spring water and the potential for contamination.

The hydraulic interaction between karst conduits and the adjacent rock matrix for different hydrologic conditions was described by means of a tracer breakthrough curve in an alpine karst system by Goldscheider (2005b). Instances of fluid transfer between karst conduits and the surrounding limestone matrix have been outlined by Raeisi et al. (2007) by specific electrical conductivity measurements within a stream cave. Another indication of conduit-matrix interaction was given by Mitrofan et al. (2015) by monitoring the natural flux of chloride in a karst spring and applying mass balance calculations.

Although there have been numerous studies focusing on karst aquifers and surface water/groundwater exchange (e.g. Lakey and Krothe, 1996; Green, 1997), questions remain about the rates and extent of mixing between conduit and matrix water, especially as they relate to lithology.

The hydrogeochemical evolution of groundwater is affected by many natural factors, including the composition of rain water, geological structures, mineralogy of the aquifer and water-rock interaction along the flow paths (e.g. Barberá and Andreo, 2015; López-Chicano et al., 2001; Yuan et al., 2017).

Previous studies showed that water chemistry, especially the spatial variations of major ion concentrations, can be used to determine recharge, flow paths, sources of solutes and the interactions between groundwater and the surrounding lithology (e.g. Andreo et al., 2016; Lang et al., 2006; Wu et al., 2009). Major ion concentrations can also be used to identify the interactions between shallow and deep aquifers (Carucci et al., 2012) and to identify groundwater mixing and the consequent implications for drinking uses (Barbieri et al., 2017).

Therefore, water chemistry can significantly contribute to understand complex aquifer hydrology and hydrological processes in the karst aquifer (e.g. Glynn and Plummer, 2005).

The purpose of this study is to examine the interaction between conduit and matrix water together with the lithology in a complex gypsum carbonate karst system in the Austrian Alps and to develop a better understanding of the hydrological processes occurring in complex karst aquifers.

The investigated spring was selected because 12 individual water samples taken during different hydrological conditions in 2014 and 2015 and analyzed for major ion concentrations indicated distinct differences, especially in sulfate concentrations and therefore pointed out the need for a more detailed monitoring campaign.

At the investigated spring, physico-chemical parameters were measured and the chemical composition of the spring water was determined during a hydrologically stable period interrupted by a rainfall event in order to identify possible variations in water characteristics caused by this rainfall event.

The main objectives of this study are 1) to systematically investigate the distribution of major ion concentrations during a hydrologically stable period interrupted by a rainfall event; 2) to identify the dominant hydrological processes and the main factors controlling the hydrogeochemical characteristics of the investigated spring; 3) to obtain insights into interaction of groundwater with the surrounding lithology and 4) to verify possible exchange of water between conduits and the surrounding matrix porosity during low-flow and high-flow conditions by means of natural tracers.

Understanding of hydrological processes and the hydraulic functioning of the investigated karst system are important for the protection of the karst spring and for the future use of this spring as drinking water source.

2.2   Study Area

2.2.1   Geological Setting

The investigated spring (Marulbach Spring, MBQ) is located in the Lechquellen Mountains in the Austrian Alps in the Federal State of Vorarlberg (Fig. 6a).

Two main geological units form the Lechquellen Mountains in the investigation area, the Penninic and Austroalpine nappes. The oldest formations in the study area are the Triassic Arlberg and Partnach Formations. These are overlain by the Raibl Fm. This formation consists of dark, indurated limestone and slatey, impermeable marls, as well as gypsum and rauhwackes. Above the Raibl Fm. lies the Hauptdolomit-Plattenkalk Fm. (upper Carnian – upper Norian) which covers most of the study area. Moderately karstifiable dolomite (Goldscheider and Goeppert,

2004) builds up most of the summits in the investigation area (Fig. 6b). The thickness of the whole formation can be up to 2000 m (Friebe, 2004).

Above 1800 m asl, most areas are poorly covered by alpine and nival vegetation. Nevertheless, some parts of the investigation area are used as cattle pasture.
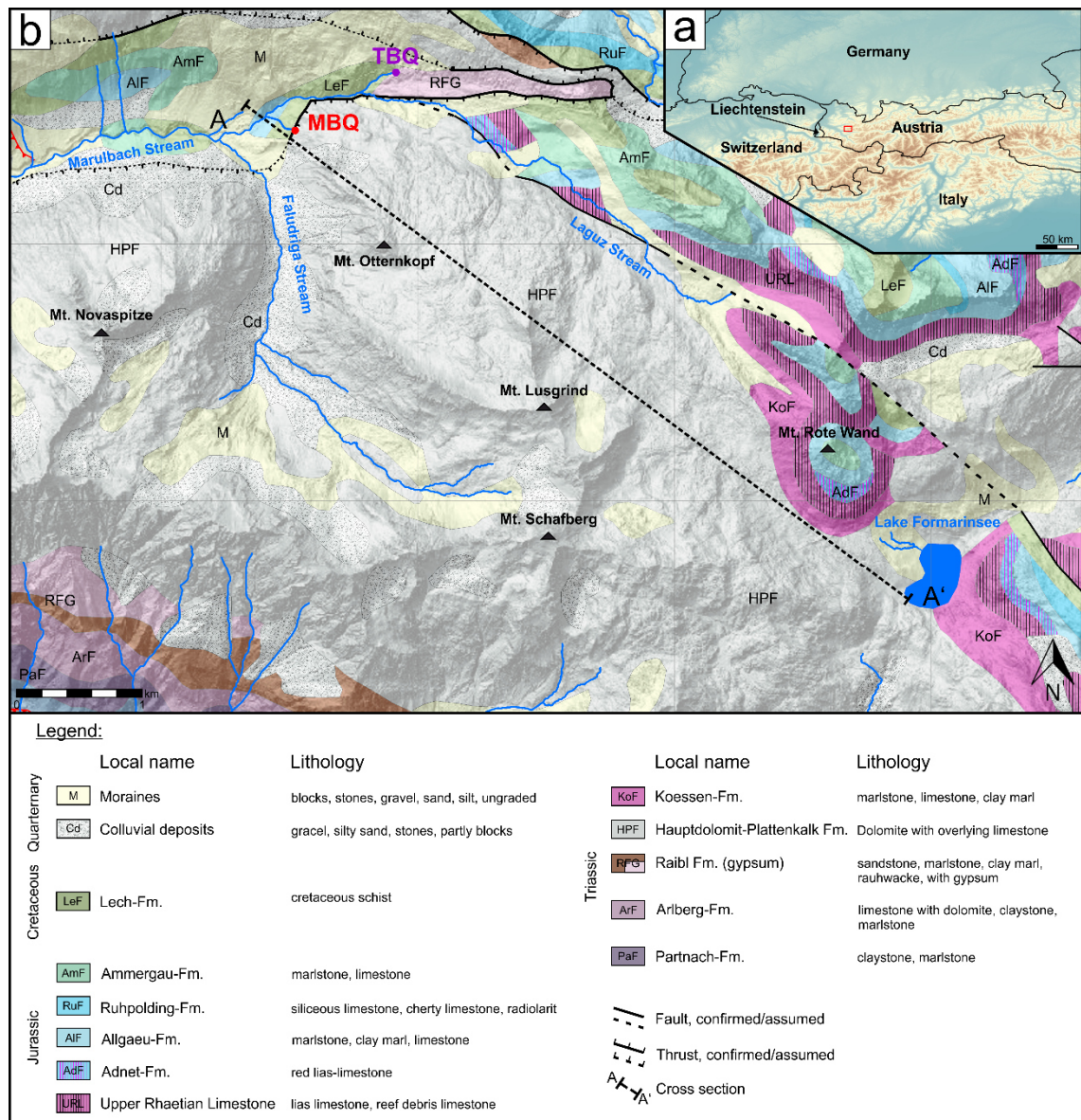
Figure 6: Location of the test site in the federal state of Vorarlberg in Austria (red rectangle); b) Geological map of the investigation area with the monitored spring (MBQ). (basemap: Land Vorarlberg – data.vorarlberg.gv.at and Geological Map of Vorarlberg, 1:100000).

2.2.2 Hydrogeology

The site is located at the continental water divide between the catchment of the Rhine (North Sea) in the northwest and the catchment of the Danube (Black Sea) in the southeast.

The large Marulbach Spring (MBQ) drains into the Laguz stream with a measured discharge of 168 L/s to 232 L/s during the study period. The minimum and maximum discharges of MBQ were

88 L/s and 909 L/s respectively (Land Vorarlberg, 2018). The spring is located directly on the border of the Lechtal nappe and the Rhenodanubian Flysch zone. The spring itself is a karst spring and the outlet lies in the Hauptdolomit-Plattenkalk formation (Fig. 7). The catchment of the second important spring (Trübbachspring, TBQ, Fig. 6b) encompasses only gypsum layers of the Raibl Fm.
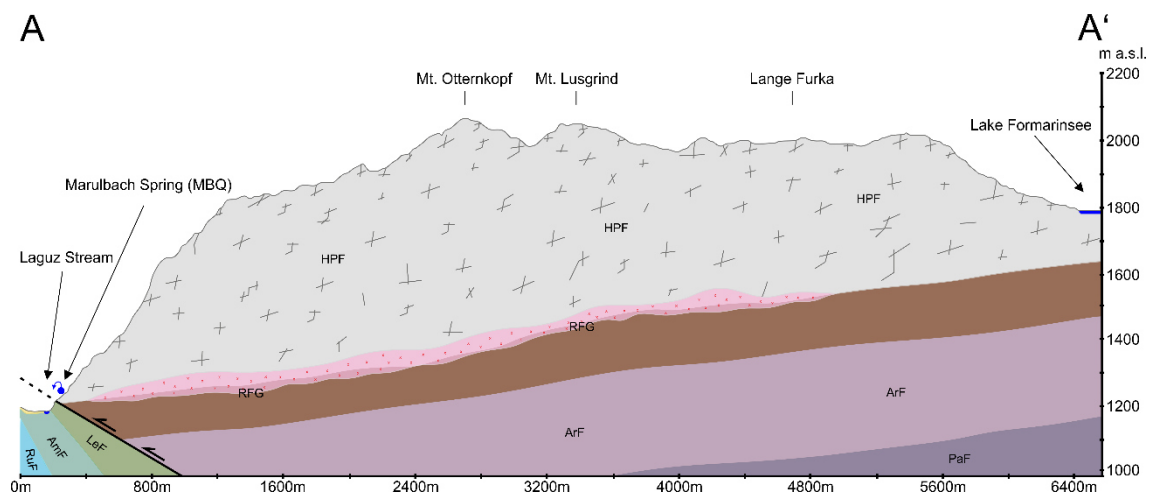
Figure 7: Cross-section A-A' through the main catchment area of Marulbach Spring, Legend see Figure 6.

In the investigation area, most precipitation contributes to recharge due to scarce vegetation and easy infiltration due to distinct fracturing and karstification. The Plattenkalk shows karren features (Goldscheider & Goeppert, 2004). The underlying Raibl Fm. with its marly layers forms a major aquitard (Plan et al., 2009). The limestone lenses within the transition zone of the Dolomite and Raibl Fm. and especially the porous rauhwackes and gypsum rocks form thin karst aquifers if they are contiguous.

2.3   Materials and Methods

Discharge, electrical conductivity (EC) and water temperature of Marulbach Spring (MBQ) have been continuously monitored (at 5 min to 15 min intervals) by the Water Management Department of the Vorarlberg State Administration since the year 2000 and these data were used for this study.

During the detailed monitoring period from 17.-29.09.2015 water samples were collected at two hour to four hour intervals, manually and with an automatic sampler, in 50 mL PE bottles (Rixius AG, Mannheim, Germany) for subsequent laboratory chemical analysis. Water samples were filtered with cellulose acetate membrane filters (0.45 μm, 25 mm, Sartorius AG, Göttingen, Germany) and split for the analysis of anions and cations. The samples for the analysis of cations were acidified with HNO_3 (65 %) on-site and all samples were stored at 4 °C until analysis. Alkalinity was measured as triplicate by volumetric titration on site using an alkalinity test (Merck KGaA, Darmstadt, Germany) and the mean value was taken, while all other major components

(Ca^{2+}, Mg^{2+}, Na^+, K^+, SO_4^{2-}, Cl^-, NO_3^-) were measured in the laboratory using an IC system (DIONEX ICS-1100 and ICS-2100, Sunnyvale, USA).

The major ions calcium, magnesium, bicarbonate and sulfate are generally provided by the dissolution of carbonates (calcite/dolomite) and gypsum. The dissolution of calcite, dolomite and gypsum can be expressed as follows:

$$CaCO_3 + H_2O + CO_2 \rightarrow Ca^{2+} + 2HCO_3^- \tag{1}$$

$$CaMg(CO_3)_2 + 2H_2O + 2CO_2 \rightarrow Ca^{2+} + Mg^{2+} + 4HCO_3^- \tag{2}$$

$$CaSO_4 \cdot 2H_2O \rightarrow Ca^{2+} + SO_4^{2-} + 2H_2O \tag{3}$$

For quality control of our ion analysis, we computed the charge balance error for every sample according to (DIN 38402-61, 2014).

$$CB = \frac{\sum_k c_{eq,k} - \sum_j c_{eq,j}}{(\sum_k c_{eq,k} + \sum_j c_{eq,j}) \times 0.5} \times 100 \tag{4}$$

where k is the index of cations, j is the index of anions and c_{eq} is the respective equivalent concentration.

The Spearman's rank correlation (r_s) was computed using PAST software (Version 3.20) to determine the nonparametric correlation based on a rank transformed method by using the following equation (Press et al., 1992).

$$r_s = \frac{\sum_{i=1}^{n}(R_i - \bar{R})(S_i - \bar{S})}{\sqrt{\sum_{i=1}^{n}(R_i - \bar{R})^2}\sqrt{\sum_{i=1}^{n}(S_i - \bar{S})^2}} \tag{5}$$

The data of two variables x_i and y_i are ranked independently among themselves to R_i and S_i. If there are identical values within one data set, called ties, the mean of the ranks was calculated.

2.4 Results and Discussion

2.4.1 Observed time series and statistical analysis

During the sampling campaign, the cumulative rainfall was 32 mm with the major rain event starting on the evening of the 22nd and lasting until noon of the 23rd for a total of 25.3 mm. The snow line during these days was at around 1900 m asl, so a large proportion of precipitation in the higher regions of the catchment was snow. The influence of the snow melt on the discharge and EC of MBQ could be seen in the subsequent days. The summary statistics of all measured parameters during the investigation period was computed using PAST software and is given in table 1.

Table 1: Summary statistics of the measured parameters during the investigation period.

	Q	T	EC	Ca^{2+}	Mg^{2+}	Na^+	K^+	HCO_3^-	SO_4^{2-}	NO_3^-	Cl^-
	[L/s]	[°C]	[µS/cm]	[mg/L]	[mg/L]	[mg/L]	[mg/L]	[mg/L]	[mg/L]	[mg/L]	[mg/L]
n	1152	748	1152	103	103	103	103	103	103	103	103
Min.	168	4.70	309	42.50	12.95	0.30	0.16	149.50	38.30	1.22	0.28
Max.	232	4.84	501	73.50	17.35	1.06	0.37	164.75	136.18	2.14	0.65
Mean	192	4.76	389	55.57	14.87	0.60	0.25	156.99	78.91	1.62	0.47
S.D.	16	0.03	48	8.36	0.96	0.17	0.05	3.23	26.60	0.19	0.09
CV [%]	8.33	0.63	12.34	15.04	6.46	28.33	20.00	2.06	33.71	11.73	19.15

The complete results of the sampling and monitoring campaign of MBQ are shown as a time series in Fig. 8. Within one hour after the start of rain, the discharge of MBQ began to increase, and reached a maximum of 232 L/s after 19 hours. During the recession period, another two distinct discharge peaks on the evenings of the 24th and 25th (resulting from snow melt in the higher areas of the catchment) were observed.

The major rainfall event led to a decrease of EC from 501 to 309 µS/cm. A five hours time lag between increase of discharge and decrease of EC was observed. The steep increase of discharge likely resulted from a hydraulic pressure pulse or piston effect, caused by the rapid rainfall infiltration (Ravbar et al., 2011). According to the method proposed by (Ashton, 1966), the resulting conduit volume is between 2160 m³ and 3485 m³. The water temperature of MBQ is almost constant between 4.7 °C and 4.8 °C, but the rain event led to a slightly higher water temperature.

The main rain event also had a significant influence on water chemistry; a distinct decrease of major ion concentrations. Ca^{2+} concentration fell from 73.5 mg/L to 42.5 mg/L (a decrease of – 41 %) around 12 h after the rainfall. The pattern of Mg^{2+} concentration is very similar to that of Ca^{2+}, it decreased from 17.4 mg/L to 12.9 mg/L. The variations in Na^+ and K^+ concentrations are almost negligible throughout the whole investigation period, even after the rain event.

The major anions are bicarbonate and sulfate with minor concentrations of nitrate and chloride. HCO_3^- shows only minor fluctuations with a slight decrease around five hours after the rainfall. A major decrease of SO_4^{2-} was measured (72 %) from 136.2 mg/L to 38.3 mg/L around eight hours after the rain event. Slight fluctuations of the sulfate concentration was measured during the two snow melt periods (corresponding to the later discharge surges).

The patterns of the saturation indices (SI, calculated using PhreeqC) of the relevant minerals calcite, dolomite and gypsum show a similar behavior as the corresponding ions. The water is saturated with respect to calcite (~ 0.08) and undersaturated with respect to dolomite (~ -0.41) and gypsum (~ -1.58). The freshly infiltrating water after the rain event causes a minor decrease of the saturation indices of calcite and dolomite but a major decrease of the saturation index of

gypsum. Therefore, after the rain event, especially the dissolution of gypsum has a greater influence on water chemistry in the spring than calcite and dolomite dissolution.

For quality control, the charge balance error of all ion samples is also given in figure 6. According to DIN 38402-61, 2014 a charge balance error of ± 5 % is acceptable. Of 103 analyzed samples, 99 are acceptable with a charge balance error less than 5 %.
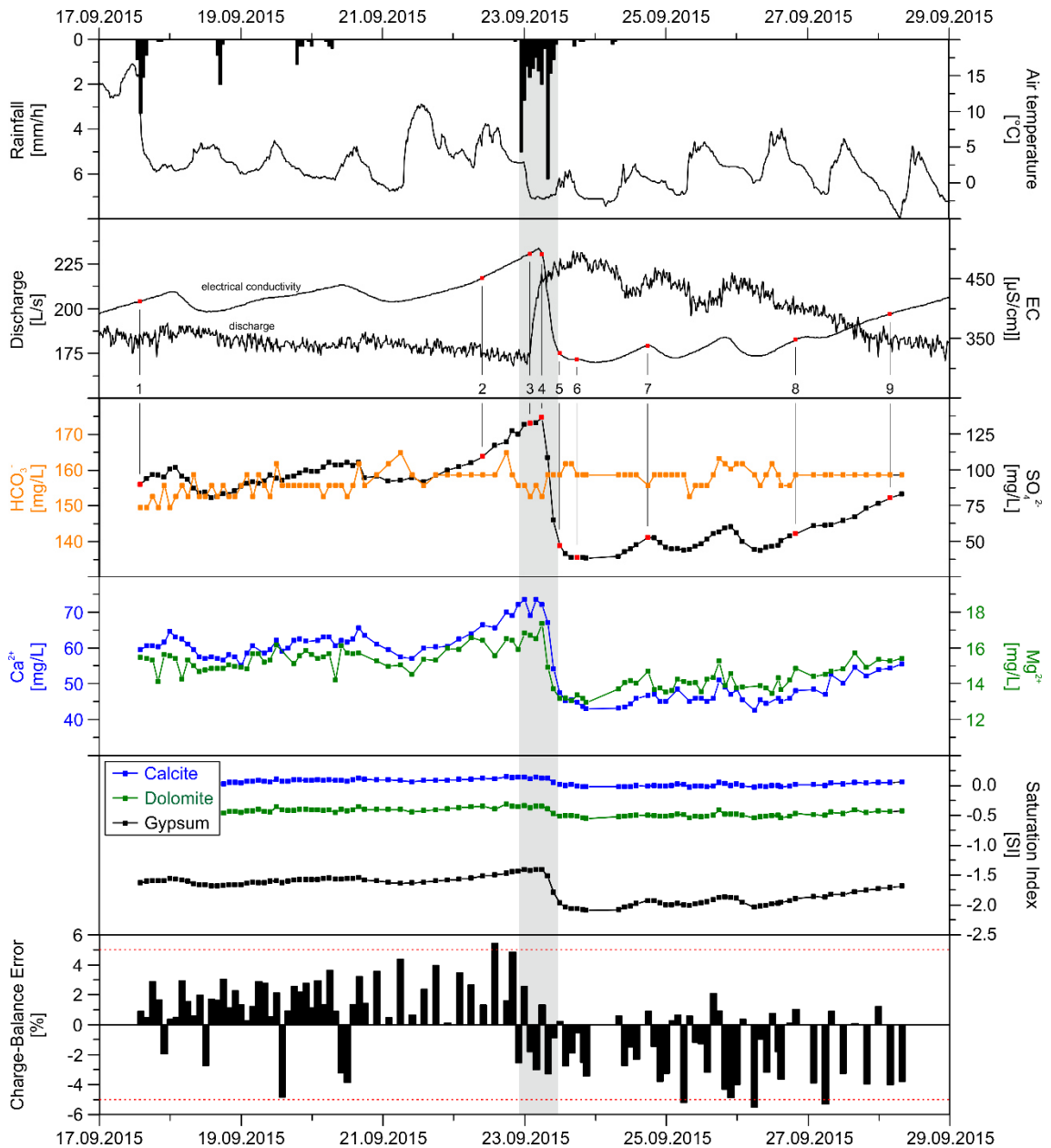
Figure 8: Temporal patterns of major ion concentrations of MBQ and saturation indices of calcite, dolomite and gypsum together with discharge, EC, rainfall and air temperature during the investigation period. As quality check for the ion analysis results, the charge balance error is given for all samples. The red dotted lines indicate the tolerable error according to DIN 38402-61. Numbers 1 to 9 indicate the position of the according ion measurements in figures 9 and 10. The grey bar indicates the main rain event.

2.4.2 Geochemical Investigations

The analysis of the spring water demonstrated that Ca^{2+}, Mg^{2+}, HCO_3^- and SO_4^{2-} are the dominant ions. If Ca^{2+}, Mg^{2+} and HCO_3^- result only from the dissolution of dolomite, the samples should be distributed along the 1:1 line (charge balance) of $Ca^{2+} + Mg^{2+}$ and HCO_3^- (Fig. 9a). If the dissolution of calcite was the only source of Ca^{2+} and HCO_3^-, the ratio of Ca^{2+} and HCO_3^- should also be 1:1 (Fig. 9b). If the dissolution of calcite and dolomite occurred side-by-side, the theoretical ratio of Ca^{2+} and HCO_3^- would be between 1:1 and 1:2. However, in this study, the water samples are located below the 1:1 line of $Ca^{2+} + Mg^{2+}$ and HCO_3^- (Fig. 9a) indicating that dissolution of dolomite is not the only source of Ca^{2+} and Mg^{2+}. The excess of Ca^{2+} indicates that another source for the excess Ca^{2+} must be present. The dissolution of gypsum leads to more Ca^{2+} in the spring water. As shown in Fig. 9c, the ratio of Ca^{2+} and SO_4^{2-} is greater than 1, indicating that gypsum dissolution is one of the Ca^{2+} sources in the spring water. In order to determine the contribution of the dissolution of carbonate and gypsum minerals to the spring water chemistry, the ratios of $Ca^{2+} + Mg^{2+}$ and $HCO_3^- + SO_4^{2-}$ were plotted (Fig. 9f).
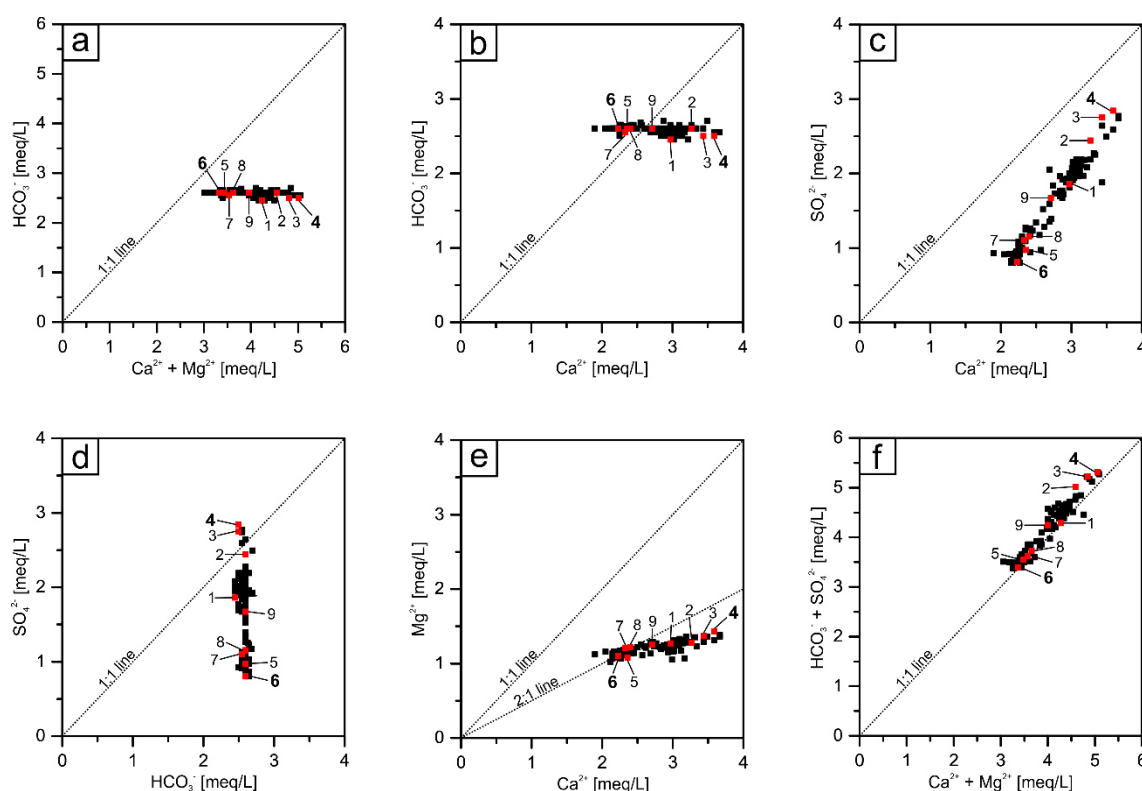
Figure 9: Ion ratios of all measurements: a) $Ca^{2+}+Mg^{2+}:HCO_3^-$; b) $Ca^{2+}:HCO_3^-$; c) $Ca^{2+}:SO_4^{2-}$; d) $HCO_3^-:SO_4^{2-}$; e) $Ca^{2+}:Mg^{2+}$ f) $Ca^{2+} + Mg^{2+}:HCO_3^-+SO_4^{2-}$; Red rectangles with numbers 1 to 9 indicate the same measurements as given in figures 6 and 8. Bold numbers 4 and 6 indicate the last value before the rain event and the first value after the rain event.

The samples from this study were distributed along the 1:1 line, showing that the dissolution of both, carbonate and gypsum rocks is the only source of the major ions, consistent with previous studies of carbonate-gypsum karst aquifers (e.g. Yuan et al., 2017). In the investigated system,

sulfate and bicarbonate are the dominating anions. While during and after the rain event the bicarbonate concentration remains more or less constant, the sulfate concentration shows a slight increase during the dry period (Numbers 1 – 4, Fig. 9d). Directly after the rain event, the sulfate concentration decreases (Numbers 5 – 6, Fig 9d) before it returns to the values prior to the rain event (Numbers 7 – 9, Fig. 9d).

Prior to the rain event, the $Ca^{2+}:Mg^{2+}$ ratio was between 2.34 and 2.51 (Numbers 1 – 4, Fig. 9e). Because of the decrease in Ca^{2+} concentration, the ratio is shifted towards Mg^{2+} after the rain event with a value of 2.02 (Number 6, Fig. 9e). Because the main source of Mg^{2+} in the area is dolomite, the Ca^{2+} can either originate from the Hauptdolomit-Plattenkalk formation or the gypsum deposits of the Raibl Group. The shift towards magnesium demonstrates the increasing influence of the Ca^{2+}-Mg^{2+}-HCO_3^--rich water after the rain event compared to the Ca^{2+} -SO_4^{2-}-water prior to the rain event.

A comparison of the $Ca^{2+}:HCO_3^-$ with the $Ca^{2+}:SO_4^{2-}$ ratio also shows the influence of the lithology on water chemistry. The pre-event water shows a $Ca^{2+}:HCO_3^-$ ratio of 1.21 to 1.44 (Numbers 1 – 4, Fig. 9b). The excess of Ca^{2+} originates from gypsum dissolution. After the rain event, the ratio drops to 0.86 (Number 6, Fig. 9b). The change in ratio of $Ca^{2+}:SO_4^{2-}$ is the inverse. Prior to rain, the ratio is between 1.60 and 1.26 (Numbers 1 – 4, Fig. 9c), while after the rain event the ratio increases to 2.75 (Number 6, Fig. 9c). The amount of water flowing through the gypsum layers of the Raibl Group decreases, and thus the $Ca^{2+}:SO_4^{2-}$ decreases, while the Ca^{2+} - HCO_3^--part increases. Further after the rain event, the influence of sulfate-rich water increases again, while the influence of bicarbonate-rich water decreases.

2.4.3   Hysteresis of sulfate and EC

To illustrate the influence of the piston effect on the sulfate concentration and EC of MBQ, the sulfate concentration and EC are displayed versus discharge (Fig. 10a and 10b). The time series shows a clear hysteresis. At the beginning of the sampling campaign, the sulfate concentration was around 89 mg/L and discharge was around 185 L/s. The smaller rain events on September 17th and 18th caused only slight EC and sulfate variations. After that, the sulfate concentration and EC increased while the discharge stayed almost constant. Initially the increase of the sulfate concentration continues, while the discharge also started to rise during the main rain event. About five hours after the start of the rain event, a notable decrease in the sulfate concentration was measured. This was caused by infiltrating meteoric freshwater reaching the spring. The influence of the snow melt and therefore the slightly increased discharge can also be seen in the two smaller loops on the 25th and 26th of September. With the subsequent decrease of discharge, an increase in EC and sulfate concentration back to values prior to the rain event was observed.
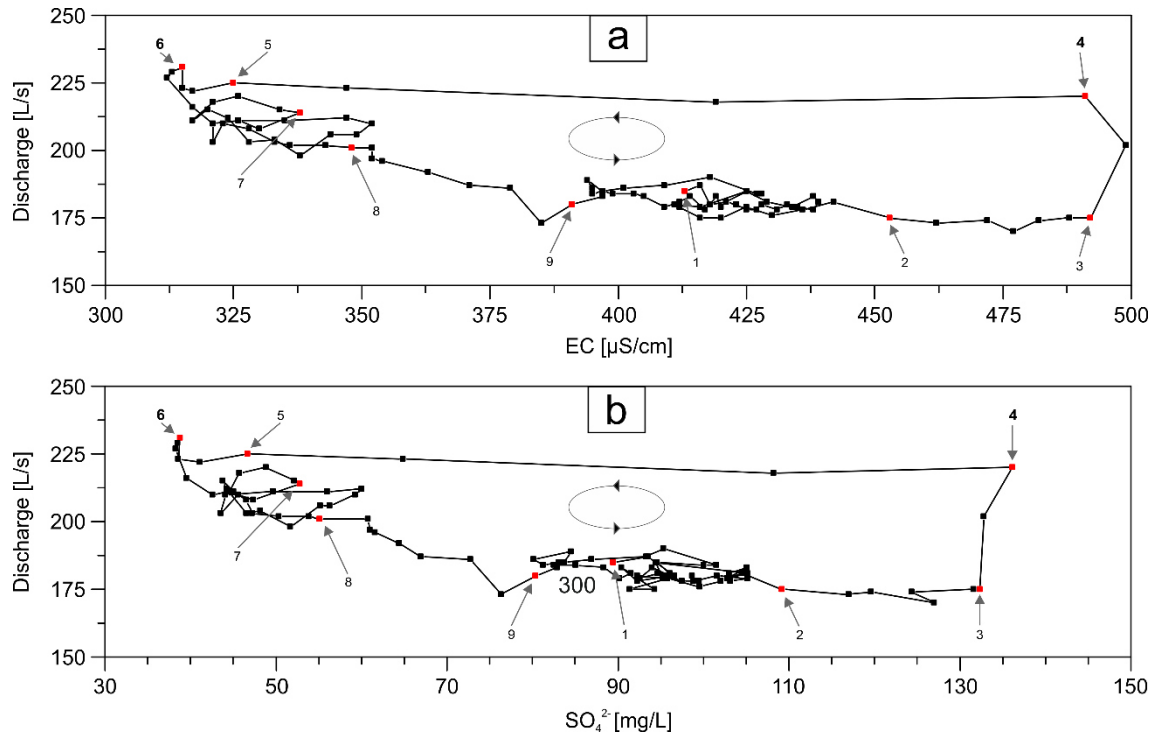
Figure 10: Electrical conductivity (EC) versus discharge and b) sulfate concentration versus discharge. Numbers 1 to 9 and red dots indicate the position of the corresponding points in Figs. 8 and 9.

2.4.4 Correlation Analysis

The investigated spring showed a fast and dramatic response for discharge and EC. The main cations also reacted to the rain event, with major changes in Ca^{2+} and Mg^{2+}-concentrations, but only minor changes in Na^+ and K^+. The main anions HCO_3^- and SO_4^{2-} also showed a fast reaction to the rainfall event. Only minor changes were measured in NO_3^- and Cl^--concentrations.

To better understand the relation between the different parameters and components, a correlation analysis was done for all parameters. In Table 2, the Spearman's rank correlation (r_s), the significance (p) and the number of samples (n) are given.

The strongest correlation exists for EC and Ca^{2+} and for EC and SO_4^{2-} with r_s values of 0.944 and 0.988. This highlights the importance of the gypsum layers for the EC and water chemistry of MBQ. The strong dependence of EC and sulfate was also confirmed by the additional water samples that were taken at MBQ during 2014 and 2015.

Strong correlations were also found for Mg^{2+} and Na^+ with EC with values of 0.820 and 0.832. Strong negative correlations were found for major cations and discharge (-0.699 to -0.715) as well as between discharge and EC (-0.801), which demonstrates the importance of EC as a stable and robust parameter to deduce the basic characteristics of a karst aquifer, especially regarding the timing of the arrival of surface water at the spring as also demonstrated by other studies (e.g. Raeisi et al., 2007; Ravbar et al., 2011).

Especially notable in water chemistry is the strong decrease of sulfate after the rain event from 136 mg/L to 38 mg/L with an almost constant HCO_3^- - concentration. This implies a significant change in the flow regime at different water levels in the system.

Table 2: Spearman's rank correlation (r_s), significance (p value) and the number of samples (n) for the sampling period at MBQ for all relevant parameters.

r_s p n	Q	EC	T	Ca^{2+}	Mg^{2+}	Na^+	K^+	HCO_3^-	SO_4^{2-}	NO_3^-	Cl^-
Q		-0.8009 < 0.0001 103	0.0971 0.3294 103	-0.7145 < 0.0001 103	-0.6991 < 0.0001 103	-0.7092 < 0.0001 103	-0.4288 <0.0001 103	0.2508 0.0106 103	-0.7694 < 0.0001 103	0.1558 0.1161 103	-0.1910 0.0533 103
EC			-0.0097 0.9227 103	0.9440 < 0.0001 103	0.8202 < 0.0001 103	0.8320 < 0.0001 103	0.4790 < 0.0001 103	-0.3722 < 0.0001 103	0.9878 < 0.0001 103	-0.0846 0.3955 103	0.3032 0.0018 103
T				-0.0066 0.9469 103	-0.0139 0.8891 103	-0.0686 0.4914 103	0.0089 0.9291 103	0.3403 0.0004 103	0.0149 0.8816 103	-0.0297 0.7657 103	0.1072 0.2811 103
Ca^{2+}					0.8012 < 0.0001 103	0.8338 < 0.0001 103	0.5100 < 0.0001 103	-0.3316 0.0006 103	0.9519 < 0.0001 103	-0.0701 0.4818 103	0.3400 0.0004 103
Mg^{2+}						0.6675 < 0.0001 103	0.4015 < 0.0001 103	-0.2510 0.0106 103	0.8141 < 0.0001 103	-0.1500 0.1304 103	0.2807 0.0041 103
Na^+							0.5206 < 0.0001 103	-0.4589 < 0.0001 103	0.8341 < 0.0001 103	-0.0751 0.4510 103	0.3063 0.0016 103
K^+								-0.1881 0.0571 103	0.4790 < 0.0001 103	0.0395 0.6922 103	0.1832 0.0639 103
HCO_3^-									-0.3541 0.0002 103	-0.0153 0.8782 103	-0.1635 0.0989 103
SO_4^{2-}										-0.0565 0.5701 103	0.3337 0.0006 103
NO_3^-											0.2311 0.0189 103

2.4.5 Mixing Calculation

The first hypotheses is that at low-flow conditions, the flow paths are almost solely along or on top of the Raibl Group (Fig. 11, low-flow) and the gypsum layers within this group lead to a Ca^{2+}-SO_4^{2-}-type water discharging at MBQ. At high-flow conditions, more water is seeping through the Hauptdolomit-Plattenkalk Fm. and the water level in the whole system rises which means that more Ca^{2+}-Mg^{2+}-HCO_3^- -type water reaches MBQ (Fig. 11, high-flow). During the dry period after the rain event, the values readjust back to low-flow as before the rain event.

This hypothesis of the flow behavior can only explain a part of the observed chemical variations at MBQ. This model implies a dilution effect of the sulfate-rich water, when fresh water infiltrates through the Hauptdolomit-Plattenkalk Fm. At MBQ, an increase of discharge from 168 L/s to

232 L/s (38 %) was observed. In contrast, the sulfate concentration decreased from over 136 mg/L to 38 mg/L (72 %).
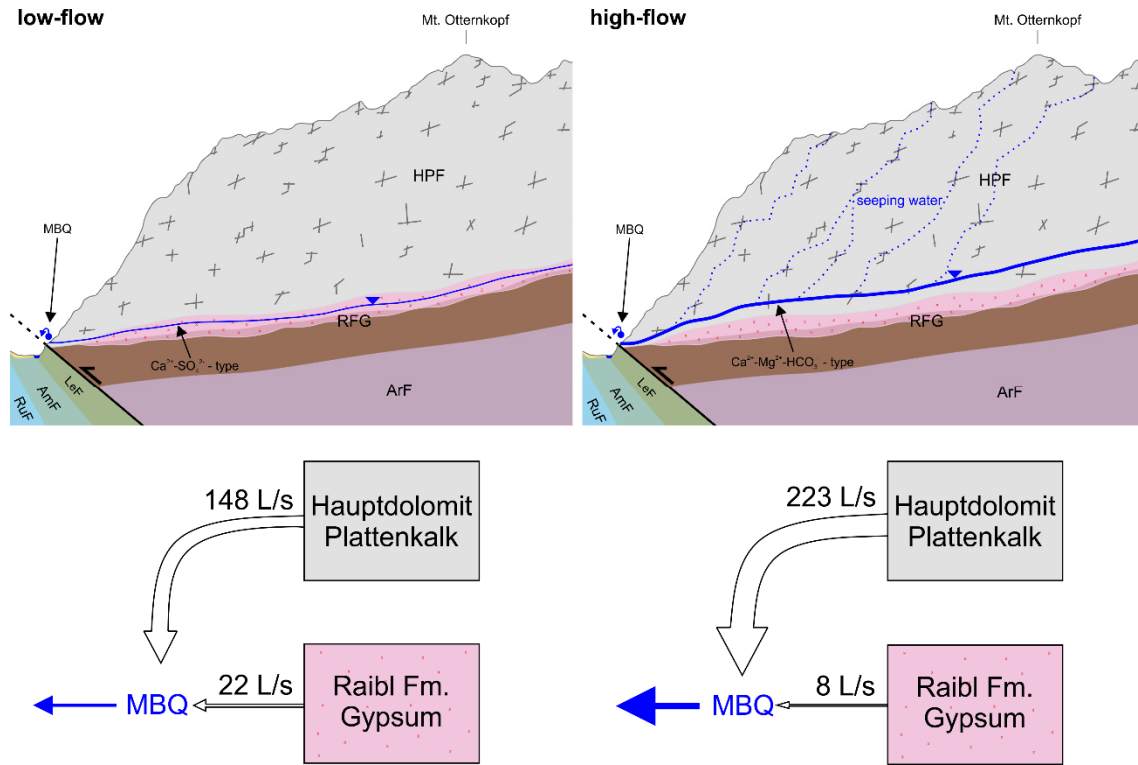
Figure 11: Cross sections and conceptual model of the flow behavior during low-flow and high-flow conditions. Legend see Figure 6.

Thus, the resulting sulfate concentration at MBQ after the rainfall event cannot result simply from dilution.

Therefore, a mixing calculation for the investigated system was conducted and can be expressed as follows:

$$Q_{MBQ} = Q_{gypsum} + Q_{carbonate} \hspace{3cm} (6)$$

$$Q_{MBQ}C_{MBQ} = Q_{gypsum}C_{gypsum} + Q_{carbonate}C_{carbonate} \hspace{2cm} (7)$$

Where Q_{MBQ} is the total discharge at MBQ and Q_{gypsum} and $Q_{carbonate}$ are the respective discharge contributions from the carbonate formations and gypsum layers. C_{MBQ} is the total sulfate concentration at MBQ and $C_{carbonate}$ and C_{gypsum} are the respective sulfate concentrations of the carbonate rocks and of the Raibl Group/gypsum. In this study, we assume that the sulfate concentration of the Raibl Group/gypsum is around 1050 mg/L, which is similar to the sulfate concentration measured at a nearby spring (TBQ, Fig. 6b) with only Raibl Group/gypsum in the catchment area (mean value of 6 measurements).

During low-flow conditions $Q_{carbonate}$ is 146 L/s compared to Q_{gypsum} with 22 L/s which gives a total discharge at MBQ of 168 L/s. During high-flow conditions Q_{gypsum} declined to 8 L/s while $Q_{carbonate}$ increased to 224 L/s which relates to a total discharge at MBQ of 232 L/s.

This mixing calculation shows a decrease of the sulfate component of 63% from low-flow conditions to high-flow conditions, while the total discharge at MBQ only increases by 38%. The discrepancy of the theoretical value of 72% compared to the calculated value of 63% may either result from the uncertainty of our model (e.g. the assumed sulfate concentration within the gypsum layers) or from geochemical processes occurring in the investigated system that we did not consider in our model (e.g. dissolution and precipitation processes). Besides conduit and matrix, the contribution of water from a "third type", small fractures and fissures, might also be a reason for the discrepancy of the measured value from the theoretical value.

However, these results are a clear evidence of conduit-matrix exchange processes occurring in this karst system.

2.4.6 Conceptual Model

The fast and marked reaction of the spring after a rainfall event indicates fast flow components, which result mainly from conduit-flow. The observed hydrochemistry also indicates that matrix-flow, together with flow in small fractures and fissures, is an important factor. During stable low-flow conditions, the main flow paths near the spring are in conduits and are located on top or within the Raibl Fm. and this sulfate-rich water contributes 22 L/s to the spring discharge. During high-flow conditions, the gradients reverse. In this case, the hydraulic head within the conduits is greater than the head in the surrounding matrix and causes a water flow from the conduits to the matrix (Fig. 12, high-flow). Therefore, more water from the overlying carbonate layers contributes to the discharge of the spring, while the percentage of the contribution of the sulfate water from the Raibl Fm. decreases. During low-flow conditions, the hydraulic head changes again and water, now with high sulfate content from the matrix, flows back to the main conduits and contributes predominantly to the spring discharge (Fig. 12, low-flow).

These findings may also help to improve hydrologic models of karst aquifers, which conceptualize the transport of a natural tracer and consider mixing and the exchange of the tracer between conduits and the matrix (Cornaton and Perrochet, 2002; Hartmann et al., 2013). The results can also improve estimations of residence times and mixing fractions of the water in karst aquifers.
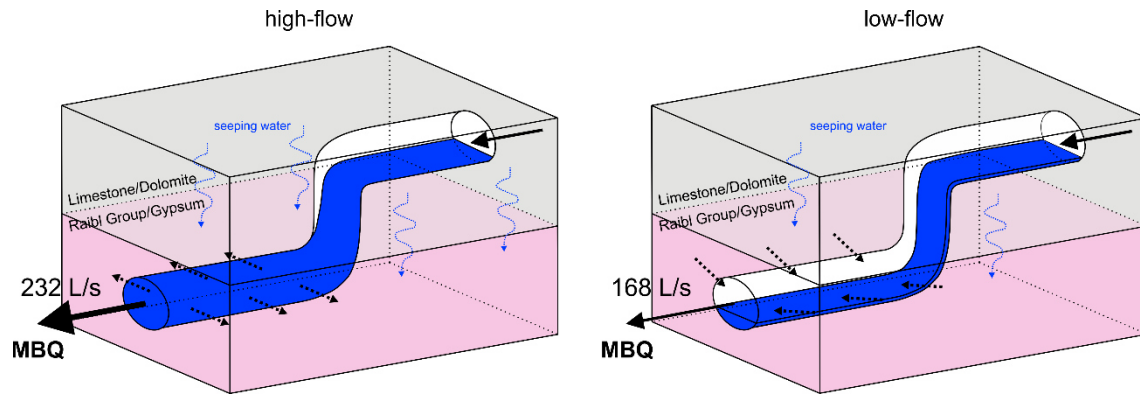
Figure 12: Interaction between the main flow paths in conduits and the surrounding matrix during high-flow conditions and low-flow conditions.

2.5   Conclusion

A high-resolution monitoring of physico-chemical parameters was conducted at an alpine karst spring (MBQ) in Vorarlberg, Austria, during a hydrologically stable period in September 2015 interrupted by one major rain event.

This study demonstrated that the lithology, especially the carbonate formations and the underlying gypsum layers play an important role for the water chemistry of the investigated MBQ.

A fast and marked response of discharge and EC to the rainfall event was observed. In response to the rain event the major cations Ca^{2+} and Mg^{2+} showed a fast and distinct reaction. Regarding major anions, SO_4^{2-} showed a significant decrease after the rain event while all other anions, including bicarbonate, remained more-or-less constant.

During low-flow conditions, the spring is characterized by high sulfate contents while during and directly after rainfall events the water chemistry is shifted to Ca^{2+} - Mg^{2+} - HCO_3^- water, infiltrating from the surface through the carbonate formations overlying the gypsum layers. These hydrogeochemical investigations indicate that the main flow paths of the whole system are located on top or within the gypsum deposits.

The behavior of the spring discharge and the sulfate content also indicates that not only a dilution effect was observed but also that conduit-matrix exchange is an important factor regarding the discharge-sulfate relationship.

Our conceptual model can explain these observed behaviors. During high-flow conditions, the hydraulic head in the main conduits is greater than in the surrounding matrix, therefore water from the conduits is pressed into the matrix and is stored there until the flow conditions reverse. During low-flow, water from the matrix, now with a high sulfate load originating from gypsum deposits within the Raibl Fm., flows back into the main conduits and is discharged at MBQ.

The results of the hydrogeochemical investigations and the developed conceptual model also show the possibility to use natural tracers to investigate complex karst systems especially in regard to water-rock and conduit matrix interaction.

To validate and to verify this conceptual model, a tracer test during different hydrological conditions at MBQ should be performed. The shape of the break-through curve can give additional information about the conduit-matrix interaction as also demonstrated by Goldscheider (2005b).

The conducted investigations can contribute to a better understanding of complex karst aquifers and to a better utilization and protection of karst springs especially in regard to contaminant transport and high and low-flow behavior of the spring. This conceptual model can also help to improve numerical models of karst aquifers if volumes and exchange rates are implemented.

Acknowledgments

Chapter 3

3 Fluorescence-based multi-parameter approach to characterize dynamics of organic carbon, faecal bacteria and particles at alpine karst springs

Abstract

Karst springs, especially in alpine regions, are important for drinking water supply but also vulnerable to contamination, especially after rainfall events. This high variability of water quality requires rapid quantification of contamination parameters. Here, we used a fluorescence-based multi-parameter approach to characterize the dynamics of organic carbon, faecal bacteria, and particles at three alpine karst springs. We used excitation emission matrices (EEMs) to identify fluorescent dissolved organic material (FDOM). At the first system, peak A fluorescence and total organic carbon (TOC) were strongly correlated (Spearman's r_s of 0.949), indicating that a large part of the organic matter is related to humic-like substances. Protein-like fluorescence and cultivation-based determination of coliform bacteria also had a significant correlation with $r_s = 0.734$, indicating that protein-like fluorescence is directly related to faecal pollution. At the second system, which has two spring outlets, the absolute values of all measured water-quality parameters were lower; there was a significant correlation between TOC and humic-like fluorescence ($r_s = 0.588$-0.689) but coliform bacteria and protein-like fluorescence at these two springs were not correlated. Additionally, there was a strong correlation ($r_s = 0.571$-0.647) between small particle fractions (1.0 and 2.0 µm), a secondary turbidity peak and bacteria. At one of these springs, discharge was constant despite the reaction of all other parameters to the rainfall event. Our results demonstrated that i) all three springs showed fast and marked responses of all investigated water-quality parameters after rain events; ii) a constant discharge does not necessarily mean constant water quality; iii) at high contamination levels, protein-like fluorescence is a good indicator of bacterial contamination, while at low contamination levels no correlation between protein-like fluorescence and bacterial values was detected; and iv) a

combination of fluorescence measurements and particle-size analysis is a promising approach for a rapid assessment of organic contamination, especially relative to time-consuming conventional bacterial determination methods.

3.1   Introduction

In Europe, about 22 % of the land surface is characterized by karstifiable rocks, in Austria about 25 % of the land surface is covered by carbonate rocks (Chen et al., 2017) and karst water contributes about 50 % to the total drinking water supply (Kralik, 2001). The largest water resources in Austria are in high alpine karst regions, which, in light of increasing water demand, offer an enormous potential for future water supply. At the same time, karst aquifers are vulnerable to contamination because recharge to karst aquifers occurs directly, through dolines, fissures or swallow holes, or indirectly through the often thin soil overlying the limestone bedrock. Almost no filtration of contaminants occurs between point of recharge and discharge at springs, which often have strong and rapid variations in discharge and water quality in response to rainfall events (Pronk et al., 2007).

Many constituents of natural fresh waters like dissolved organic material (DOM) or bacteria can be used as a signature of its origin (Birdwell and Engel, 2009). Improvements in fluorescence spectroscopy allow the characterization of fluorescent dissolved organic matter (FDOM) and have led to the understanding that DOM is a complex mixture of soluble organic compounds that vary in their reactivity and ecological role in natural spring waters. The samples in this study were measured with a technique that is based on the simultaneous scanning of emission and excitation wavelengths to generate excitation-emission matrices (EEMs). The excitation wavelengths (ex) are wavelengths delivered to the aqueous sample, thus inducing fluorescence, whereas the emission wavelengths (em) are the wavelengths of the resulting fluorescence (Butturini and Ejarque, 2013). Most identifiable fluorophores in natural, non-contaminated waters are attributed to humic-like and protein-like fluorescence (Coble, 1996; Baker and Genty, 1999; Fellman et al., 2010).

Dissolved humic substances in natural waters are mostly derived from dead and decaying soil detritus, aquatic plants, animals, and debris (Hongve, 1999). Aquatic fulvic substances are derived from tree and other plant residues, which contain more phenolic and lignin-derived organic compounds than those found in soil (Chen et al., 2003). Protein-like fluorescence is related to a mixture of amino acids, free or bound in proteins or other organic materials with similar fluorescence characteristics, and is described as an indicator of biologic activity (Maie et al., 2007; Fellman et al., 2010). So far, more studies have investigated the fluorescence properties of organic matter in marine waters (e.g., Coble et al., 1990; Senesi et al., 1991; Mobed et al., 1996) than in

freshwater, and protein-like fluorescence is less well understood than humic- and fulvic-like fluorescence.

Some studies of freshwaters have used organic matter fluorescence as a tracer of groundwater flow in aquifers by comparing fluorescence with other natural tracers (e.g. Baker and Lamont-Black, 2001) or for the understanding of the interaction between surface water and groundwater and their biogeochemical processes (Lapworth et al., 2009). Studies of karst aquifers have investigated the fluorescence properties of organic material present in cave waters (e.g., Baker and Genty, 1999; Ban et al., 2008), and the relation between DOM in spring waters and infiltration processes (Mudarra et al., 2011). Quiers et al. (2014) used the fluorescence signal of DOM to characterize the recharge to and vulnerability of a karst aquifer.

Determann et al. (1998) investigated protein-like fluorescence from marine ecosystems relative to that of bacterial (laboratory) cultures. The data of Determann et al. (1998) and Quiers et al. (2014) show tryptophan-like fluorescence to be directly related to the microbial activity of bacteria. Other studies also strongly support the relation between amino- acid-like DOM and biological activity and further indicate that amino-acid-like DOM is produced during conditions of high bacterial growth (e.g., Stedmon and Markager, 2005; Elliott et al., 2006; Hudson et al., 2008; Fellman et al., 2010).

Faecal pollution of spring waters is typically determined via faecal indicator organisms such as *E. coli*. Although the use of *E. coli* as a faecal indicator is under discussion, the study of Sinreich et al. (2014) concluded that *E. coli* proved to be an adequate indicator for the arrival of bacterial pathogens, viruses and protozoa at karst springs. Standard culture-based techniques to determine *E. coli* require between 18 and 24 h incubation time, which is often too long to prevent contaminated water from entering the distribution network. Contamination of drinking water can lead to infectious diseases, caused by pathogenic bacteria, viruses, or other parasites (WHO, 2011).

Other indirect methods to determine faecal contamination in near real-time, like the measurement of the enzymatic activity, were investigated by Ryzinska-Paier et al. (2014) and Ender et al. (2017). Both studies show only a low level of correlation between *E. coli* and β-D-glucuronidase (GLUC) enzymatic activity and conclude that the measurement of GLUC activity cannot substitute conventional culture-based determinations of *E. coli*. Stadler et al. (2010) used the spectral absorption coefficient (SAC) at 254 nm as a real-time early warning proxy for faecal pollution events. They concluded that SAC254 measures the detectable fractions of DOM that are leached from the land surface (e.g. humic substances) but their approach is only suitable for diffuse faecal pollution sources and point pollution sources are unlikely to be detectable. Furthermore the quantity of faecal pollution can only be determined by using event type, site

specific calibrations. This fact highlights the need for other advanced measurement techniques, such as fluorescence spectroscopy, to determine faecal contamination in near real-time.

Sorensen et al. (2015) used tryptophan-like fluorescence as a real-time indicator of faecal contamination in drinking water supplies. They compared tryptophan-like fluorescence with other traditional indicators and found tryptophan-like fluorescence to be the most effective indicator of the presence/absence of thermotolerant (faecal) coliforms. Sorensen et al. (2016) found tryptophan-like fluorescence to be predominantly associated with fluorophores <0.22 µm, hence is likely more mobile and transported more easily in groundwater than bacterial index organisms. Thus, tryptophan-like fluorescence can also serve as a more precautionary indicator of smaller enteric viruses. Khamis et al. (2015) tested two in-situ tryptophan-like fluorometers and the influence of turbidity and temperature on the measurements. They concluded that in-situ monitoring of reactive DOM using submersible sensors represents a sensitive and cost-effective solution.

To confirm the suitability of fluorescence measurements to determine organic and faecal contamination, in this study other water quality parameters, such as faecal indicator bacteria (*E. coli*), particle-size distribution and turbidity, were determined and compared to fluorescence measurements. Although the measurement of turbidity provides no information about the origin and nature of the measured particles, the analysis of the particle-size distribution (PSD) itself can be a valuable tool for specifying the type of turbidity and to identify particle classes related to microbial contamination (Pronk et al., 2007; Ender et al., 2017). Especially in karst conduits, where suspended mineral particles play an important role in the transport and attenuation of contaminants, such as pathogenic microorganisms (Mahler et al., 2000; Goldscheider et al., 2010), the PSD was used to study the sediment dynamics and sediment-contamination interactions (Mahler and Lynch, 1999; Vesper and White, 2004). The studies of Baker (2005) and Khamis et al. (2015) showed the need to measure turbidity and temperature simultaneously with fluorescence because both parameters are used for correcting the fluorescence measurements.

The aim of this study is to characterize the dynamics of organic matter in three different spring waters, collected from karst springs in the Lechquellen Mountains using fluorescence spectroscopy. Here we measured faecal-indicator bacteria (FIB, *E. coli*) using both fluorescence-based and conventional culture-based methods to test the reliability of the fluorescence method to measure organic faecal contamination of natural karst springs. Therefore, the relation between fluorescence, total organic carbon (TOC), bacteria, and PSD was investigated. The principal research questions are:

- How do the measured parameters react to hydrological events and are there any differences between the springs and catchments?

- What information about the contamination dynamics can be obtained from turbidity and particle-size measurements?
- Is there any relation between fluorescence values and other water quality parameters, especially between TOC and fluorescence and between protein-like fluorescence and cultivation-based determinations of bacteria?

Is fluorescence spectroscopy a valuable tool to measure organic and faecal contamination? Can a certain combination of the techniques be used as a real-time indication system?

3.2 Study site and Methods

3.2.1 Study Site

The springs investigated are in the Lechquellen Mountains in the Austrian Alps in the federal state of Vorarlberg (Figure 13a). The relief ranges from 560 m a.s.l. (at the district capital of Bludenz) to the summit of Mt. Rote Wand (2704 m a.s.l.). Two geological units form the Lechquellen Mountains in the investigation area, the Penninic and Austroalpine nappes. The Hauptdolomit-Plattenkalk formation covers most of the study area and the Hauptdolomit, in particular, constitutes most of the summits. According to Goldscheider and Goeppert (2004), the Hauptdolomit is only moderately karstified while the Plattenkalk is the main karst aquifer.

One of the two karst aquifers investigated has one spring (Marulbach Sping, MBQ) as the only outlet (Figure 13b). The catchment area is mainly overlain by Hauptdolomit, which is underlain by the Raibler formation. The second karst aquifer has two springs (Weißbach Spring, WBQ, and Schwarzbach Spring, SBQ) as outlets (Figure 13c). The southern part of this catchment is mainly overlain by Arlberg limestone and the Raibler formation, whereas the summits on the northern border of the catchment consist of Hauptdolomit (Geologische Bundesanstalt, 2007).

MBQ (1220 m a.s.l.) is located at the southern side of the Großes Walsertal Valley (Figure 13b) and is one of the sources of the Marulbach Stream. As there are some areas in the Großes Walsertal with water shortage in the summer months, MBQ is continuously monitored by the Water Management Department of Vorarlberg and is planned to be used as drinking water source in the future. WBQ (1540 m a.s.l.) and SBQ (1529 m a.s.l.) are the two main springs in the Upper Lech Valley, and are located about 4.5 km west of the village Lech (Figure 13c). In both catchments, which are about the same size, there are some alpine cattle pastures (Figures 13b and 13c).

The three springs were selected for investigation because they are the largest karst springs in the Upper Lech Valley and the Großes Walsertal Valley. They already are or could be used for drinking water supply in the future. The WBQ acts as overflow of the SBQ, which has an almost

constant discharge of 140 L/s and is used as main drinking water supply of the village Lech, whereas discharge from WBQ is highly variable, ranging from less than 100 L/s to more than 1200 L/s.
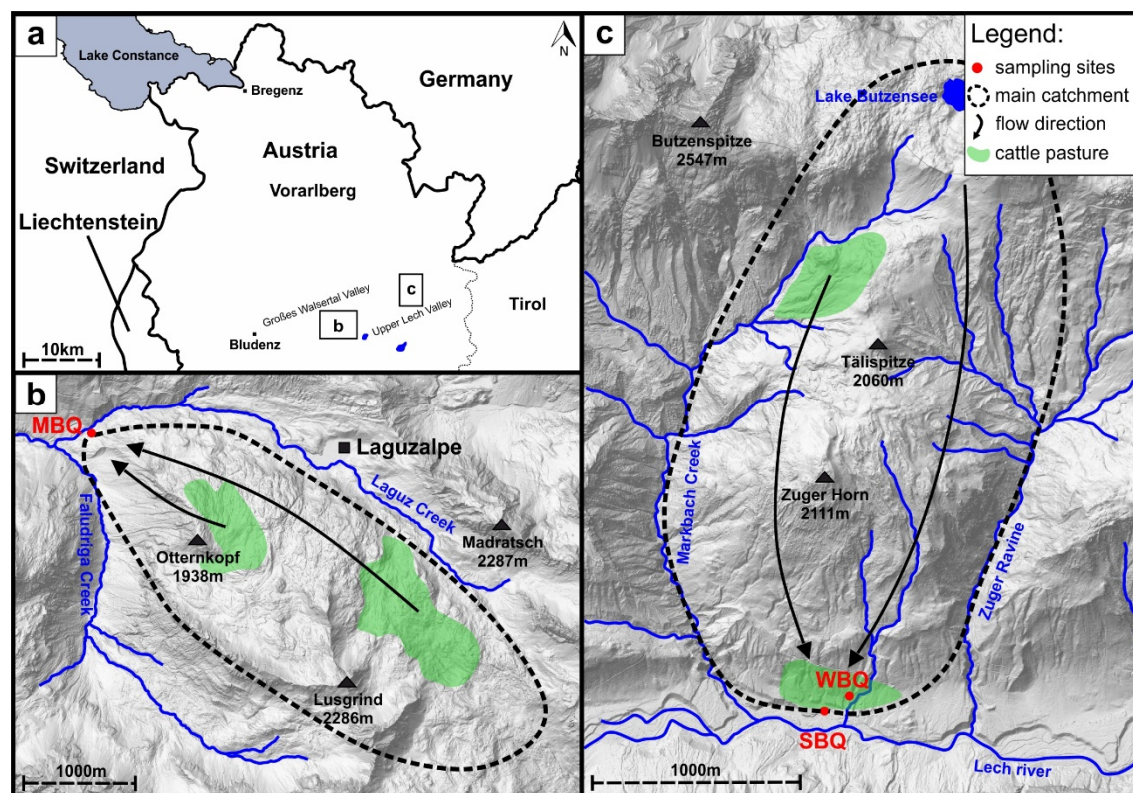
Figure 13: a) Location of the two test sites in the federal state of Vorarlberg in Austria; b) Marulbach Spring (MBQ) with the main catchment area and cattle pasture areas; c) Schwarzbach Spring (SBQ) and Weißbach Spring (WBQ) with main catchment and cattle pasture areas (basemap: Land Vorarlberg – data.vorarlberg.gv.at).

3.2.2 Physicochemical data

The three springs were monitored continuously for 10 days (MBQ) and 6 days (WBQ and SBQ), respectively, in September 2015. WBQ and SBQ also were continuously monitored for 6 days in September 2013. Water temperature and electrical conductivity (EC) were measured continuously at 5 to 15 minutes intervals. At WBQ, a CTD sensor (Ott Hydromet GmbH, Kempten, Germany) was used to measure water temperature (precision ± 0.1 °C), EC (± 1 µS/cm) and water level (± 0.1 cm). Discharge measurements were done using the salt dilution method with point injection. Water level was converted into continuous discharge using the following stage (x) – discharge (y) relationship which was obtained by plotting the 13 measured discharge values versus the according water level data (polynomial regression):

$$y = 0.8108x^2 - 31.753x + 422.69 \tag{8}$$

At SBQ, water temperature (± 0.05 °C) and EC (± 1 µS/cm) was measured using a multi-parameter sensor (MPS-K16, Seba Hydrometrie GmbH & Co. KG, Kaufbeuren, Germany), which was installed inside the spring house. Discharge at SBQ was calculated by adding the

discharge from the overflow (discharge measurements were done using the salt dilution method and water level data were recorded with a CTD sensor, Ott Hydromet GmbH, Kempten, Germany) to the extracted water data provided by the water supplier. MBQ is continuously monitored by the Water Management Department of Vorarlberg, and their data for EC, discharge and temperature were used for this study.

3.2.3 Total organic carbon (TOC) and faecal indicator bacteria (FIB)

At MBQ, water samples for TOC were collected at 2h intervals, and at WBQ and SBQ, at 2- to 4h intervals; all samples were collected in 50-mL brown glass bottles. The samples were acidified with HCl (37 %) to stabilize the sample and to prohibit algae growth. The removal of inorganic carbon (HCO_3^-) is achieved by acidifying and by air injection prior analysis. Measurements were done in the laboratory at the Institute of Applied Geosciences, Karlsruhe Institute of Technology (KIT), with a TOC analyzer (vario TOC cube, Elementar Analysensysteme GmbH, Hanau, Germany). All samples were analysed in triplicate and the mean value was computed and used as TOC concentration.

For the analysis of faecal indicator bacteria, 97 water samples were collected at MBQ at mostly 2h intervals in 100 mL bottles containing sodium thiosulfate. The bottles were stored in the dark at 4 °C and analysed within 10 h after sampling for total coliforms and *E. coli*, which is widely accepted as faecal indicator. The same procedure was used for the 58 samples collected at WBQ and the 56 samples collected at SBQ. Bacteria were identified as the most probable number (MPN) per 100 mL following the Colisure-Quanti-Tray/2000 method (IDEXX Laboratories Inc. Westbrook, USA), which is approved by the U.S. EPA and included in the Standard Methods for Examination of Water and Wastewater. This method was used because it enabled a higher temporal flexibility during the sampling campaigns. The microbial detection range of the testing method is from 1 MPN/100 mL to 2419 MPN/100 mL.

3.2.4 Fluorescence spectroscopy

The state-of-the-art measurement technique for CDOM fluorescence is the excitation-emission matrix (EEM). EEMs were obtained by using the Aqualog fluorometer (Horiba, Ltd., Kyoto, Japan) for the samples collected in 2015 and an LS 55 fluorescence spectrometer (PerkinElmer, Waltham, USA) for the samples collected in 2013. Briefly, an EEM is acquired by simultaneous scanning of the absorbance (excitation) spectrum and of the fluorescence emission spectrum at each excitation wavelength. The samples were analysed in a quartz cuvette with a path length of 10 mm maintained at a constant temperature of 20 °C. For each sample, a simultaneous scan of excitation and emission wavelength from 240-600 nm with 3 nm intervals was performed. A deionized water blank was used to validate the performance of the instrument and to measure the

signal-to-noise ratio. First and second order Rayleigh scattering was removed by nullifying the signal intensities of the Rayleigh lines. The Raman scatter line is removed by subtracting the blank from the sample EEM. EEMs were corrected for inner filter effects (IFE) using the parallel absorbance measurement from the blank and from the sample (Gilmore, 2011). The algorithm used for correction is based on Eq. 2 applied to each excitation-emission wavelength coordinate of the EEM.

$$F_{ideal} = F_{obs}\, 10^{\frac{Abs_{Ex}+ Abs_{Em}}{2}} \tag{9}$$

where F_{ideal} is the ideal fluorescence-signal spectrum expected in the absence of IFE, F_{obs} is the observed fluorescence signal, and Abs_{Ex} and Abs_{Em} are the measured absorbance values at the respective excitation and emission wavelength-coordinates of the EEM (Gilmore, 2011). Fluorescence intensity calibration to Raman Units (R.U.) was done using the Raman peak of pure water, following the procedure of Lawaetz and Stedmon, (2009). To determine the fluorescence intensities, the peak-picking technique was used (Coble, 1996).

In accordance with Coble (1996), peak A was identified at excitation wavelength (ex) 240-260 nm and emission wavelength (em) 400-480 nm in all samples, while peak C was mainly identified at ex 330-360 nm and em 420-480 nm. Protein-like fluorescence was identified at ex 270-280 nm and em 300-350 nm and marked with peak T. The samples were not diluted.

3.2.5 Particle-size distribution

At WBQ (2013 and 2015) and SBQ (2013), the PSD was measured using a portable particle counter (Abakus mobile fluid, Markus Klotz GmbH, Bad Liebenzell, Germany), which counts suspended particles in the range of 0.9-139 µm and groups them into up to 32 definable size classes. The measuring procedure starts with a rinsing process followed by the actual measurement in which 10 mL of the sample pass through a small glass tube. The tube is irradiated by a laser beam and the particles contained cause a decrease in the laser light at the detector. The extent of the decrease is determined by assuming an equivalent spherical diameter of the particle and thereby the size of the particle. In this study, 32 particle size classes were measured but only four particle-size classes were of special interest: 0.9-1.0 µm (hereinafter 1.0 µm), 1.1-2.0 µm (2.0 µm), 2.1-5.0 µm (5.0 µm) and 5.1-10.0 µm (10.0 µm). These size fractions were compared with FIB as coliform bacteria and *E. coli* have a size of about 1-3 µm (Reshes et al., 2008).

3.3 Results and discussion

3.3.1 Single-spring system (Marulbach Spring)

The Marulbach Spring had a low TOC content ranging from 0.66 mg/L to 2.05 mg/L (Table 3). The lowest values were measured before the rain event that started on the evening of the 22nd of September 2015, and the maximum value was measured shortly after the end of this event. The values for intrinsic fluorescence for peaks A, C, and T correspond to the values of TOC. Peak A (humic-like) reached a maximum of 2.47 R.U. with mean values before the rain event of around 1.00 R.U. The maximum measured fluorescence intensity for peak C (humic-like) was 1.23 R.U. with mean values of around 0.40 R.U. before the rainfall. Peak T (protein-like) reached a maximum of 0.47 R.U. The coefficients of variation (CV) for peaks A, C and T were in the range of 13.9-34.8 %, which was very similar to the CV for TOC (33.1 %). Coliform bacteria reached a maximum of 816 MPN/100 mL about 12 h after the start of the rainfall event. The values for *E. coli* range from <1 to 53 MPN/100 mL and correspond temporally to the total coliforms. In addition, EC and discharge (Q) were recorded. There is a large difference between the minimum and maximum EC values (309-501 µS/cm). The maximum occurred during the rain event and was followed by a steep decrease, reaching the minimum 16 h after the start of the rain event. The discharge showed the reverse pattern with a steep increase starting around 4 h before the decrease of EC. The steep increase in Q likely resulted from a hydraulic pressure pulse, also known as the piston effect, caused by the rainfall (Ravbar et al., 2011). The maximum discharge recorded during the monitored time period was 232 L/s.

Table 3: Summary statistics for total organic carbon (TOC), bacteria, fluorescence peaks A, C, and T, electrical conductivity (EC), temperature (T), and discharge (Q) measured during the investigation periods in September 2013 and September 2015 for the three springs. S.D., standard deviation; CV, coefficient of variation; n.m., not measured.

		MBQ (2015)	**SBQ (2013)**	**SBQ (2015)**	**WBQ (2013)**	**WBQ (2015)**
	Altitude [m a.s.l.]	1220	1529	1529	1540	1540
TOC	n	96		50		45
	Min. [mg/L]	0.66		0.19		0.20
	Max. [mg/L]	2.05	n.m.	0.78	n.m.	0.77
	Mean [mg/L]	1.21		0.30		0.29
	S.D.	0.40		0.12		0.11
	CV [%]	33.1		40.0		37.9
total coliforms	n	97		56		58
	Min. [MPN/100 mL]	13.4		2		< 1
	Max. [MPN/100 mL]	816.4	n.m.	119.8	n.m.	214.3
	Mean [MPN/100 mL]	77.0		34.4		47.2
	S.D.	115.8		33.0		45.1
	CV [%]	150.4		95.9		95.6
E. coli	n	97		56		58
	Min. [MPN/100 mL]	< 1		< 1		< 1
	Max. [MPN/100 mL]	53.0	n.m.	14.8	n.m.	14.8
	Mean [MPN/100 mL]	6.9		3.0		3.3
	S.D.	10.9		4.3		4.1
	CV [%]	158.0		144.7		124.2
Peak A	n	96	14	50	18	45
	Min. [R.U.]	0.82	0.20	0.23	0.25	0.23
	Max. [R.U.]	2.47	0.50	0.52	0.42	0.51
	Mean [R.U.]	1.41	0.36	0.32	0.29	0.31
	S.D.	0.49	0.09	0.08	0.04	0.07
	CV [%]	34.8	25.0	25.0	13.8	22.6
Peak C	n	96	14	50	18	45
	Min. [R.U.]	0.39	0.15	0.10	0.11	0.10
	Max. [R.U.]	1.23	0.29	0.23	0.22	0.24
	Mean [R.U.]	0.69	0.21	0.13	0.14	0.13
	S.D.	0.25	0.04	0.03	0.03	0.04
	CV [%]	36.2	19.0	23.1	21.4	30.8
Peak T	n	96	14	50	18	45
	Min. [R.U.]	0.28	0.16	0.09	0.13	0.02
	Max. [R.U.]	0.47	0.18	0.29	0.17	0.27
	Mean [R.U.]	0.36	0.17	0.15	0.15	0.14
	S.D.	0.05	0.01	0.07	0.01	0.04
	CV [%]	13.9	5.9	46.7	6.7	28.6
EC	n	904	772	601	725	601
	Min. [μS/cm]	309	165	186	165	177
	Max. [μS/cm]	501	212	218	212	209
	Mean [μS/cm]	388	193	207	192	198
	S.D.	53.3	13.7	10.4	13.3	10.4
	CV [%]	13.7	7.1	5.0	6.9	5.3
T	n	1160	1728	601	725	601
	Min. [°C]	4.31	3.95	3.65	3.88	4.02
	Max. [°C]	4.46	4.28	3.84	4.15	4.63
	Mean [°C]	4.37	4.08	3.76	3.98	4.20
	S.D.	0.03	0.08	0.06	0.08	0.12
	CV [%]	0.7	2.0	1.6	2.0	2.9
Discharge	n	905	1619	601	1728	601
	Min. [L/s]	168	136	134	144	139
	Max. [L/s]	232	148	145	652	480
	Mean [L/s]	194	142	140	393	229
	S.D.	17.3	3.5	3.0	128,8	89.8
	CV [%]	8.9	2.5	2.1	32.8	39.2

At spring MBQ, marked changes were measured in fluorescence peak intensity, TOC, FIB, EC, and Q in response to rainfall on September 23, 2015 (Figure 14). Similar temporal patterns for fluorescence intensities and TOC were recorded at 11 smaller karst springs in the Großes Walsertal Valley (Supplementary 1).

Figure 14: Temporal patterns in peak A, C, and T fluorescence intensities at MBQ Spring. Temporal patterns in TOC, bacteria, EC, discharge, and rainfall are also shown. The numerals 1, 2, and 3 indicate the position of the EEMs shown in Figure 13.

Coliform bacteria, *E. coli*, TOC, and fluorescence started to increase about 6 h after rainfall began and reached maximum values about 15 h after the start of rain.

The EEM spectra of MBQ evolved from before the rain event to about 3 days afterwards reveal three main fluorescence peaks (Figure 15). Humic-like substances, peak A and peak C are described to represent widespread aromatic humic substances with a high molecular weight and are highest in wetlands and forested environments. Both substances are mainly derived from terrestrial plant or soil organic matter (Fellman et al., 2010). In our study, protein-like fluorescence could not be attributed either to pure tryptophan or pure tyrosine. Excitation wavelengths of both substances are 270-280 nm but tryptophan has a maximum fluorescence at an emission wavelength of 348 nm and tyrosine at 303 nm (Ghisaidoobe and Chung, 2014). The tryptophan and tyrosine signals represent amino acids, free or bound in proteins. In our samples, we found either a complex mixture of both substances or their respective degradation products, which are in both cases shifted to slightly higher emission wavelengths (Determann et al., 1998). Determann et al. (1998) also found the fluorescence signal from living bacteria to be remarkably

constant and dominated by a blue-shifted tryptophan fluorescence. In our study, this fluorescence peak was referred to as protein-like fluorescence which was identified at ex 270-280 nm and em 300-350 nm and marked with T. This fluorescence resembles free tryptophan or tyrosine and may indicate intact proteins or less degraded peptide material. This material may originate either from terrestrial plant or soil organic matter as well as from microbial processing (Fellman et al., 2010). The results of our fluorescence measurements at MBQ, especially peak T, compared to the obtained bacterial values, indicate a strong relation of these parameters and that the obtained fluorescence signature may originate from the decay of bacteria or cell dissolved organic material originating from the land surface as also described by Coble et al. (2014).

Figure 15: Temporal evolution of the EEM spectra recorded at MBQ. Peak A and C indicate humic-like fluorescence while peak T indicates protein-like fluorescence. Numbers 1 (21.09.2016, 6 a.m.), 2 (23.09.2016, 8 p.m.) and 3 (25.09.2016, 10 p.m.) show the position of the EEMs in the timeline of Figure 14.

3.3.2 Dual-spring system (Schwarzbach- and Weißbach Spring)

At WBQ and SBQ, which drain the same karst aquifer, measured values for fluorescence, TOC, coliform bacteria, *E. coli* and EC are similar (summary statistics provided in Table 3), but discharge at the two springs follow very different temporal patterns even though WBQ is considered to be the overflow outlet of SBQ (Figures 16 and 18). For the investigation period in September 2015 the minimum values for TOC are 0.19 (SBQ) and 0.20 mg/L (WBQ), while the maximum values were observed after the major rainfall event and are 0.78 and 0.77 mg/L. The highest values for the fluorescence peaks A and C were measured at the same time as maximum TOC values were recorded. Peak A reached values of 0.52 (SBQ) and 0.51 R.U. (WBQ) respectively, peak C reached 0.23 (SBQ) and 0.24 R.U. (WBQ) respectively while protein-like fluorescence (peak T) showed values between 0.29 (SBQ) and 0.27 R.U. (WBQ) but no clear correlation with the other parameters could be identified. The range in coefficient of variation for fluorescence was similar to that of TOC (22.6-46.7 %). These values are comparable to the MBQ

Spring. The minimum and maximum values for coliforms and *E. coli* at WBQ and SBQ were substantially lower than at MBQ Spring. The maximum for *E. coli* was 14 MPN/100 mL at both springs for the measurements conducted in September 2015.
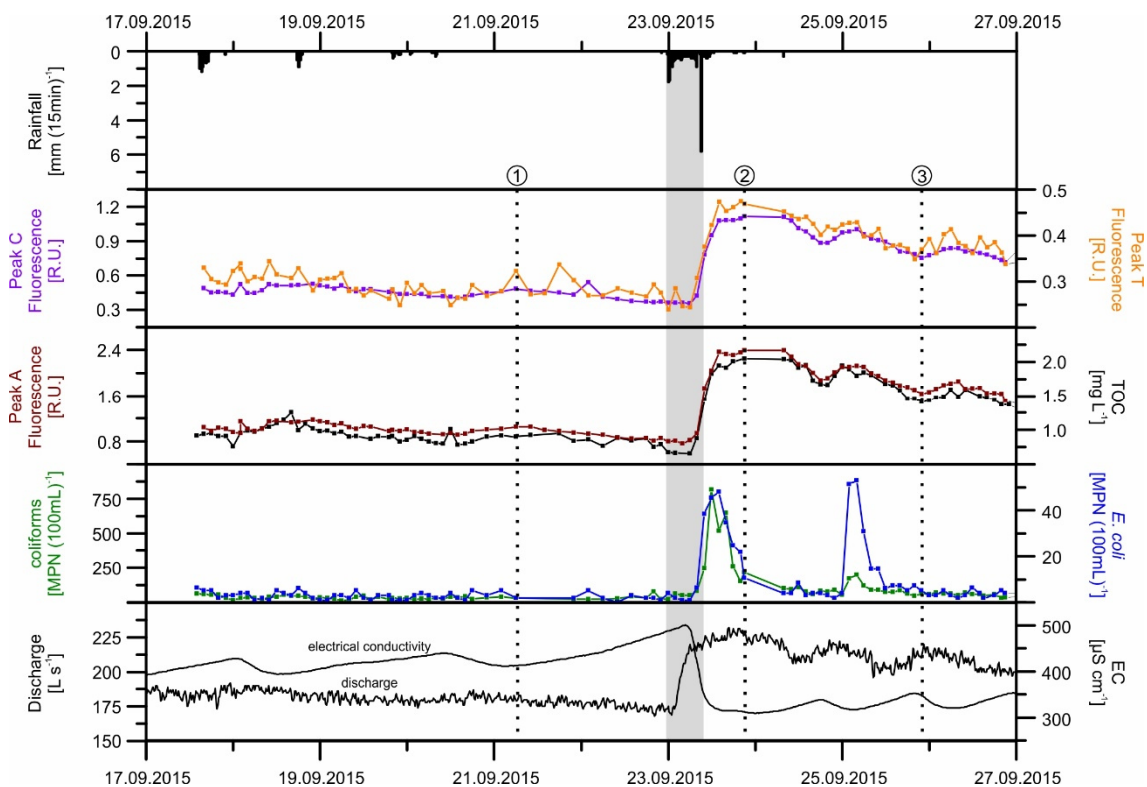

Figure 16: Temporal patterns of Peak A, C and T fluorescence intensities of WBQ together with TOC, bacteria, EC, discharge and rainfall during the investigation period. Numbers 1, 2 and 3 indicate the position of the EEMs shown in Figure 13. The figure also shows the particle-size distribution of 4 different fractions. Dotted lines (a) and (b) indicate the peak position of the particle fractions and turbidity.

Similar to MBQ, there was a marked response in all parameters measured at WBQ, with the exception of peak T, to the rain event (Figure 16). Discharge began to increase about 6 h after the

major rainfall event began and about 1 h before the decrease of the EC. Fluorescence peaks A and C reached their maximum about the same time that the maximum TOC values were recorded. Fluorescence peak T remained relatively constant during the whole time. Coliform bacteria and *E. coli* became much more variable after the major rain event, but showed no distinct peak and no clear correlation to other parameters. Measured bacteria values and peak T at WBQ are much lower than those at MBQ.

Turbidity and all particle fractions first peaked about 9 h after rainfall began, but still during the rising limb of the hydrograph (Figure 16; dotted line a). This turbidity and particle signal likely originates from a hydraulic pressure pulse that leads to a remobilization of sediments from inside the karst network (autochthonous). The turbidity and the 1.0 μm particle fraction had a second peak about 25 h after rainfall began (Figure 16; dotted line b). This second peak is attributed to the arrival of turbid water from the land surface that entered the karst network (allochthonous). This second peak also correlated with the fluorescence peaks A and C and the TOC peak, consistent with TOC and humic-like and fulvic-like substances originating from the soil and the land surface. These results are similar to those of previous studies of turbidity and particle-size investigations in karst springs (e.g. Massei et al., 2003; Goldscheider et al., 2010). The slight increase of coliform bacteria occurred at about the same time as the second turbidity peak and the second peak of the 1.0 μm fraction of the particles, indicating the arrival of faecal bacteria originating from the land surface, as described by Pronk et al. (2007).

The measured EEM spectra for WBQ, similar to MBQ, show three distinct peaks which represent humic-like substances (peaks A and C) and protein-like substances (peak T, Figure 17).
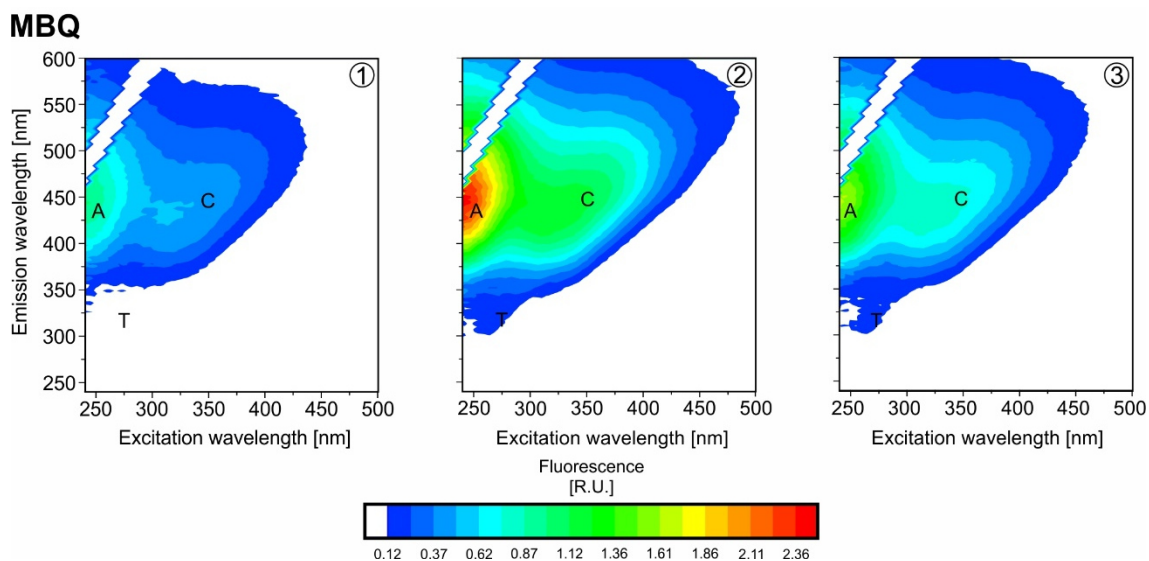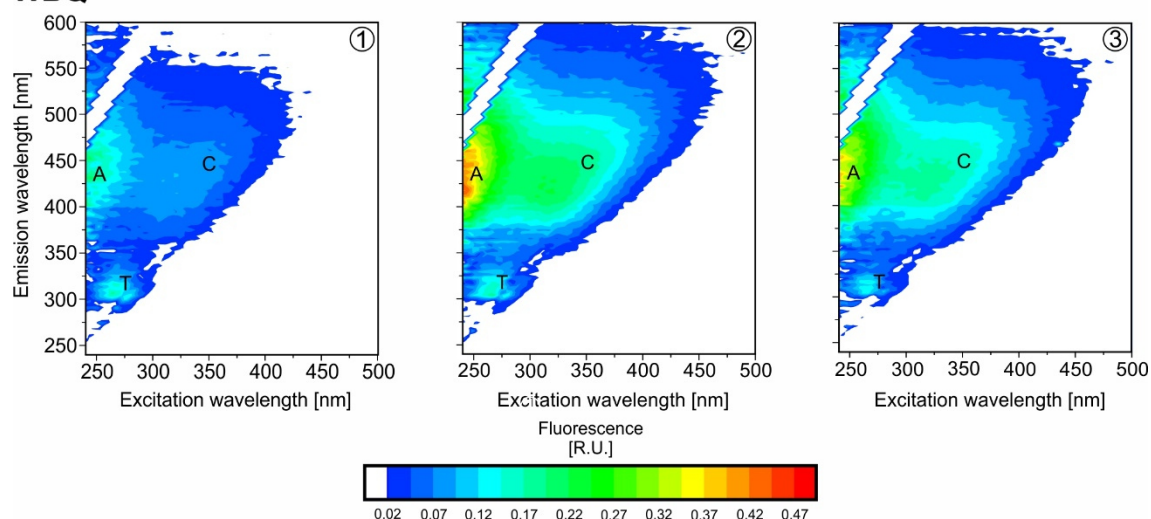

Figure 17: Temporal evolution of the EEM spectra recorded at WBQ. Peak A and C indicate humic-like fluorescence while peak T indicates Tryptophan-like fluorescence. Numbers 1 (03.09.2016, 2 a.m.), 2 (04.09.2016, 4 p.m.) and 3 (05.09.2016, 10 a.m.) show the position of the EEMs in the timeline of Figure 16.

The temporal evolution of the data from the September 2013 measurement period for WBQ is given in Supplementary 2. The results from 2015 are largely consistent with the results from 2013.

Water quality parameters measured at SBQ varied similar to those measured at WBQ, even though SBQ has an almost constant discharge of 140 L/s (Figure 18). Fluorescence peaks A and C reached their maximum at the same time that the TOC peak occurred. The peaks arose around 26 h after the start of rainfall and 1 h later than at WBQ. For fluorescence peak T no clear correlation to other parameters could be identified, although a slight increase after the rain event was observed.
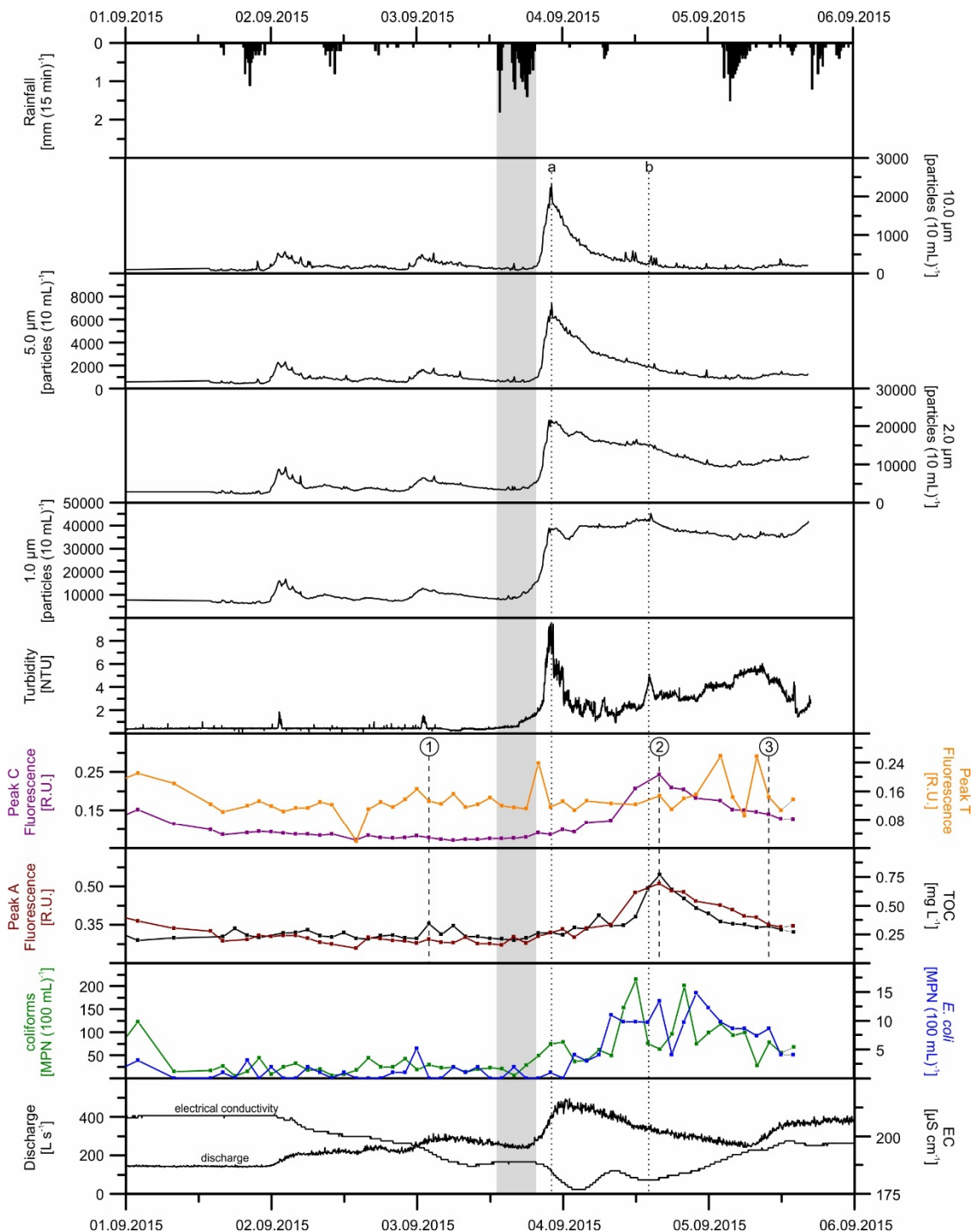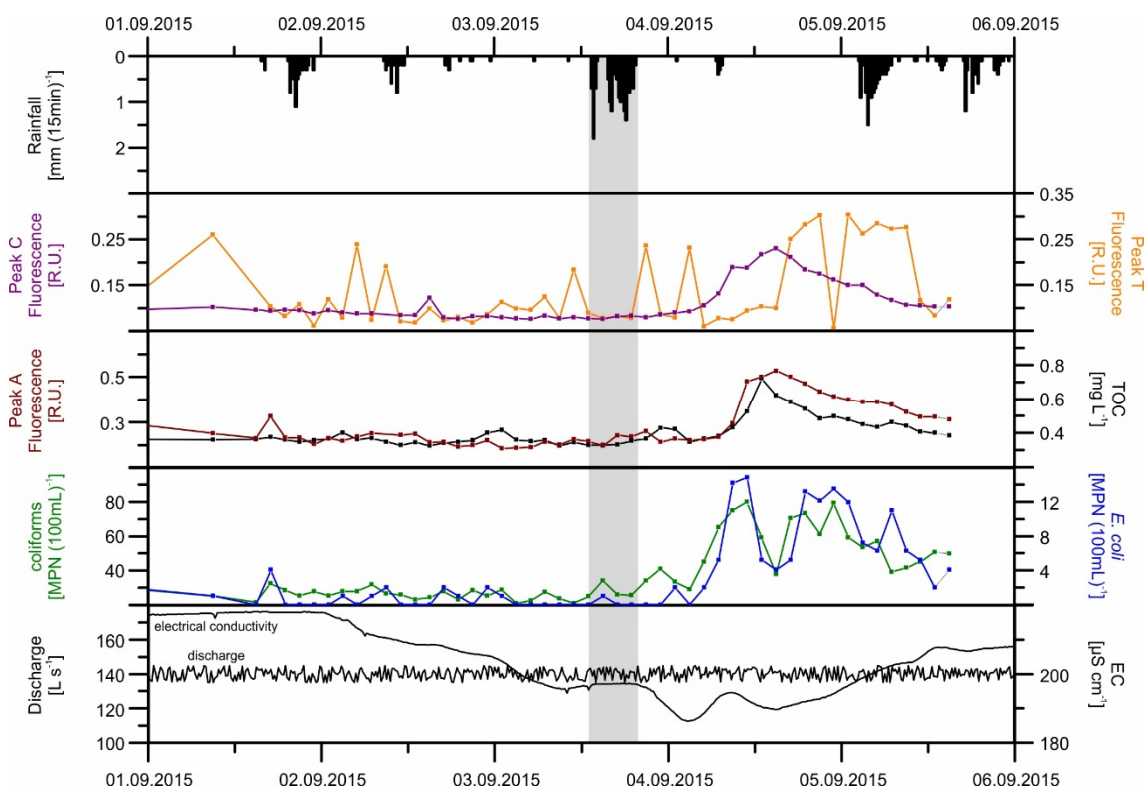

Figure 18: Temporal patterns of Peak A, C and T fluorescence intensities of SBQ together with TOC, bacteria, EC, discharge and rainfall during the investigation period 2015. Note the almost constant discharge of 140 L/s.

Time series for all parameters measured during September 2013 are given in Supplementary 3. Discharge, EC and the other parameters show again almost the same behavior as in 2015. In 2013 the particle-size distribution was also measured at SBQ Spring. The particles showed the same behavior as at WBQ Spring, with two distinct peaks for the 1.0 and 2.0 μm fractions. The second peak of the smaller particle fractions correlated with peak A and peak C fluorescence, indicating the arrival of the recharging surface water.

3.3.3 Comparison of the three springs

All three springs showed fast and marked responses to rainfall events for virtually all of the parameters measured. The only exception is the SBQ Spring, where an almost constant discharge

of 140 L/s was recorded (Figure 18), while all other parameters reacted to the rainfall. We hypothesize that SBQ (base-flow spring) is fed by a conduit of finite capacity so that discharge does not increase but instead the water overflows into conduits which then feed WBQ (overflow spring; Fig. 19). The measurements at SBQ demonstrate that constant discharge does not necessarily signify invariable water quality.

TOC concentrations and fluorescence intensities for Peaks A, C and T at MBQ were typical of those reported for other studies of karst spring waters (e.g. Batiot et al., 2003; Mudarra et al., 2011; Tissier et al., 2013). Fluorescence intensities and TOC concentrations at WBQ and SBQ dual-spring system are lower than those at MBQ, likely as a result of the higher altitude of the dual-spring system, which corresponds to thin soils and minor or absent vegetation in the catchment areas. Nevertheless, a marked increase in TOC concentration and fluorescence intensities of peaks A, C and T was recorded at all three springs after a major rainfall event. The fluorescence intensity values of peaks A, C and T were correlated with the TOC concentration at each spring.
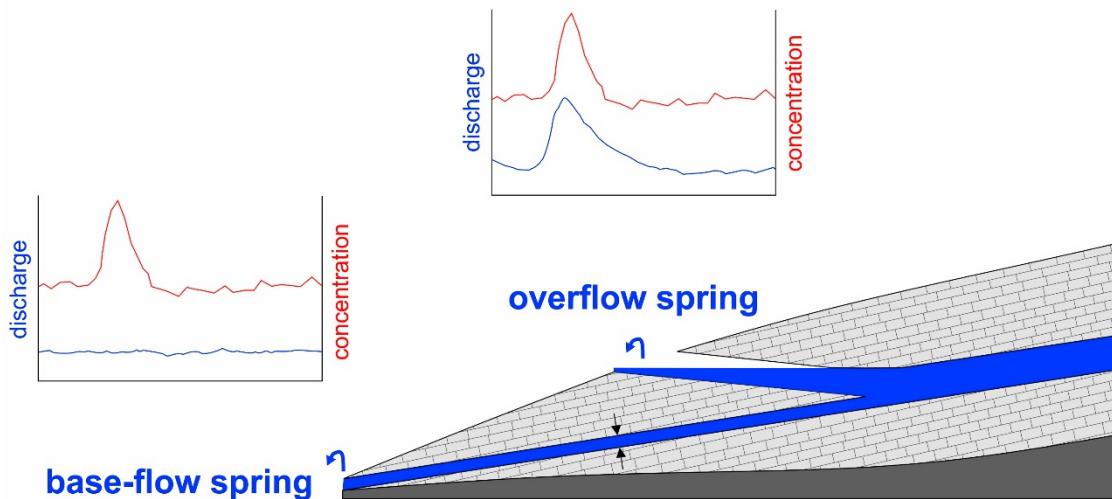
Figure 19: Conceptual diagram to illustrate the functioning of WBQ-SBQ system. The base-flow spring is fed by a conduit of finite capacity, the excess water discharges via the overflow spring.

The best correlation between TOC and fluorescence was at MBQ with calculated coefficients of determination (R^2) between 0.91 and 0.98 between TOC and peaks A, C and T. For SBQ and WBQ, the correlation was 0.69 and 0.76 for fluorescence peaks A and C, respectively, which indicates a strong correlation between the two variables. Only for peak T, no correlation was found at SBQ and WBQ Springs.

In Table 4, the Spearman's rank correlation (r_s), the significance (p), and the number of samples (n) are given for MBQ.

Table 4: Spearman's rank correlation (r_s), significance (p value) and the number of samples (n) for the sampling period at Marulbach Spring (MBQ) for all relevant parameters.

r_s p n	Q	EC	coliforms	*E. coli*	TOC	Peak A	Peak C	Peak T
Q		-0.827 <0.001 96	0.773 <0.001 96	0.598 <0.001 96	0.801 <0.001 96	0.806 <0.001 96	0.786 <0.001 96	0.809 <0.001 96
EC			-0.728 <0.001 96	-0.584 <0.001 96	-0.949 <0.001 96	-0.964 <0.001 96	-0.940 <0.001 96	-0.887 <0.001 96
coliforms				0.596 <0.001 96	0.729 <0.001 96	0.706 <0.001 96	0.684 <0.001 96	0.734 <0.001 96
E. coli					0.601 <0.001 96	0.567 <0.001 96	0.601 <0.001 96	0.578 <0.001 96
TOC						0.949 <0.001 96	0.934 <0.001 96	0.883 <0.001 96
Peak A							0.962 <0.001 96	0.880 <0.001 96
Peak C								0.881 <0.001 96

The strongest correlations were between TOC and the three fluorescence peaks. Correlations between coliform bacteria, *E. coli* and the three fluorescence peaks were less strong but still significant, with the best correlation between coliforms and peak T. This supports the findings of Elliott et al. (2006), who reported that at least some of the tryptophan-like fluorescence can have a direct bacterial origin. Sorensen et al. (2015) and Sorensen et al. (2016) also report that tryptophan-like fluorescence is more resilient in groundwater than bacteria and therefore could also be an indicator of some smaller, more easily transported pathogenic enteric viruses which are beyond the scope of this study. Furthermore, tryptophan-like fluorescence has the advantage of potentially detecting the presence of coliforms in viable but nonculturable states Sorensen et al. (2015). The IDEXX test, used in this study only measures the viable bacterial state. Correlations between EC and TOC and EC and fluorescence peaks were significant and negative; recharging rain water leads to an increase of discharge and, with a slight delay, to a decrease of EC. As EC decreased, TOC, fluorescence values, and FIB began to increase, indicating the arrival of the fresh surface water. EC is a simple and robust parameter to deduce the characteristics of the investigated karst aquifers, with respect to the arrival of surface water at the springs.

Correlations between parameters also were investigated for WBQ and SBQ (September 2015 data, Table 5).

Table 5: Spearman's rank correlation (r$_s$) with significance (p value) and the number of samples (n) for all relevant parameters measured for SBQ (light blue) and WBQ (white).

r$_s$ p n	Q	EC	TOC	coliforms	*E. coli*	Peak A	Peak C	Peak T	1.0 µm	2.0 µm	5.0 µm	10.0 µm
Q		-0.907 <0.001 45	0.651 <0.001 45	0.530 <0.001 45	0.477 <0.001 45	0.383 0.004 45	0.226 0.094 45	-0.005 0.969 45	0.877 <0.001 45	0.898 <0.001 45	0.789 <0.001 45	0.602 <0.001 45
EC	-0.036 0.802 50		-0.582 <0.001 45	-0.493 <0.001 45	-0.463 <0.001 45	-0.324 0.015 45	-0.187 0.167 45	-0.005 0.971 45	-0.809 <0.001 45	-0.793 <0.001 45	-0.672 <0.001 45	-0.439 <0.001 45
TOC	0.086 0.553 50	-0.373 0.008 50		0.561 <0.001 45	0.653 <0.001 45	0.588 <0.001 45	0.524 <0.001 45	-0.026 0.847 45	0.774 <0.001 45	0.744 <0.001 45	0.660 <0.001 45	0.343 0.010 45
coliforms	0.129 0.373 50	0.490 <0.001 50	0.772 <0.001 50		0.575 0.001 45	0.681 <0.001 45	0.649 <0.001 45	0.233 0.084 45	0.647 <0.001 45	0.613 <0.001 45	0.475 <0.001 45	0.167 0.219 45
E. coli	0.131 0.366 50	-0.350 0.013 50	0.778 <0.001 50	0.811 0.001 50		0.664 <0.001 45	0.635 <0.001 45	0.192 0.156 45	0.641 <0.001 45	0.571 <0.001 45	0.415 0.001 45	0.094 0.491 45
Peak A	0.050 0.729 50	-0.225 0.116 50	0.689 <0.001 50	0.683 <0.001 50	0.703 <0.001 50		0.897 <0.001 45	0.327 0.014 45	0.584 <0.001 45	0.526 <0.001 45	0.415 0.001 45	0.097 0.477 45
Peak C	0.118 0.416 50	-0.247 0.083 50	0.743 <0.001 50	0.724 <0.001 50	0.718 <0.001 50	0.809 <0.001 50		0.366 0.005 45	0.472 <0.001 45	0.398 0.002 45	0.268 0.045 45	-0.060 0.660 45
Peak T	-0.107 0.461 50	-0.061 0.676 50	0.364 0.009 50	0.164 0.254 50	0.252 0.077 50	0.415 0.003 50	0.338 0.016 50		0.022 0.871 45	-0.037 0.785 45	-0.039 0.777 45	-0.122 0.369 45
1.0 µm										0.972 <0.001 45	0.883 <0.001 45	0.606 <0.001 45
2.0 µm											0.929 <0.001 45	0.699 <0.001 45
5.0 µm												0.857 <0.001 45

The correlations between TOC and the three fluorescence peaks were at SBQ and WBQ lower than at MBQ. Similar, the correlations between coliform bacteria, *E. coli* and the three fluorescence peaks also were slightly lower than at MBQ. The lowest correlations were for bacteria and peak T fluorescence at both springs. We hypothesize that this is because TOC and bacteria values at WBQ and SBQ are substantially lower than at MBQ, because of less developed soil and vegetation and fewer cattle farming activities in the dual-spring catchment. In this study a good correlation between bacteria and peak T fluorescence was detected at MBQ, where coliform bacteria and *E. coli* reached values of 816 MPN/100 mL and 53 MPN/100 mL respectively. The corresponding values for peak T fluorescence were up to 0.47 R.U. At WBQ/SBQ, coliform bacteria and *E. coli* only reached values up to 214 MPN/100 mL and 14 MPN/100 mL. Peak T fluorescence was measured with 0.29 R.U. This also supports the findings of Sorensen et al. (2016) who described tryptophan-like fluorescence to be an effective indicator of coliform bacteria only where tryptophan-like fluorescence exceeded 0.4 µg/L

dissolved tryptophan. At WBQ the Spearman's r_s was also computed for the correlations between bacteria and particles. For both coliform bacteria and *E. coli*, the correlation decreased as particle size increased.

3.4   Conclusion

Three alpine karst springs in Austria were monitored at high resolution during two hydrologically stable periods in September 2013 and 2015 interrupted by one major rain event. Fluorescence characteristics, particle-size distribution and physico-chemical parameters were used to characterize the dynamics of organic carbon, faecal bacteria, and particles discharging from the springs following a rainfall event.

A fast and marked response of all recorded water quality parameters to rainfall events was observed at all three investigated springs. Even though a constant discharge at SBQ was measured, all other parameters at this spring reacted to the rainfall event. These findings demonstrated that a constant discharge does not necessarily mean constant water quality.

We found a high correlation at all three springs and a simultaneous response to the rain event of TOC and fluorescence peaks A and C. These observations showed that an important amount of TOC from the two catchments is related to FDOM, especially to humic-like and protein-like substances and mainly originated from the decomposition of organic material from plants and animals from the land surface.

We detected a simultaneous increase of turbidity and all measured particle fractions after the rain event, followed by a secondary turbidity peak, where a further increase of the smaller particle fractions as well as TOC and fluorescence was observed. The first peak is attributed to autochthonous turbidity originating from the remobilization of sediments from the karst network itself while the second turbidity peak represents the allochthonous sediments from the soil and land surface. Because TOC and faecal bacteria also mainly originate from the land surface, they showed a good correlation with the secondary turbidity peak and the second peak of the 1.0 and 2.0 µm particle fraction as also detected by Pronk et al. (2007).

At high contamination levels, as at MBQ, a strong correlation between protein-like fluorescence peak T and faecal indicator bacteria was detected. At this spring, fluorescence spectroscopy (tryptophan-like fluorescence) could be used for a near real-time assessment of faecal contamination. Sorensen et al. (2016) concluded that tryptophan-like fluorescence is only an effective indicator of coliforms where it exceeds 0.4 µg/L dissolved tryptophan. Therefore, peak T fluorescence measurements are not suitable to determine precise bacterial values.

A difference in the strength of the correlation between TOC, bacteria and fluorescence was observed between the two spring systems, which originated from higher values of TOC, bacteria and fluorescence at MBQ compared to WBQ/SBQ. We hypothesize, that the higher values were caused by the different altitude and therefore the different soil formation and vegetation in the two catchments as well as different cattle farming activities.

Because of a significant negative correlation between EC, discharge, TOC, FIB and fluorescence, EC is a simple but stable parameter to determine the basic characteristics of the investigated karst aquifers and is a good indicator for the arrival of surface water.

Neither the measurement of tryptophan-like fluorescence nor the determination of the particle-size distribution can substitute conventional bacterial determination methods to determine faecal pollution, but the simultaneous monitoring of particle-size distribution and intrinsic fluorescence might be a valuable tool to act as an early warning system for organic contamination processes, originating from the land surface, and can also help to estimate bacterial contamination in near real-time.

The results presented in this study highlight the vulnerability of karst aquifers to organic contamination, especially during and after rainfall events, and demonstrate the utility of advanced measurement techniques, such as fluorescence spectroscopy and particle-size measurements, to detect and predict the contamination variability, especially with regard to the time consuming conventional methods.

Acknowledgments

Chapter 4

4 Field tracer tests to evaluate transport properties of Tryptophan and humic acid in karst

Abstract:

The monitoring of water quality, especially of karst springs, requires methods for rapidly estimating and quantifying parameters that indicate contamination. In the last few years, fluorescence-based measurements of tryptophan and humic acid have become a promising tool to assess water quality in near real-time. In this study, we conducted comparative tracer tests in a karst experimental site to investigate the transport properties and behavior of tryptophan and humic acid in a natural karst aquifer. These two tracers were compared with the conservative tracer uranine. Fluorescence measurements were conducted with an online field fluorometer and in the laboratory. The obtained breakthrough curves (BTCs) and the modeling results demonstrate that i) the online field fluorometer is suitable for real-time fluorescence measurements of all three tracers; ii) the transport parameters obtained for uranine, tryptophan and humic acid are comparable in the fast flow areas of the karst system; iii) the transport velocities of humic acid are slower and the resulting residence times are accordingly higher, compared to uranine and tryptophan, in the slower and longer flow paths; iv) the obtained BTCs reveal additional information about the investigated karst system. As a conclusion, the experiments show that the transport properties of tryptophan are similar to those of uranine while humic acid is partly transported slower and with retardation. These findings allow a better and quantitative interpretation of the results when these substances are used as natural fecal and contamination indicators.

4.1   Introduction

To protect drinking water from contamination, the rapid estimation of water-quality parameters has become a major task. In the last few years, fluorescence-based measurements of tryptophan and humic substances have become a promising tool for the rapid assessment of bacterial and other organic contamination (Sorensen et al., 2015; Frank et al., 2018; Sorensen et al., 2018). With this method, it is possible to locate contamination origin and to monitor how contamination spreads through the karst aquifer network in near real-time (Ediriweera and Marshall, 2010).

Dissolved humic substances in natural waters are mainly derived from dead and decaying soil detritus, aquatic plants and debris (Hongve, 1999). Humic substances are heterogeneous molecular compounds resulting from abiotic and biotic reactions in soil (Piccolo et al., 2018). The presence of humic acid in water can have a significant adverse impact on the treatability of that water and decreases the success of disinfection processes (Oliver et al., 1983).

Tryptophan is a fluorescent amino acid containing an amino group, a carboxylic acid group and a side chain indole. Tryptophan is essential for humans and is used in the biosynthesis of proteins. Tryptophan is often used as an indicator of biological activity (Fellman et al., 2010; Maie et al., 2007). Determann et al. (1998) and Quiers et al. (2014) showed that tryptophan-like fluorescence is directly related to microbial activity of bacteria, and Sorensen et al. (2015) demonstrated that it can be used to investigate the biological quality of drinking water.

So far, several studies use dissolved tryptophan and humic substances as indicators of water quality (e.g. Cumberland et al., 2012; Baker et al., 2015; Sorensen et al., 2018), however, the behavior and transport properties of these substances with respect to flow velocities, residence times and especially degradation processes are still insufficiently known, although they are crucial to accurately determine organic contamination, especially at fast reacting karst springs.

To determine these relevant parameters, we conducted a tracer test, comparing tryptophan and humic acid to the conservative tracer uranine in a well-studied karst experimental site. The fluorescent dye uranine is commonly used as an almost ideal conservative tracer because of its low detection limit and favorable properties (Käss, 2004).

Generally, tracer tests are powerful tools to study groundwater flow and contaminant migration, especially in karst systems (Göppert and Goldscheider, 2007). Artificial tracers have been applied in the identification of recharge areas, flow directions and velocities and groundwater vulnerability (Käss, 2004; Goldscheider, 2008; Massei et al., 2006) and to characterize transport processes in natural streams (Boulton et al., 2010; Lemke et al., 2013). Numerous mathematical models have been developed to estimate transport parameters from the observed break through curves (BTC, e.g. Kreft and Zuber, 1978; Maloszewski et al., 1992; Berkowitz et al., 2006).

In this study, we compared tryptophan and humic acid with the conservative tracer uranine in a pristine karst experimental site in the Austrian Alps, in order to identify differences between the ideal conservative tracer and the two natural organic compounds that were used as artificial tracers in this study. We determined flow velocities, residence times, dispersion and retardation of tryptophan and humic acid in a natural karst groundwater system during different hydrological conditions in order to achieve a better understanding of these two substances, which is important with respect to their utilization as water quality indicators. Additionally, we compared novel fluorescence-based online field measurements and conventional laboratory analyses of water samples in order to test and evaluate the near real-time detection and quantification of tryptophan and humic-acid by means of field instruments.

4.2 Materials and Methods

4.2.1 Study Site

A well-investigated small-scale epikarst system representing a model karst aquifer that can be used as an ideal experimental site for field-scale tracer tests was chosen as test site (Goeppert and Goldscheider, 2019). The karst system is located west of Lake Formarin in Western Austria (Fig. 1a) and consists of a swallow hole, where the three tracers were injected, and a downstream spring that served as monitoring and sampling site (Fig. 1b). At high-flow conditions, an overflow spring exists between the swallow hole and the sampling point (Fig. 1b). The catchment area consists of highly karstified limestone (Plattenkalk Formation) and the spring can be characterized as a typical epikarst spring with shallow flow paths between the swallow hole and the outlet. The main advantages of this study area for the conducted comparative tracer tests are:

- short distances (linear distance between the injection point and the spring outlet is 235 m) and relatively high flow velocities resulting in short experiment durations
- relatively simple hydrogeological conditions with an active swallow hole connected to a perennial karst spring
- low and constant background concentrations of tryptophan and humic substances at the spring
- good accessibility of the study site

These advantages make this study area an ideal site for the evaluation of the transport properties of different substances in groundwater.
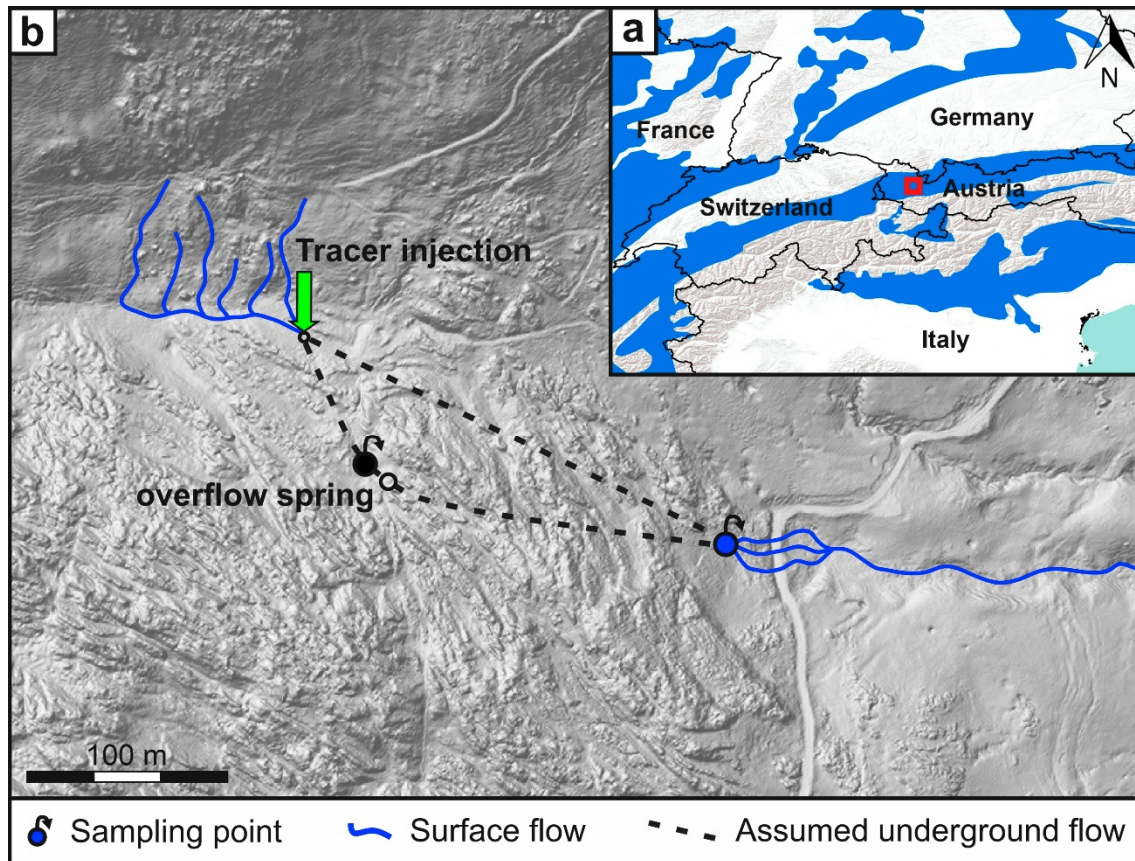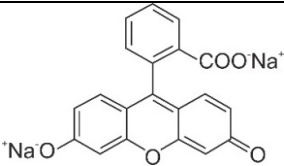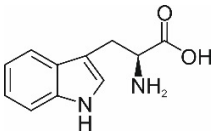
Figure 20: a) Location of the test site in Western Austria (basemap: World Karst Aquifer Map, modified after Chen et al., 2017); b) detailed view of the karst experimental site (basemap: data.vorarlberg.gv.at).

The injection and monitoring for the first test series were done from 16. to 18. August 2017 under the same conditions for all three tracers, with direct injection of the dissolved tracers into flowing water and constant spring discharge between 29 L/s and 31 L/s (mean to high flow) during the monitoring period. The second test series was conducted from 7. to 9. September 2017 with constant discharge conditions between 7.5 and 8.5 L/s (low-flow conditions). A third test with uranine and tryptophan was conducted from 6. to 7. July 2017 under low to mean flow conditions (discharge between 14 L/s and 14.5 L/s). To compare the three tracers, within each test series, water samples were taken manually and analyzed in the laboratory. An online field fluorimeter (FF) was used for each test series, to test its applicability to detect and to measure the three tracers in real time and in higher resolution.

4.2.2   Used Tracers

Uranine (AppliChem GmbH, Darmstadt, Germany), L-Tryptophan (Sigma-Aldrich/Merck KGaA, Darmstadt, Germany) and humic acid (as Humic Acid sodium salt, Sigma-Aldrich/Merck KGaA, Darmstadt, Germany) were used as tracers. The structural formulas, the solubility in water and the main optical properties of the three tracers are given in Table 1.

Table 6: Structural formula and properties of the three used tracers.

	uranine	l-tryptophan	humic acid
structural formula			macromolecule without defined structural formula
solubility [g/L] (H_2O, 20°C)	>600[a]	10[b]	n.n.
peak λ_{em} [nm]	512[a]	350[c]	Peak 1: 380-480[d] Peak 2: 420-480[d]
peak λ_{ex} [nm]	491[a]	280[c]	Peak 1: 250-260[d] Peak 2: 330-350[d]

[a] Käss 2004 [b] Römpp Enzyklopädie Online [c] Lakowicz 2006 [d] Parlanti et al. 2000

Uranine shows the strongest fluorescence of all fluorescence tracers (Käss, 2004). The detection limit of uranine is extremely low (~0.005 μg/L); its solubility is very high, and it is harmless for the environment (Behrens et al., 2001). Therefore, uranine is widely used for hydrogeological tracer tests.

L-Tryptophan is an aromatic, proteinogenic amino-acid with a carboxylic acid group and a side chain indole and is one of three fluorescent amino acids. The fluorescence properties of tryptophan are used to investigate the dynamics of dissolved natural organic material (Wagner, 2014).

Humic substances have a polymeric composition without a reproducible structure. They consist of aliphatic and heterocyclic structures which give them the optical property of fluorescence (Sun et al., 2010). Humic substances are decomposition products of dead herbal and animal material which develop through biological conversion in soil and water. Depending on their origin, humic substances created in water have a smaller size and are generally younger than humic substances from soil. The fluorescence properties of humic substances are depending on the amount of aromatic structures and their actual size (Wagner, 2014).

Because environmental conditions can have a complex influence on the characteristics of especially tryptophan and humic acid fluorescence (Sun et al., 2010; Chen and Kenny, 2007), a comparative tracer test with uranine was conducted to determine the transport properties

(transport velocities, residence times, dispersion and retardation) of the two used substances. Sorensen et al. (2018) used tryptophan as an indicator of fecal pollution and observed good correlation between dissolved tryptophan (tryptophan-like fluorescence) and thermotolerant coliforms, and Sorensen et al. (2016) demonstrated that the majority of the tryptophan-like fluorescence signal was within the <0.22 µm size fraction. Therefore, for this study a tryptophan solution was used as tracer.

4.2.3   Tracer measurements

The three tracers were analyzed directly on site with an online field fluorometer (FF) GGUN-FL30 (Albillia Co., Neuchâtel, Switzerland) with optics for uranine, tryptophan and amino G acid. In addition, water samples were taken in 4 to 30 min intervals for analysis in the laboratory. All water samples were collected in 50 mL brown glass bottles and stored in the dark at 4 °C until analysis. In the laboratory, uranine was measured with a LS55 fluorescence spectrometer (Perkin Elmer Inc., Waltham, USA) and tryptophan and humic acid were analyzed with the Aqualog fluorometer (Horiba Ltd., Kyoto, Japan). All samples were analyzed in a quartz cuvette with a path length of 10 mm maintained at a constant temperature of 20 °C.

With the Aqualog, excitation-emission matrices (EEMs) were acquired by simultaneous scanning of the absorbance (excitation) and the fluorescence emission spectrum at each excitation wavelength. For the samples analyzed with the Aqualog, a simultaneous scan of excitation and emission wavelength from 240 to 600 nm with 5-nm intervals was performed. A deionized water blank was used to validate the performance of the instrument and to measure the signal-to-noise ratio. First and second order Rayleigh scattering was removed by nullifying the signal intensities of the Rayleigh lines. The Raman scatter line was removed by subtracting the blank from the sample EEM. EEMs were also corrected for inner filter effects (IFE) using the parallel absorbance measurement from the blank and from the sample, following the procedure of Gilmore (2011). To determine the fluorescence intensities, the peak-picking technique was used (Coble, 1996). In accordance with Fellman et al. (2010), the tryptophan peak was identified at excitation wavelength (λ_{ex}) 270-280 nm and emission wavelength (λ_{em}) between 330-370 nm. In the field, humic acid was determined using the Amino G Acid channel of the FF. In the EEM, it was identified at λ_{ex} 320-375 nm and λ_{em} 430-500 nm. 20 µL of a pH 10 buffer solution were added to the water samples analyzed for uranine (with LS55) and tryptophan (with Aqualog) to increase the fluorescence yield. Samples were not diluted.

4.2.4 Modelling of the breakthrough curves (BTCs)

To model the BTCs in this karst system (with major conduits), the commonly used advection-dispersion model (ADM, Kreft and Zuber, 1978) was used:

$$C_f(x,t) = \frac{M}{Q \cdot t_0 \cdot \sqrt{4\pi \cdot P_D \cdot \left(\frac{t}{t_0}\right)^3}} exp\left[\frac{\left(1-\frac{t}{t_0}\right)^2}{4 \cdot P_D \cdot \frac{t}{t_0}}\right] \tag{10}$$

Where C is the tracer concentration in the water (µg/L), M is the injected tracer mass (mg), Q is the discharge or pumping rate (m³/s), t_0 is the mean flow time, P_D is the dispersion parameter (reciprocal Péclet Number, $P_D = \frac{D_L}{v \cdot x}$), t is a time variable (s), D_L is the longitudinal dispersion coefficient ($D_L = \alpha_L \cdot v$) (m²/s), v is the effective flow velocity $v = \frac{x}{t_0}$ (m/s), x is the distance between injection and sampling point (m) and α_L is the longitudinal dispersivity (m).

The observed BTCs during low-flow conditions show a more pronounced tailing compared to mean- to high-flow conditions. To model these BTCs a 2-Region Nonequilibrium model (2RNE, Field and Pinsky, 2000) was used. This model accounts for exchange between mobile and immobile fluid regions in a karst system. Water in the immobile fluid region is assumed as stagnant relative to the water flowing in the mobile fluid region. Therefore, the advection-dispersion equation is extended by two parameters, a partitioning coefficient β between mobile and immobile fluid regions and a mass transfer coefficient ω between the two regions. For simplification, only the dimensionless form is given here (modified after Field and Pinsky, 2000 and Toride et al., 1999).

$$\beta \frac{\partial C_1}{\partial T} = \frac{1}{Pe} \frac{\partial^2 C_1}{\partial Z^2} - \frac{\partial C_1}{\partial Z} - \omega(C_1 - C_2) \tag{11}$$

$$(1 - \beta)\frac{\partial C_2}{\partial T} = \omega(C_1 - C_2) \tag{12}$$

where C represents the dimensionless solute concentration and T and Z dimensionless time and space variables. The Péclet number Pe is defined by the model parameters mean flow velocity (v_m) and dispersion coefficient D.

$$Pe = \frac{x v_m}{D} = \frac{x}{\alpha} \tag{13}$$

where x is the flow distance and α the dispersivity. The dimensionless partitioning coefficient β ($0 \leq b \leq 1$) indicates the proportion of mobile water, while the mass transfer coefficient ω describes the exchange rate between the two fluid regions.

The 2RNE model was already successfully applied to the simulation of breakthrough curves from tracer tests in karstic and non-karstic environments (e.g. Birk et al., 2004; Geyer et al., 2007; Lauber et al., 2014; Ender et al., 2018).

Because the observed BTCs of all three tracers show two individual peaks during mean- to high-flow conditions, both peaks were modelled separately according to the multi-dispersion model (MDM) from Maloszewski et al. (1992). The different peaks can be modeled by superposition of two or more advection-dispersion models (Seaman et al., 2007). For each peak, t_0 and D have to be determined individually.

The modelling was done with the software package CXTFIT (Toride et al., 1999) where both, the ADM and the 2RNE model, are implemented.

4.2.5 pH-dependence of tracer fluorescence

For all three tracers, a laboratory experiment was conducted to investigate the pH dependence of fluorescence. Diluted solutions were prepared from a stock solution (1 g/L) for each tracer. The pH adjustment was done by adding microliters of concentrated NaOH and HCl respectively. The pH reading was conducted with a WTW SenTix 940 sensor (Xylem Analytics Germany Sales GmbH & Co. KG, WTW; Weilheim; Germany). The fluorescence intensities of all samples were measured at a constant temperature of 20 °C with a LS55 fluorescence spectrometer (uranine) and an Aqualog fluorimeter (tryptophan and humic acid). The fluorescence peaks were identified at the wavelength described above. The results of the fluorescence measurements at different pH values for all three tracers are given in the following figure.
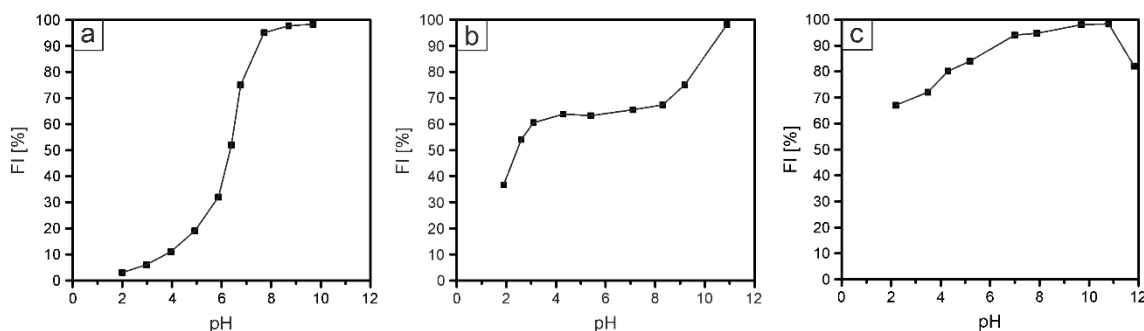
Figure 21: Dependency of the fluorescence intensity of the pH value for a) uranine; b) tryptophan; c) humic acid; the highest measured fluorescence intensity was assumed as 100 %.

Uranine fluorescence is highly influenced by the pH; the highest fluorescence intensities (FI) were measured at alkaline pH over 10, as also described in Käss (2004). Tryptophan also shows higher FI at alkaline pH, but the fluorescence is more or less constant in the pH range between 5 and 8 (Sun et al., 2010). The influence of the pH is also visible for humic acid, which shows higher fluorescence at alkaline values but is also more or less constant in the range 6 to 8. During the investigation period, the spring water had constant pH between 7.8 and 8.0.

4.3   Results and Discussion

4.3.1   Comparison of field and laboratory measurements

A comparison of the measured uranine concentrations with the LS55 and the FF gives a satisfying consistency, with an R² of 0.995 and a = 0.960 (Appendix 1a). For tryptophan, comparison of the measured concentrations with the Aqualog in the laboratory and the FF shows an R² value of 0.98 and a = 1.003 which also indicates a satisfying consistency (Appendix 1b). For humic acid, comparison between the laboratory and on-line measurements indicate a good performance of the FF with an R² of 0.97 and a = 0.995 (Appendix 1c), slightly lower than for uranine and tryptophan.

The measurement of an uranine sample with the Aqualog produced an EEM that reveals the maximum fluorescence at λ_{ex} 490 nm and λ_{em} of 515 nm (Fig. 22a). The EEM scan also shows a secondary fluorescence maximum at λ_{ex} 320 nm (Fig. 22a).

The produced EEM spectrum for Tryptophan shows a clearly identifiable peak at λ_{ex} between 270 and 280 nm and λ_{em} between 330 and 370 nm (Fig. 22b), which is very similar to other studies (e.g. Fellman et al., 2010; Coble, 1996).

The produced EEM spectrum for humic acid sodium salt shows more than one identifiable peak (Fig. 22c). The excitation and emission wavelengths where the peak was identified in this study with the Aqualog were λ_{ex} 320-350 nm and λ_{em} 400-480 nm (according to Coble, 1996 and Parlanti et al., 2000). To identify the humic acid with the FF, the channel for amino G acid was used, which is at a similar wavelength than the one used from the EEMs.
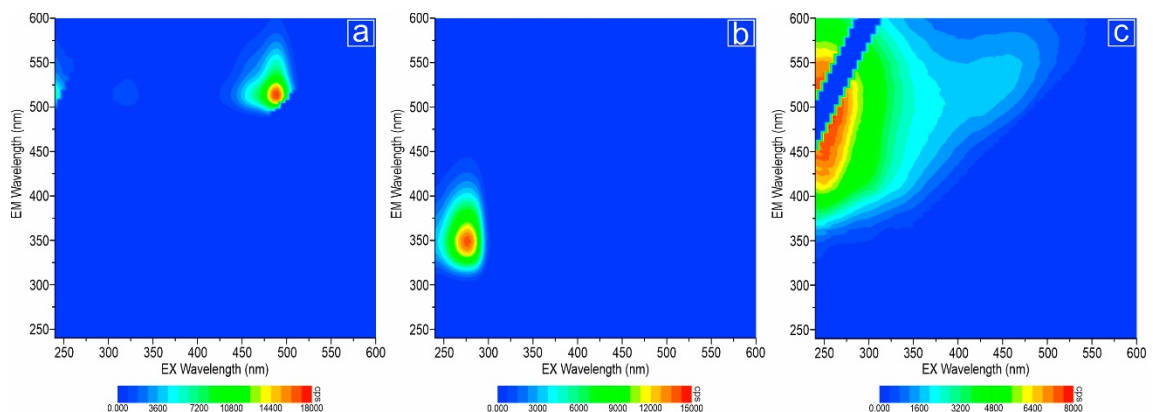
Figure 22: a) EEM spectra of uranine recorded with the Aqualog, which shows λex and λem of the main and secondary uranine fluorescence peak; b) EEM spectra of tryptophan which shows the main tryptophan fluorescence peak; c) EEM spectra of humic acid.

4.3.2   BTCs and obtained transport parameters

To obtain high-resolution results, the breakthrough curves (BTCs) for all test series (mean- to high-flow, low- to mean-flow and low-flow) were produced from the FF data that were also used

for modeling. During mean- to high-flow, uranine was first detected 22 min after the injection and reached a maximum of 20.1 µg/L after 32 min (Fig. 23a). The BTC shows a second peak after 63 min with a concentration of 4.2 µg/L. The total recovery was 74 % which indicates that the monitored spring is the major outlet of the system, but infiltration into deeper parts of the aquifer also occurs. This conclusion is supported by other tracer tests performed in this system (Goeppert and Goldscheider, 2019).

An explanation of the observed multi-peaks and tailing effects could be different flow-paths with different lengths, dispersivities, and flow velocities (Goldscheider et al., 2008). The overflow spring (Fig. 1b), which is only active during high-flow conditions at the main spring (>25 L/s), indicates the existence of at least a secondary flow path.

The observed BTC for tryptophan (Fig. 23b) has an almost identical shape compared to the uranine BTC. Tryptophan was first detected 22.5 minutes after injection and reached a maximum concentration of 80.4 µg/L after 32 minutes. Again, the BTC shows a second peak after 62.5 minutes with a concentration of 15.3 µg/L. The calculated total recovery of tryptophan was 70.6 %, slightly lower than for uranine.

Although the recovery rates of uranine and tryptophan are comparable, additional processes in the aquifer, such as degradation and sorption, can occur. Some studies found for example, that bacteria were able to degrade aromatic amino acids (Janke, 1950; Aklujkar et al., 2014), which might be a possible explanation for the slightly lower recovery, although it is quite unlikely that these processes occur in the investigated system because of the short transit times, high flow velocities, and short distances.

The BTC of humic acid again shows two distinct peaks: the first occurs after 33 min with a maximum concentration of 1373.0 µg/L, while the second peak was recorded after 78 min with a concentration of 218.4 µg/L (Fig. 23c). This is a delay of about 15 min compared to uranine and tryptophan. The shape of the first peak is similar to uranine and tryptophan, while the second peak is flatter and wider compared to the other two tracers. The total recovery of humic acid is 76 %, which is slightly higher compared to uranine and tryptophan.
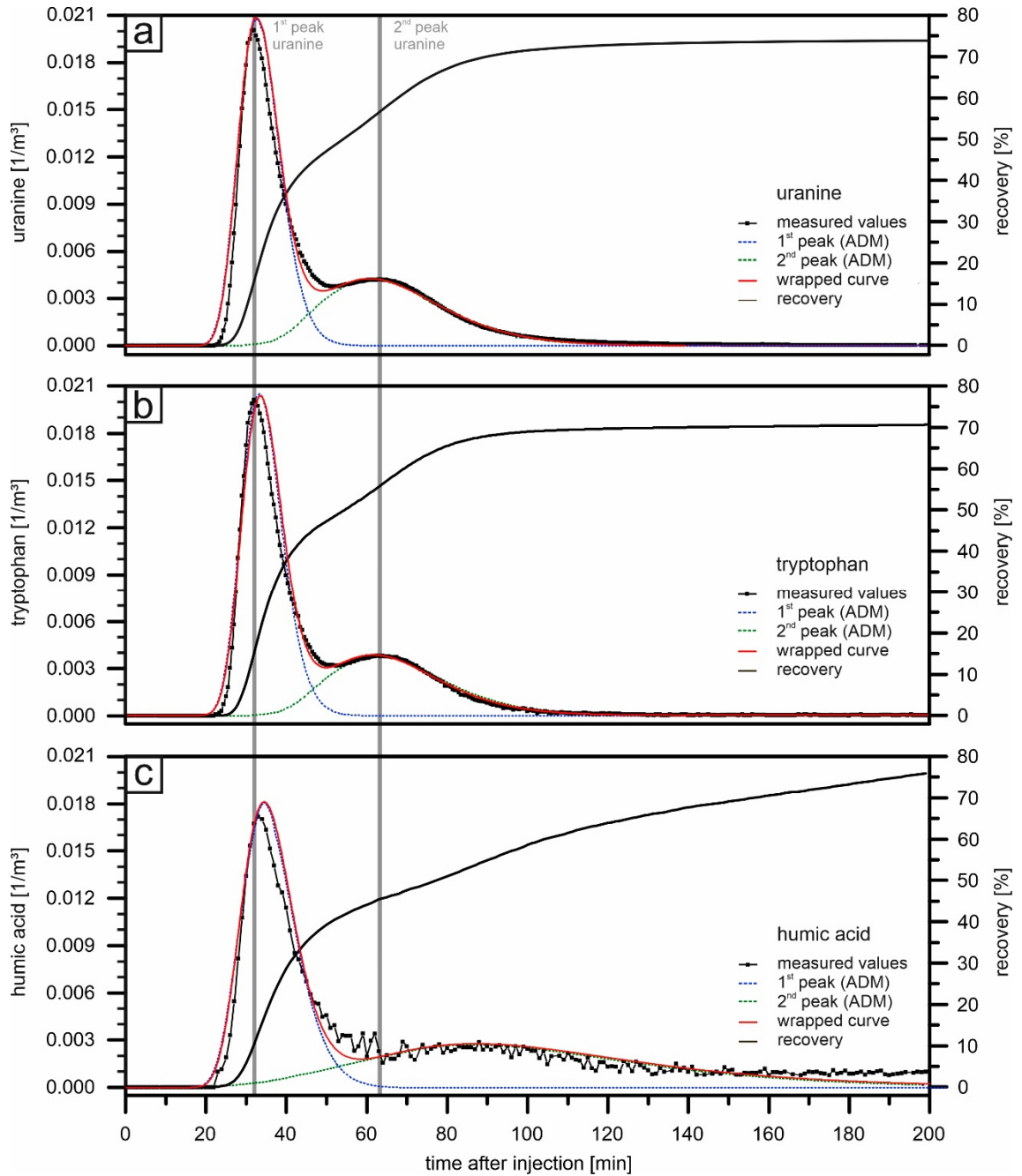
Figure 23: Breakthrough curves (BTCs) of the tracer a) uranine, together with the recovery and the modelled BTC for both peaks and the wrapped curve; b) tryptophan, together with the recovery and the modelled BTC for both peaks and the wrapped curve, c) humic acid, together with the recovery and the modelled BTC for both peaks and the wrapped curve. Concentrations are normalized [c/M].

The second test series was conducted in the same system during low-flow conditions. The results show BTCs for all three tracers with only one identifiable peak (Fig. 24) which show a more pronounced tailing compared to the BTCs observed during high-flow conditions. The modelling for these BTCs was done with a two – region nonequilibrium model (2RNE).
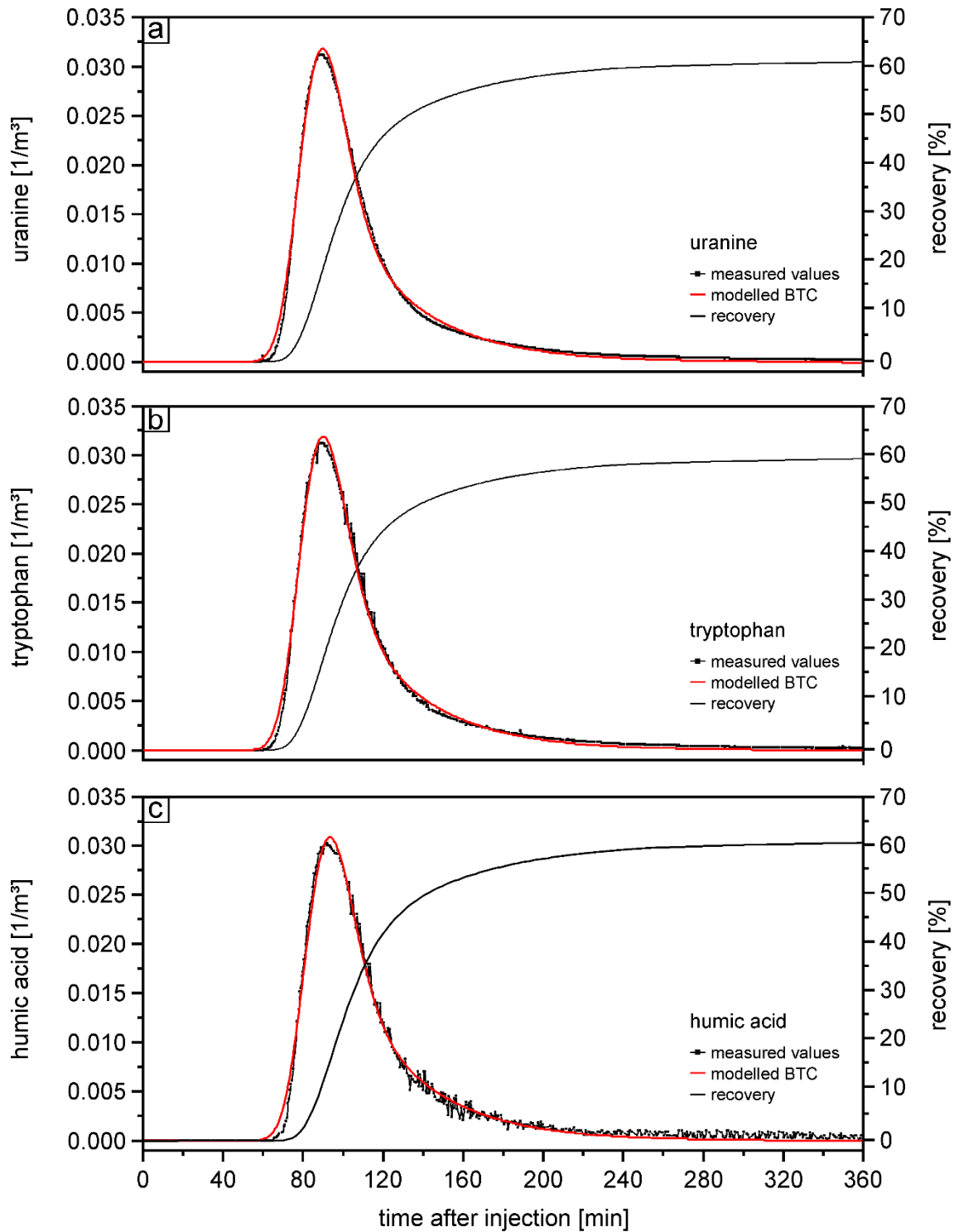
Figure 24: Breakthrough curves (BTCs) during low-flow conditions of a) uranine; b) tryptophan; c) humic acid, each time together with the recovery and the modelled BTC.

During low-flow, uranine was first detected 59.5 min after the injection and reached a maximum of 24.8 µg/L after 89 min (Fig. 24a). These observed time values are 2.7 times higher compared to high-flow conditions. The total recovery was 60.8 % which is lower than during high-flow and also indicates that the monitored spring is the major outlet of the system, but infiltration into deeper parts of the aquifer also occurs.

The observed BTC for tryptophan (Fig. 24b) has an almost identical shape compared to the uranine BTC. Tryptophan was first detected 60.5 minutes after injection and reached a maximum concentration of 99.2 µg/L after 90.5 minutes. This is again 2.7 times more compared to low-flow conditions. The calculated total recovery of tryptophan was 59.7 %, slightly lower than that for uranine.

The recovery rates of uranine and tryptophan are also comparable during low-flow conditions, but additional processes in the aquifer, such as degradation and sorption, can occur and cannot be excluded. Compared to high-flow conditions, the transit times are higher and the resulting flow velocities are lower.

The BTC of humic acid shows a similar shape compared to uranine and tryptophan (Fig. 24c). Humic acid was first detected 65 min after injection and the peak occurred after 92.5 min with a concentration of 1885 µg/L. This is a slight delay compared to uranine and tryptophan. The total recovery of humic acid is 60.5 %, which is in a similar range as the other two tracers. The partitioning coefficient β is between 0.77 for uranine and 0.68 for humic substances. This means that between two-thirds and three-quarters of the water can be considered as mobile.

A third tracer test was conducted with uranine and tryptophan during low- to mean discharge conditions (14.5 L/s and 14 L/s respectively). The BTCs show only one peak with a similar shape compared to the curves obtained during low-flow conditions. The obtained values for uranine and tryptophan are also comparable. The BTCs, modelled BTCs, recovery rates and the corresponding data are given in Appendix 2 and Table 2.

Table 2 gives an overview of all parameters obtained from the three tracer tests.

During mean- to high-flow conditions, the time of first detection (t_1), t_p and the corresponding v_{max} and v_p for the first tracer peak, are comparable for all three tracers. The modelled parameters v, t_0 and longitudinal dispersion (D) were determined for both peaks for the conservative tracer uranine. The retardation factor was set to 1.0. The determined values for v and t_0 for uranine were used as fixed input parameters for the modelling of the other two tracers. While the mean transit time is comparable for uranine and tryptophan, the mean transit time for the second peak of humic substances is about 20 % higher compared to the other two tracers. The modelled retardation factor for the secondary humic acid peak is 1.5 compared to uranine (1.0 = no retardation).

During low-flow conditions, t_1, t_p and the corresponding velocities v_{max} and v_p are comparable for all three tracers with a slight delay and slighty lower velocities for humic substances. To determine retardation, the same procedure as during high-flow was applied. Compared to uranine and tryptophan, a retardation factor of 1.11 was determined for humic substances.

Retardation processes seem to have no influence on tryptophan because the modelled retardation factor is also 1.0 for both peaks during high-flow and for the BTC during low-flow (like the conservative uranine). Retardation seems to have a larger influence on the humic acid tracer, especially on the second peak during high-flow but it is also visible during low-flow.

Because uranine can be considered as an almost ideal conservative tracer, the slower transport of humic acid can be attributed to a reactive transport behaviour of the humic substances. For these kinds of substances, adsorption and desorption processes are of particular importance. Because of the higher flow velocities in the main flow path during mean- to high-flow (one major conduit), these factors are almost negligible. Factors influencing the retardation are different surface conditions and different properties of the aquifer material (Aklujkar et al., 2014), which play a more important role in the secondary flow path, which is longer, more diffuse and the transport occurs slower.

The blurrier peak in the EEM spectrum of humic acid apparently also leads to a more blurred signal in the FF, which might also influence the shape of the humic acid BTC. The tracers uranine and tryptophan produce a clear fluorescence signal which can be seen in the smooth BTCs of these two tracers (Fig. 3a and b). In comparison to this, the humic acid FF signal is associated with a certain degree of variation, especially at lower concentrations.

*Table 7: Overview of the obtained and calculated transport parameters for all three test series. Bold numbers indicate fixed values during modelling. * BTCs and modelled BTCs are shown in Appendix 2.*

	symbol	unit	mean- to high-flow (ADM/MDM) Uranine 1st Peak	2nd Peak	Tryptophan 1st Peak	2nd Peak	Humic acid 1st Peak	2nd Peak	low- to mean-flow* (2RNE) Uranine	Tryptophan	low-flow (2RNE) Uranine	Tryptophan	Humic acid
Experimental conditions													
Injection quantity	M	g	1.0		4.0		80.0		0.8	3.2	0.8	3.2	65
Spring discharge	Q	L/s	30		31		29		14.5	14.0	8.5	7.5	7.5
Basic parameters													
Time of first detection	t_1	min	22.0		22.5		23.0		57.5	58.0	59.5	60.5	65.0
Peak time	t_p	min	32.0	63.0	32.0	62.5	33.0	78.0	81.5	81.5	89.0	90.5	92.5
Peak concentration	C_p	µg/L	20.1	4.2	80.4	15.3	1372.9	218.4	20.8	101.0	24.8	99.2	1885
Normalized peak concentration	C_p/M	m^{-3}	0.020	0.004	0.020	0.004	0.017	0.003	0.038	0.032	0.031	0.031	0.029
Maximum velocity	v_{max}	m/min	10.7		10.4		10.2		4.1	4.1	3.9	3.9	3.6
Peak velocity	v_p	m/min	7.3	3.8	7.3	3.8	7.1	3.0	2.9	2.9	2.6	2.6	2.5
Recovery	R	%	73.9		70.6		76.1		69.1	67.8	60.8	59.7	60.5
Modelled parameters													
Coefficient of determination	R^2	-	0.98		0.98		0.96		0.98	0.98	0.99	0.99	0.99
Mean flow velocity	v	m/min	7.0	3.5	**7.0**	**3.5**	**7.0**	**3.5**	2.6	2.6	2.4	**2.4**	**2.4**
Mean transit time	t_0	min	33.6	67.1	33.6	67.1	33.6	67.1	90.4	90.4	97.9	97.9	97.9
Partitioning coefficient	☐	-	-	-	-	-	-	-	0.83	0.81	0.78	0.76	0.70
Transfer coefficient	☐	-	-	-	-	-	-	-	1.05	1.01	1.12	1.06	1.01
Longitudinal dispersion	D	m^2/min	15.7	23.7	**15.7**	**23.7**	**15.7**	**23.7**	6.2	6.2	5.0	**5.0**	**5.0**
Retardation factor	R_f	-	**1.00**	**1.00**	1.00	1.00	1.03	1.48	**1.00**	1.00	**1.00**	1.00	1.11

4.4   Conclusion

Given the importance of real time water quality indicators, many studies use tryptophan as fecal indicator (e.g. Sorensen et al., 2015; Frank et al., 2018) and humic substances as contaminant vector. There is the need to enhance the knowledge about the transport behaviour of these two substances.

In this study, we conducted three tracer tests in a karst experimental site, where we compared the transport of tryptophan and humic acid with the conservative tracer uranine. The main conclusions can be summarized as follows:

- Tracer test results show that modern online field fluorometers can be used to measure fluorescence of tryptophan and humic acid in near real-time and in high resolution.
- The transport parameters obtained for the conservative tracer uranine and tryptophan, especially the flow velocities, transit times, and dispersion, are almost identical. The recovery rates of uranine and tryptophan are also comparable. All three tracer tests indicate that no reduction or retardation occurs in the investigated flow system for dissolved tryptophan.
- However, humic acid is transported slower compared to uranine and tryptophan. Therefore, the calculated and modelled transport parameters of humic substances are different. In this case, retardation occurs. The retardation factors for humic substances (between 1.1 and 1.5 in our study) indicate that sorption processes have a distinct influence on humic substances.

The tracer test also led to a better understanding of the investigated aquifer. During mean- to high-flow conditions, the breakthrough curves of all three tracers show two clearly identifiable peaks, which indicate at least two flow paths. This was also verified with subsequent tracer tests conducted in this system and is dependent on the discharge of the spring. At low-flow conditions only one flow path is active and the resulting BTCs have only one peak.

The observed and calculated transport parameters (residence time, mean flow-velocity, retardation) in the investigated system, lead to the conclusion that tryptophan behaves like a conservative tracer without retardation and reduction, at least in fast-flowing karst aquifer systems. On the other hand, this study also shows that humic substances underly no reduction in fast-flowing areas, but reduction and retardation occur in slower flow-paths.

Therefore, these results can contribute to a better and quantitative interpretation when these two substances are used as fecal and contamination indicators.

Acknowledgments

Chapter 5

5 Improved understanding of dynamic water and mass budgets of high alpine karst systems obtained from studying a well defined catchment area

Abstract

Large areas of Europe, especially in the Alps, are covered by carbonate rocks and in many alpine regions, karst springs are important sources for drinking water supply. Because of their high variability and heterogeneity, the understanding of the hydrogeological functioning of karst aquifers is of particular importance for their protection and utilization. Climate change and heavy rainfall events are major challenges in managing alpine karst aquifers which possess an enormous potential for future drinking water supply. In this study, we present research from a high alpine karst system in the UNESCO Biosphere Reserve Großes Walsertal in Austria, which has a clearly defined catchment and is drained by only one spring system. Results show that (i) the investigated system is a highly dynamic karst aquifer with distinct reactions to rainfall events in discharge and electrical conductivity; (ii) the estimated transient atmospheric CO_2 sink is about 270 t/a; (iii) the calculated carbonate rock denudation rate is between 23 and 47 mm/1000a and (iv) the rainfall-discharge behavior and the internal flow dynamics can be successfully simulated using the modelling package KarstMod. The modelling results indicate the importance of matrix storage in determining the discharge behavior of the spring, particularly during low-flow periods. This research can contribute and initiate a better understanding and management of alpine karst aquifers under conditions of climate change.

5.1   Introduction

Carbonate rocks, representing potential karst aquifers, cover about 15% of the world's land surface (Goldscheider et al., 2020) and karst water resources are important for the drinking water supply of approximately 750 million people worldwide (Stevanović, 2018). In Austria, 25% of the land surface is covered by carbonate rocks (Chen et al., 2017), but over 50% of the population, including large cities like Vienna, Salzburg and Innsbruck, depend on drinking water from alpine karst aquifers (Kralik, 2001).

High-alpine karst aquifers offer a high potential for future water supply. Karst aquifers have complex and original characteristics, which make them different from other aquifer types (Bakalowicz, 2005) and often very vulnerable to contamination, especially after rain events, because recharge occurs directly through dolines, fissures or swallow holes. Consequently, karst springs often show strong and rapid variations in discharge and water quality in response to rain events (Pronk et al., 2007).

The complex hydrogeological behavior of karst aquifers results from the complex interaction of many geological and hydrological variables as the evolving porosity and permeability of carbonate rocks, which are the result of chemical interaction of the carbonate rocks and water flowing through them. The water flow is important for the aquifer development, because this flow serves as primary transport mechanism in the dissolution of carbonate rocks (Petalas et al., 2018).

Several studies have been conducted in order to understand and describe the hydrogeological functioning of karst aquifers and the complex behaviors of karst springs (e.g. Birk et al., 2004; Goldscheider, 2005b; Liñán Baena et al., 2009; Vigna and Banzato, 2015; Filippini et al., 2018). Because springs in this environment are often directly related to precipitation and recharge in the catchment, especially shallow and fast flow karst systems can be investigated by means of tracer tests and hydrograph and chemograph analysis (Hilberg and Kreuzer, 2013). Another important process, which is often described in the literature (e.g. Martin and Dean, 2001; Frank et al., 2019), is the interaction between karst conduits and the surrounding matrix. This process is important, as the matrix can act as a water storage, particularly during dry periods. Nevertheless, a qualitative and quantitative description of this process is rare. Within this study, this process was investigated for the investigated karst system in Austria and its importance during low-flow conditions is shown.

In addition to the already complex behavior of karst systems, climate change is a challenge in managing such alpine karst aquifers. The understanding of the functioning of these complex karst aquifers is important for the utilization and protection of karst springs, particularly in high alpine regions.

Models of karst aquifers can provide valuable information about the functioning of the aquifer. Many models were applied to alpine karst aquifers (e.g. Hartmann et al., 2012; Dobler et al., 2013; Chen and Goldscheider, 2014). Distributed karst models discretize the karst system in two- or three-dimensional grids and require the assignment of characteristic hydraulic parameters and system states to each grid cell (Hartmann et al., 2014). Lumped approaches conceptualize the physical processes at the scale of the whole karst system without modeling spatial variability in detail (Hartmann et al., 2014). Such reservoir models usually have a quite simple structure and are well suited to simulate the relation between input (rainfall) and output (discharge at the spring). These models can not only contribute to a better understanding of the aquifer but also provide a valuable tool to manage these aquifers in regard to climate change.

To predict future climate change and its consequences, it is also crucial to quantify the sources and sinks of the greenhouse gas CO_2. Carbonate rock weathering (both dissolution and reprecipitation of carbonate) plays an important role, especially in karst areas (e.g. Hartmann, 2009; Liu and Zhao, 2000).

Within this study, we investigated a high alpine karst system in Vorarlberg, Austria, which has only one spring as major outlet and very clear catchment boundaries. Such hydrological systems are quite rare but scientifically valuable for water- and mass balance calculations that can then be transferred to other hydrogeological systems with less clear boundaries.

This study aims to provide new insights into the dynamics of high-alpine karst systems using a well-defined catchment as study area. The possible atmospheric CO_2 sink for the studied karst system was calculated according to the hydrochem-discharge method of Liu and Zhao (2000). In addition, the denudation rates for carbonate rocks in the investigated system were calculated and compared to values from other studies and finally, the KarstMod modelling package (Mazzilli et al., 2017) was used to simulate the rainfall-discharge behavior during a time period not affected by snowmelt. The modelling results were also used to assess the internal flows within the karst aquifer and to demonstrate the importance of the matrix for water storage in low-flow periods.

5.2   Materials and Methods

5.2.1   Study Area

The alpine study site Disnergschroef (Figs. 25 and 26) is located in the UNESCO Biosphere Reserve Großes Walsertal in the federal state of Vorarlberg in Austria (Fig. 26a). The study site receives the highest precipitation amounts in Austria. According to Werner (2007) the mean annual precipitation in the Disnergschroef area is between 2100 mm and about 2700 mm in the peak areas. Precipitation data from gauging stations at Koerbersee (1675 m a.s.l.), Sonntag/Stein

(1750 m a.s.l.) and Formarinalpe (1880 m a.s.l.), which are located west, east and southeast of the study area, confirm the precipitation variations. Highest precipitation rates are during the summer months, while lowest rates are measured during winter.
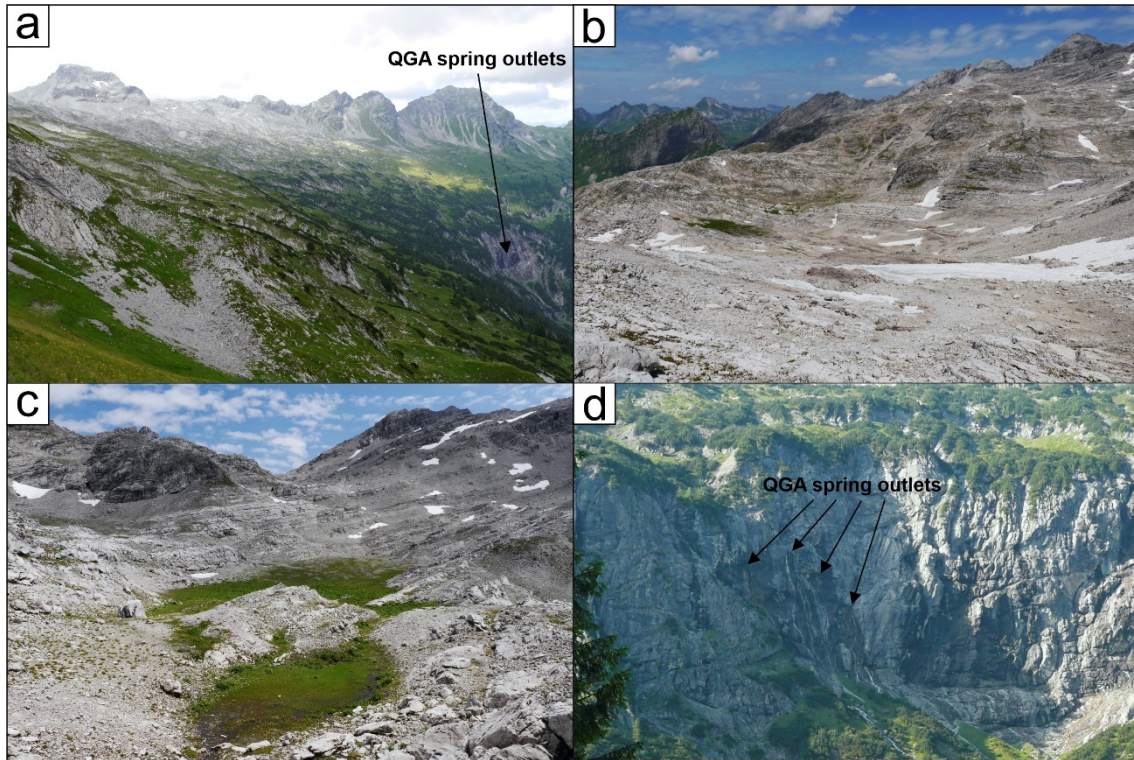

Figure 25: Overview of the Disnergschroef Karst Plateau; b) Top of the karst plateau with typical karst features, dolines and depressions; c) Depression in the karst plateau, where water directly enters the karst aquifer; d) View of the QGA spring outlets.

The relief of the investigation area (catchment of Gadenalpe spring = QGA, Figs. 25d, 26b) ranges from 1400 m a.s.l. to over 2400 m a.s.l. with steep slopes and deep valleys. The Disnergschroef karst area (Figs. 25a, 26b) belongs to the Northern Calcareous Alps and consists of a thick Main Dolomite-Limestone complex (Carnian – Norian) with distinct karst features. The karst plateau shows no surface runoff and is characterized by dolines, depressions, shafts and small caves.

The Main Dolomite also constitutes most of the summits surrounding the karst area. The cross section through the investigation area (A'-A, Fig. 26c) shows that a main fault separates the Triassic Main Dolomite-Limestone formation from Cretaceous and older deposits. The dolomite-limestone formation is underlain by the Raibl Fm. which consists of dark, indurated limestone and slatey, impermeable marls, as well as gypsum and rauhwackes and locally overlain by Jurassic limestone formations. In the area below the spring outlet, the Cretaceous and older deposits are covered by morainic sediments (Fig. 26c).

The spring consists of 4 main outlets very close to each other (Fig. 25d, summarized as QGA in the following). The point of measurement (QGA) is a few meters further downstream where the

individual spring outlets flow together. The springs emerge from the dolomite/limestone formation.

Above 1800 m a.s.l. most of the area is sparsely covered by alpine vegetation (Fig. 25). The study site and the springs are only accessible in the summer month because of high amounts of snow in winter and due to the risk of avalanches.

Two tracer tests, performed in July/August 2013 and July/August 2015, indicate that the whole karst plateau is principally drained by QGA. Two kilograms of the fluorescent tracer Amidorhodamine G were used for each tracer test. The injection points were located near the top of the Disnergschroef karst plateau at an elevation of about 2300 m a.s.l. (Fig 26b/c). The tracer was injected into a small stream, fed by snow melt water, which seeps into the karst aquifer a few meters further downstream and had a discharge of about 0.4 L/s. The injection was conducted after several days without rain. In total 25 springs and river locations in the Großes Walsertal valley and in the upper Lech valley were investigated with water samples or activated charcoal bags (Fig. 26b). Only one sampling location (QGA) led to positive tracer detection results in water samples and charcoal bags. Positive water samples were also collected further downstream following the small stream fed by QGA. All other water samples and charcoal bags were negative. This is evidence that the karst plateau is principally drained by the QGA spring system. The karst plateau can therefore be considered as a sort of natural lysimeter. Such an alpine system is quite unique and scientifically valuable because transferable detailed water and mass balances can be calculated.
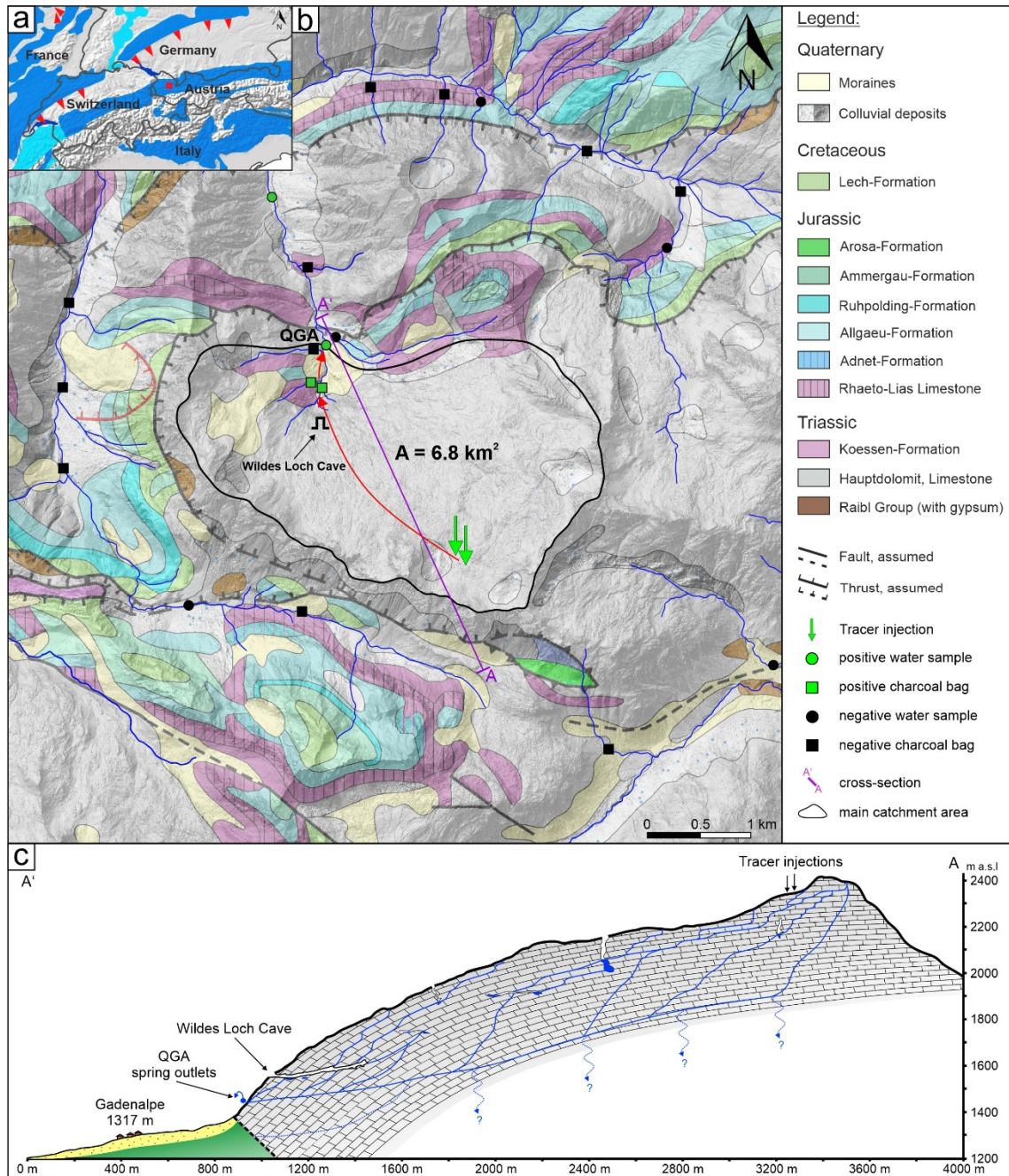
Figure 26: a) Location of the study area in the federal state of Vorarlberg in Austria (basemap: World Karst Aquifer Map, modified after Chen et al., 2017), b) Detailed view of the study site Disnergschroef with the tracer test sampling locations (basemap: Land Vorarlberg – data.vorarlberg.gv.at) and c) geological cross section through the test site.

5.2.2 Hydrological- and physicochemical data

The QGA spring was monitored continuously from 25.07.2016 to 12.07.2019. Water level (precision ± 0.1 cm), water temperature (± 0.1 °C) and specific electrical conductivity (EC, ± 1 µS/cm) were measured at 15 min intervals with a CTD sensor (Ott Hydromet GmbH, Kempten, Germany). Discharge measurements were undertaken using the salt dilution method with point injection. Water level was converted into continuous discharge using the following

stage (x in cm) – discharge (y in L/s) relationship, which was obtained by plotting the 22 measured discharge values versus the corresponding water level data (polynomial regression).

$$y = 1.437x^2 - 8.2128x \tag{14}$$

The obtained R^2 value for the polynomial regression was 0.99.

Rainfall data were obtained from three stations Koerbersee, Formarinalpe and Sonntag/Stein. For this publication the mean values of the three stations were taken as representative precipitation values.

Potential evapotranspiration (PET) was estimated by using the Haude method (DVWK, 1996).

$$PET = f \cdot (e_{s14} - e_{a14}) \tag{15}$$

$$e_{s14} = 6.11 \cdot 10^{(\frac{7.48 \cdot T}{237+T})} \tag{16}$$

$$e_{a14} = U \cdot e_{s14} \tag{17}$$

Where f is the Haude factor for the individual months (f = 0.25 for August, f = 0.23 for September, f = 0.22 for October, f = 0.20 for November) and e_{s14}-e_{a14} is the vapor saturation deficit of air at 14:00 MEZ, calculated using measured air temperature (T) and relative humidity U at 14:00 MEZ. For this calculation, the air temperature and humidity data of the station Koerbersee were taken as humidity data were only available from this station.

To estimate the contribution of carbonate rock weathering to the atmospheric CO_2 sink, the hydrochem-discharge method was employed (Liu and Zhao, 2000). The flux (F) of the atmospheric CO_2 consumed in carbonate rock weathering can be estimated by:

$$F = \frac{1}{2} \cdot [HCO_3^-] \cdot Q \cdot \frac{M_{CO_2}}{M_{HCO_3^-}} \tag{18}$$

Where $[HCO_3^-]$ is the HCO_3^- concentration in water, M_{CO2} and M_{HCO3-} are the respective molecular weights, Q is the discharge and ½ means that only half of the carbon in solution is from atmospheric CO_2 (Liu and Zhao, 2000).

Alkalinity was measured as triplicate by volumetric titration on site, using an alkalinity test (Merck KGaA, Darmstadt, Germany) and the mean value was taken as result. In total, 34 alkalinity measurements were conducted in different time intervals and during different hydrological conditions. The 34 individual bicarbonate concentrations were plotted versus the electrical conductivity measured at the same time. A continuous bicarbonate time series was then obtained by a linear regression.

$$y = 1.4743x + 20.218 \tag{19}$$

Where y is the electrical conductivity in µS/cm and x is the bicarbonate concentration in mg/L.
The obtained R² value for the linear regression was 0.93.

5.2.3   Modelling with KarstMod

The modelling platform KarstMod (Mazzilli et al., 2017) is dedicated to karstic groundwater flow
simulation. It provides an adjustable modelling platform for discharge simulations and
hydrodynamic analysis and can reproduce the conceptual structure of karst models known in the
literature (e.g. Fleury et al., 2007; Butscher and Huggenberger, 2008). The model is set up as a
two-level structure. Level 1 consists of compartment E (soil and epikarst), which represents the
infiltration zone and is influenced by precipitation (P) and evapotranspiration (ET). The water
flows then to the second level, which consists of compartments C (conduits), M (matrix) and L
(highly capacitive matrix) which represent the different sub-systems of the saturated zone (Sivelle
et al., 2019). The configuration of the KarstMod reservoir model used in this study is shown in
Figure 3. For better realism, all output discharge is set through reservoir C and compartment L is
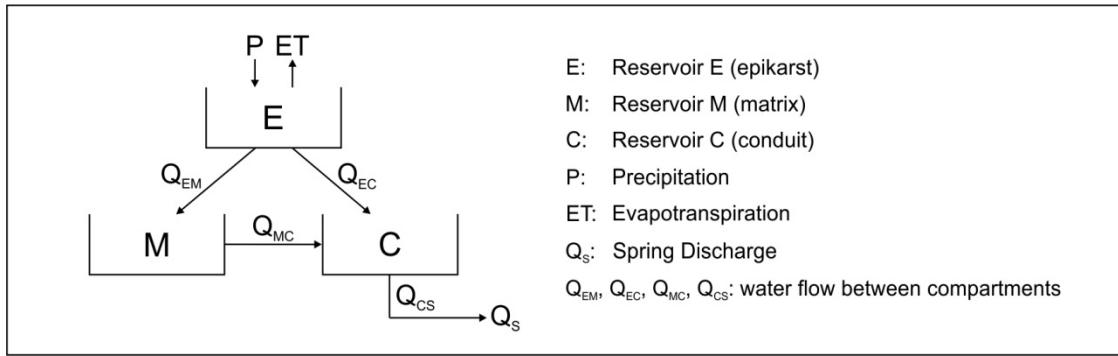not used as the investigated system is a very responsive watershed.

Figure 27: Structure of the selected rainfall-discharge reservoir model.

The modelling is based on the balance equations given by Mazzilli et al. (2017) and consists of
compartments E, M and C.

$$\frac{dE}{dt} = P - ET - Q_{EM} - Q_{EC} \tag{20}$$

$$\frac{dM}{dt} = Q_{EM} - Q_{MC} - Q_{MS} \tag{21}$$

$$\frac{dC}{dt} = Q_{EC} + Q_{MC} - Q_{CS} \tag{22}$$

$$Q_{EM} = k_{EM} \times E_t \text{ if } E_t > 0, \text{ otherwise } Q_{EM} = 0 \tag{23}$$

$$Q_{EC} = k_{EC} \times (E_t - E_{ThresholdC}) \text{ if } E_t > E_{ThresholdC}, \text{ otherwise } Q_{EC} = 0 \tag{24}$$

$$Q_{MS} = k_{MS} \times M_t \tag{25}$$

$$Q_{CS} = k_{CS} \times C_t \tag{26}$$

E_t, M_t and C_t are the water levels in the Epikarst, Matrix and Conduit reservoirs. k_{AB} is the recession coefficient associated with the flow from reservoir E → M, E → C, M → C and C → S. Q_{AB} is the discharge from A to B (e.g. E → C) and is computed by the product of Q_{AB} (e.g. Q_{EC}) and the total surface of the recharge area (R_A). With the model configuration chosen for this study, the discharge at the outlet QS is given by:

$$Q_S = R_A \times Q_{CS} \tag{27}$$

The rainfall-discharge model is calibrated using a quasi-Monte-Carlo procedure with a Sobol sequence sampling of the parameter space (Sobol, 1977; Mazzilli et al., 2017). The performance criteria in KarstMod are the Nash-Sutcliffe efficiency coefficient (NSE, Nash and Sutcliffe, 1970) and the modified Balance Error (BE), defined as follows:

$$NSE = 1 - \frac{\Sigma(Q_{obs} - Q_{sim})^2}{\Sigma(Q_{obs} - Q_{mean})^2} \tag{28}$$

$$BE = 1 - \left| \frac{\Sigma(Q_{obs} - Q_{sim})}{\Sigma Q_{obs}} \right| \tag{29}$$

where Q_{obs} is the observed discharge, Q_{sim} is the simulated discharge and Q_{mean} is the average observed discharge. A NSE of 1 is a perfect match between model and observations while a NSE of 0 indicates that the model performs equally to the mean of the observed data. A BE of 1 means that the simulated discharge is equal to the observed discharge. The KarstMod platform uses an aggregated objective function defined as the weighted sum of the two performance criteria (Baudement et al., 2017) according to equation:

$$W_{obj} = wNSE + (1 - w)BE \tag{30}$$

With W_{obj} as the objective function and w as the weight defined by the user ($0 \leq w \leq 1$). In this study we used w = 0.9. KarstMod proposes to use the simulation results from all parameter sets with a $W_{obj} > 0.7$ to evaluate the uncertainty of the simulation results. This approach is derived from the Regional Sensitivity Analysis (Hornberger and Spear, 1981) and the Generalized Likelihood Uncertainty Estimation (Beven and Binley, 1992).

In the model, three periods must be taken into account, the warm-up, calibration and validation periods. The warm-up period corresponds to the time interval after which the initialization bias is deemed to be negligible (Baudement et al., 2017). The simulation results of this period are not considered for the calibration.

For this study, time periods during summer and autumn (August – November, August – October), which are not influenced by snowmelt, were chosen for three consecutive years (2016 – 2018) for modelling in order to simulate the rainfall-discharge behavior and the internal flows within the karst aquifer as a reaction to rainfall events.

A sensitivity analysis was also carried out. Indices are calculated using the Sobol procedure as described in Saltelli (2002). The sensitivity index S_i for parameter X_i with respect to the simulated discharge Q_S is defined as the fraction V_i of the variance $V(Q_S)$ of the simulated discharge, which is due solely to the parameter X_i (Baudement et al., 2017).

$$S_i = \frac{V_i}{V_{Q_S}} \tag{31}$$

The total sensitivity index S_{Ti} measures the contribution of X_i to the output variance, including the interactions of X_i, of any order, with other input variables (Saltelli et al., 2007). By default, the sensitivity indices provided by KarstMod are obtained based on $N = 1000 \times (n_{par} + 2)$ parameter set, where n_{par} is the number of parameters to be calibrated (Baudement et al., 2017).

5.3 Results and Discussion

5.3.1 Temporal evolution of discharge, EC and bicarbonate

During the investigation period from 25. July 2016 to 12. July 2019, the cumulative rainfall was 6287 mm (Tab. 1). The temporal evolution of the monitored parameters discharge, electrical conductivity and rainfall are shown as time series in Figure 28. The hydrograph reveals distinct increases in response to recharge events with a delay of only a few hours, as also observed by many other studies of karst aquifers (e.g. Mudarra and Andreo, 2010; Vigna and Banzato, 2015; Frank et al., 2019). The highest discharge values, with up to 2200 L/s, were recorded after major rainfall events in the summer month of 2016, 2017 and 2019. Low-flow values during time periods without rainfall in autumn and winter are as low as 10 L/s. The mean discharge for the whole investigation period was 237 L/s. After each recharge period, EC rose progressively during the recession period until the next rainfall event. The mean EC for the whole period was 168 µS/cm.
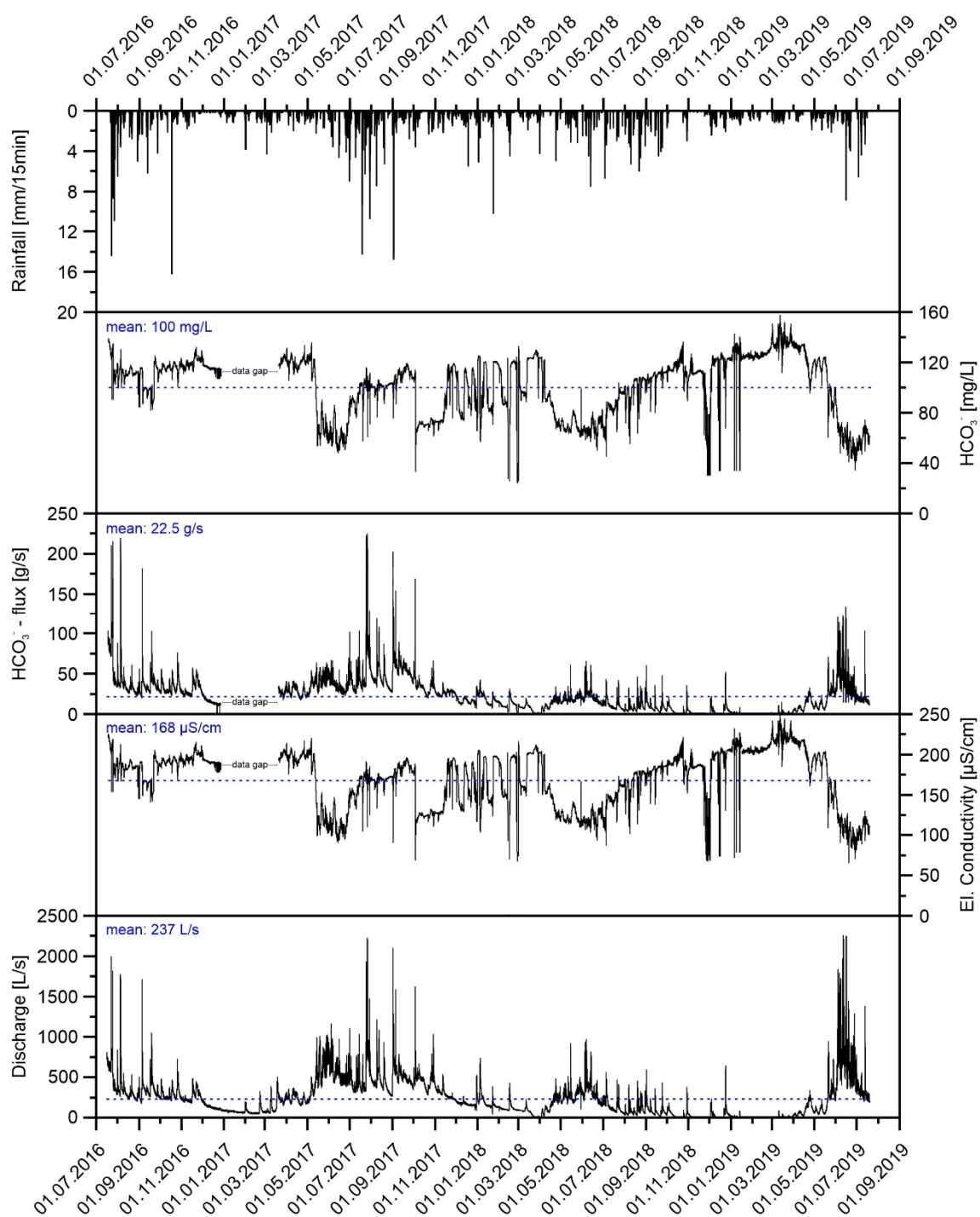
Figure 28: Time series of rainfall, electrical conductivity and discharge of the investigated spring as well as calculated bicarbonate concentration and bicarbonate flux.

The bicarbonate flux of the investigated spring was obtained using the calculated continuous HCO_3^- data and the according discharge values. The flux varies between 1 g/s and over 210 g/s after heavy rain events with a mean of 22.5 g/s. The exceptionally dry summer 2018 shows clearly the lowest discharge values and accordingly the lowest bicarbonate flux. Table 7 gives an overview of the previously mentioned parameters for different time periods.

Table 8: Overview of the values for mean discharge, mean EC, mean bicarbonate, mean bicarbonate flux and rainfall for different time periods.

Time	mean discharge [L/s]	mean EC [µS/cm]	mean HCO$_3^-$ [mg/L]	mean HCO$_3^-$ - flux [g/s]	sum rainfall [mm]
total period	237	168	100	22.5	6284
hydrological year (Nov. 16 – Oct. 17)	335	166	99	38.0	2218
hydrological year (Nov. 17 – Oct. 18)	164	159	94	14.0	1759
low-flow (Nov. 16 - Feb. 17)	137	194	118	24.4	403
low-flow (Nov. 17 - Feb. 18)	197	160	95	18.4	839
low-flow (Nov. 18 - Feb. 19)	20	186	113	2.2	749
snowmelt (March 17 - June 17)	371	158	94	33.9	706
snowmelt (March 18 - June 18)	205	145	85	14.9	389
snowmelt (March 19 - June 19)	254	179	108	18.4	623

The mean discharge is significantly lower for the hydrological year 2017/2018 compared to the hydrological year 2016/2017 because of the dry summer 2018. Accordingly, the rainfall during the hydrological year 2016/2017 was almost 500 mm more compared to 2017/2018. The mean discharge during the snowmelt periods is always greater compared to low-flow periods in autumn and winter. The mean EC is greater during low-flow periods and accordingly the calculated mean bicarbonate concentration is greater during low-flow. Because discharge is always higher during snowmelt, the calculated mean bicarbonate flux is therefore more or less the same. An exception is the low-flow period from November 2018 to February 2019 because of the exceptionally dry summer 2018. The rainfall during the period March 2018 to June 2018 was only 389 mm while during the same periods in the year 2017 and 2019, the rainfall is two times higher. During this period in 2018, the mean discharge is as low as 20 L/s and accordingly the mean bicarbonate flux is also very low.

For the time periods August – November 2016, August – November 2017 and August – October 2018 (used for modelling and not influenced by snow melt), cross-correlations were calculated to compare rainfall with the discharge and EC behavior of the investigated spring (Fig. 5). Highest correlation was found for rainfall vs. discharge with a time lag of 5.5 hours. Negative correlations were calculated for rainfall vs. EC and for discharge vs. EC. The time lag for rainfall vs. EC is 8.5 hours while the time shift for discharge vs. EC is 3.0 hours. This means that discharge starts to rise 5.5 hours after the rain event and EC starts to decrease about 8 h after the rain event. The time lag between increase of discharge and decrease of EC likely results from a hydraulic pressure pulse, also known as piston effect (Ravbar et al., 2011). These results also coincide with the results obtained from the tracer tests, where time of first detection was 8.5 hours after the injection.
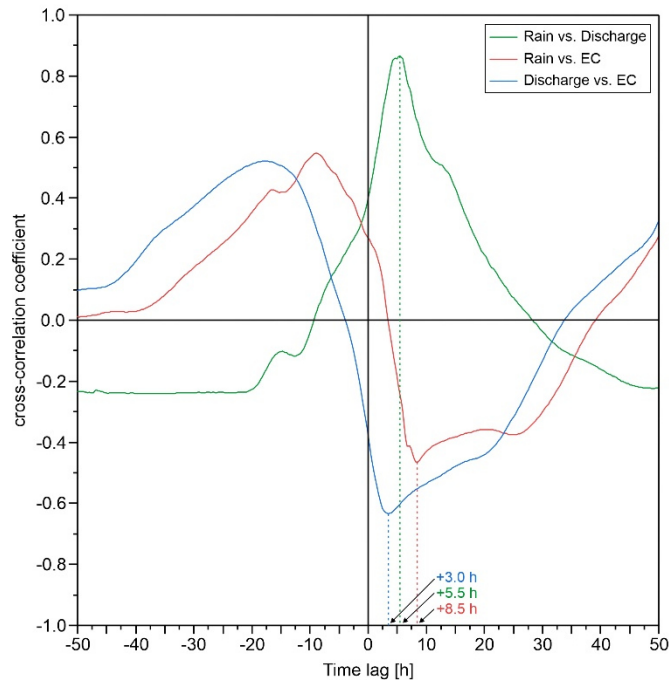
Figure 29: Cross correlation between time series of rainfall, discharge and electrical conductivity (for the same time periods that were used for modelling. There is a slight time lag of a few hours between each correlation.

5.3.2 Denudation rates and carbonate rock weathering

By using hydrochemical and discharge data, the flux of atmospheric CO_2 consumed in carbonate rock weathering can be estimated using formula 5. The CO_2 sink was calculated for different time periods, given in Table. 2. During the three investigated low-flow periods (November 2016 – February 2017, November 2017 – February 2018, November 2018 – February 2019) the CO_2 sink varies between 3.7 and 31.3 t a^{-1} km^{-2}. The very low value of 3.7 t a^{-1} km^{-2} is again related to the very dry summer 2018. Accordingly, the estimated transient CO_2 sink for the investigated karst plateau is between 25.2 and 212.8 t a^{-1} during low-flow. For the snowmelt periods (March 2017 – June 2017, March 2018 – June 2018 and March 2019 – June 2019) the CO_2 sink varies between 29.1 and 58.3 t a^{-1} km^{-2}. Again, the lowest value is related to the dry summer 2018. For the whole karst plateau, the transient CO_2 sink is between 197.9 and 396.4 t a^{-1}. during snowmelt. For the whole investigation period, the calculated atmospheric CO2 sink is 39.7 t a^{-1} km^{-2} which means 270 t a^{-1} for the entire karst plateau.

Table 2 gives an overview of the relevant parameters for the calculation of the CO_2 sink.

These values show that the investigated karst system contributes to the atmospheric CO_2 sink, at least on relatively short time scales.

Table 9: Relevant parameters and the calculated CO2 sink. For comparison, values for the Tsanfleuron-Sanetsch area (mean values for one hydrological year, Zeng et al., 2012) and South China and North China (Liu & Zhao, 1999) are given.

Test site	Time period	Area [km²]	HCO$_3^-$ concentration [g/L]	runoff module [L s^{-1}km^{-2}]	atmospheric CO$_2$ sink [t a^{-1}km^{-2}]
	total period	6.8	0.100	34.9	39.7
	hyd. year (Nov. 16 – Oct. 17)	6.8	0.099	49.3	55.5
	hyd. year (Nov. 17 – Oct. 18)	6.8	0.094	24.1	25.8
	Nov. 16 - Feb. 17	6.8	0.118	20.1	27.0
Disnergschroef (A)	Nov. 17 - Feb. 18	6.8	0.095	29.0	31.3
	Nov. 18 - Feb. 19	6.8	0.113	2.9	3.7
	March 17 - June 17	6.8	0.094	54.6	58.3
	March 18 - June 18	6.8	0.085	30.1	29.1
	March 19 - June 19	6.8	0.108	37.4	45.9

Other studies of the atmospheric CO$_2$ sink in alpine regions also found that the CO$_2$ sink is about four times higher in the melting season compared to the freezing season, because the effect of higher flow rates overrides the effect of lower bicarbonate concentrations (Zeng et al., 2012). Our study also shows higher values during the melting season but approximately only two times higher compared to low-flow periods. Other studies also showed that CO$_2$ consumption by chemical weathering is highly sensitive to climate change, especially to changes in precipitation, temperature and runoff patterns (Hartmann, 2009), which is especially important for the alpine region and can be seen during the dry summer period in 2018 in this study.

In addition to the CO$_2$ sink, the denudation rates for calcite and dolomite in the investigated system were also calculated, assuming that pure calcite and pure dolomite occur as a mixture in the aquifer. The denudation rate is considered as the rate of lowering of a karst surface due to the chemical dissolution of bedrocks (Gabrovšek, 2009). Kaufmann and Braun (2002) showed that denudation processes result in a landscape evolution almost twice as effective as the purely erosional evolution of an insoluble landscape. Denudation rates depend on climatic, lithological and structural factors (Gabrovšek, 2009). Input parameters are the mean Ca^{2+} concentration (15 individual measurements) with 21.1 mg/L and the mean Mg^{2+} concentration (15 individual measurements) with 9.9 mg/L. The denudation rates were calculated for the hydrological year 2016/2017 and for the hydrological year 2017/2018. The assumed runoff was 335 L/s (2016/2017) and 164 L/s (2017/2018) respectively and the recharge area is 6.8 km². The density of pure calcite is 2.7 t/m³ and 2.9 t/m³ for pure dolomite.

Approximately 126 t/a of calcite are removed from the system by dissolution, which equals a calcite denudation rate of 6.9 mm/1000 years. Some 794 t/a of dolomite are removed from the system annually, which means a denudation rate of 40.2 mm/1000 a. In total, the calculated denudation rate for the carbonate rocks in the investigated system is therefore 47.1 mm/1000 a, calculated with values of the hydrological year 2016/2017. With values of the following

hydrological year, 62 t/a of calcite and 389 t/a of dolomite are removed from the system, which equals a denudation rate of 3.4 mm/1000 a for calcite and 19.7 mm/1000 a for dolomite. In total, the denudation rate for carbonate rocks is 23.1 mm/1000 a.

The main factors affecting denudation rates are climate (infiltration, temperature and the amount of CO_2 available) and lithology (Dreybrodt, 1988; Appelo and Postma, 2005; Gabrovšek, 2009). The denudation rates, calculated in other studies, vary between 4 and 193 mm/1000 a (Fig. 30).
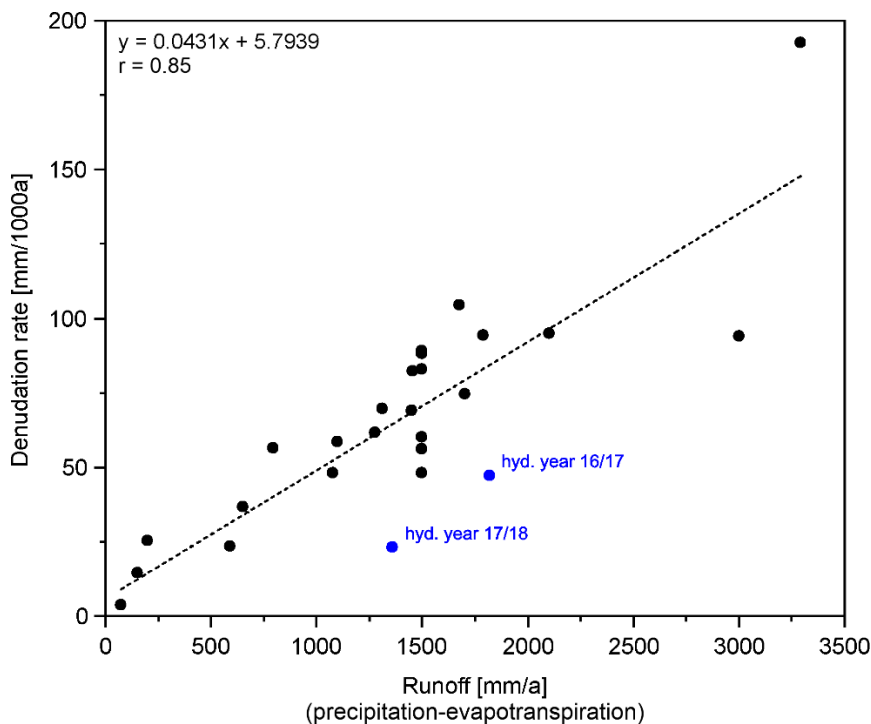
Figure 30: Relation between denudation rate of carbonate rocks and runoff. Data from Bakalowicz (1979), Gams (2004), Gunn (1981), Kunaver (1979), Plan (2005), Yoshimura & Inokura (1997), White (1984).

The relation between the denudation rate of carbonate rocks and runoff (Fig. 30) clearly reflects the sensitivity of denudation and carbonate rock weathering from the runoff change. The larger the runoff, the more intensive is the carbonate rock weathering and denudation. The calculated values from the investigated system are about 40 to 60 % lower compared to expected values (Fig. 30). The reason for that might be either the quite low mean annual temperature in this area or the general geological situation. The rocks in the study area are described as dolomite/limestone formation while the majority is less soluble dolomite.

5.3.3   Modelling Results with KarstMod

The model has been calibrated and validated for the outlet of the karst plateau (QGA) using hourly data for discharge and rainfall. The observed and modelled discharge together with the rainfall during the investigation period are given in Fig. 31a and 31c. Time periods not influenced by snowmelt were chosen (August-November 2016 and 2017, August – October 2018), in order to

reduce the uncertainty of the model introduced by snowmelt and to simulate the direct reaction to rainfall events.
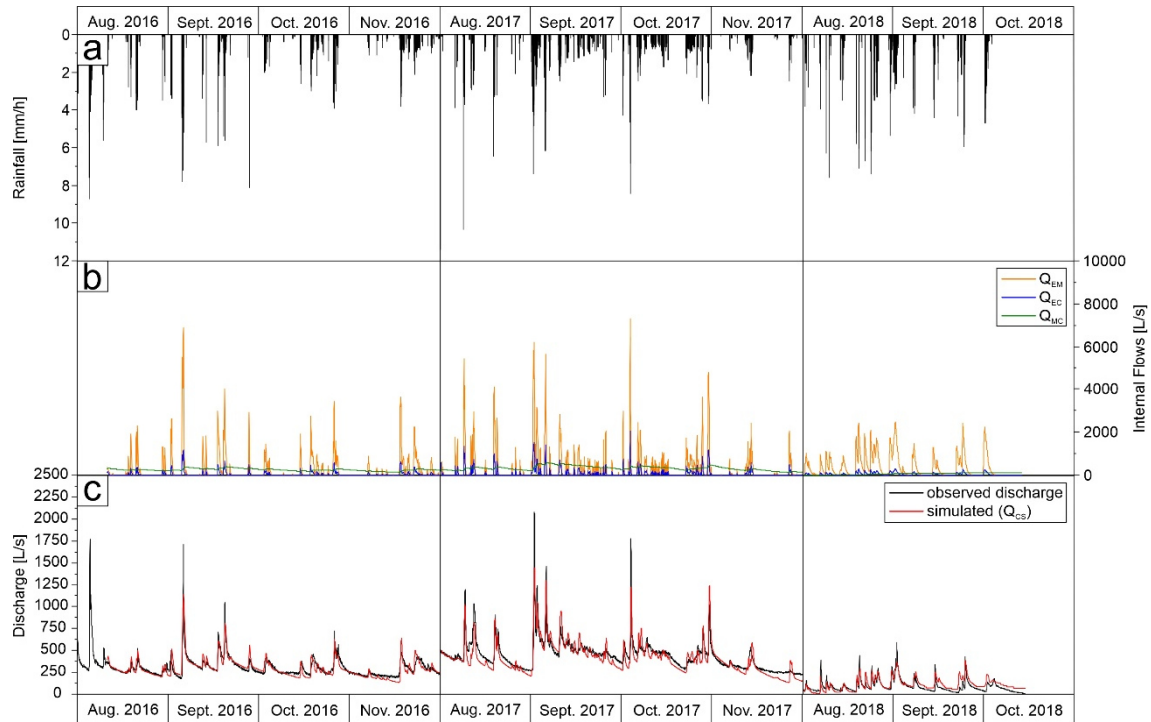

Figure 31: a) Rainfall during the investigation periods in 2016, 2017 and 2018, together with b) the internal flows between the different compartments and c) observed and simulated discharge values for the respective time period.

According to the performance criteria (Tab. 9) and the shape of the simulated discharge curve, the model shows a good fit to the observed data. The NSE is 0.83 for the calibration period and 0.76 for the validation period. The BE is close to 1 for both, the calibration period and the validation period. The objective function gives values of 0.85 for the calibration period and 0.79 for the validation period. These performance values are similar to those from other studies using KarstMod (e.g. Baudement et al., 2017; Poulain et al., 2018; Sivelle et al., 2019).

The optimum value determined for the recharge area is 6.9 km². This modelling result confirms the delineation of the recharge area by geographical and geological information (6.8 km², see Fig. 2b) and also demonstrates that the karst system is mainly drained by the investigated QGA spring.

Table 10: Performance of the model for calibration and validation period (NSE = Nash Sutcliff Efficiency, BE = Balance Error, Wobj = Objective function).

Performance criteria	Calibration period	Validation period
NSE	0.83	0.76
BE	0.99	0.99
$W_{obj} = 0.9NSE + 0.1BE$	0.85	0.79

All simulations (10000) with a performance criteria Wobj > 0.8 are graphically represented in figure 8. For each parameter calibrated, a scatterplot of the values of the objective function

(calibration period) against the values of the parameter is given. Based on a equifinality analysis, these plots show that the model has found an optimum for the calibration. The parameter set associated with the highest performance criteria was kept and used to draw the simulated discharge curve given in figure 31.
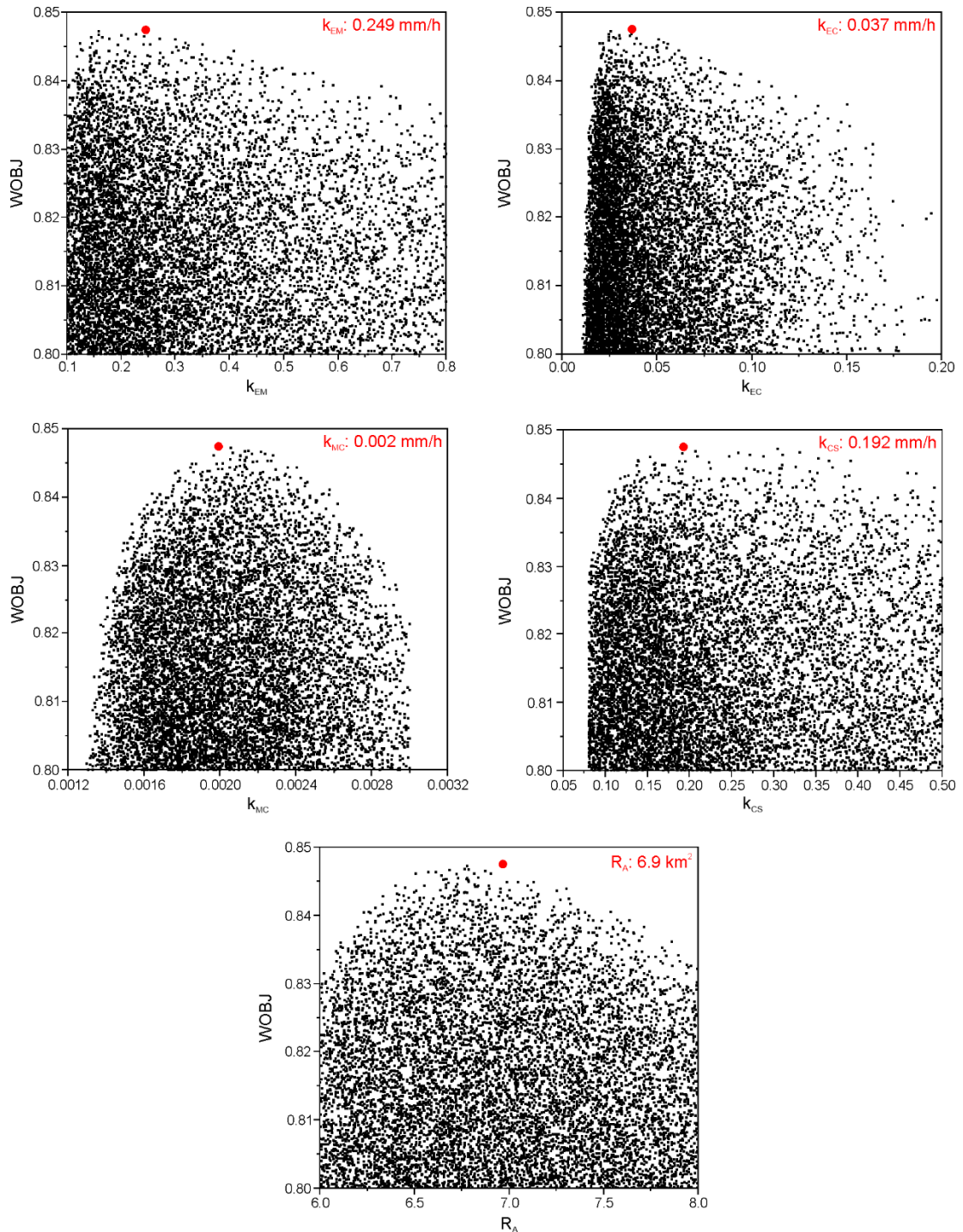

Figure 32: Analysis of the sensitivity of the input parameters of the rainfall-discharge model with a Monte-Carlo procedure. Wobj = objective function. The best fit with the objective function chosen is marked with a red dot and the respective value is given for each parameter.

In addition, table 10 gives the first-order and total-effect sensitivity indices. The total-effect index indicates the overall sensitivity of the model performance (assessed by the objective function) to the parameters, within the previously user-defined range of variations. The most sensitive parameters are k_{MC}, R_A and k_{EC}, while the least sensitive parameters are k_{EM} and k_{CS}.

Table 11: Sensitivity indices (first-order index and total-effect index).

Parameter	first-order index (S_i)	total-effect index (S_{Ti})
k_{MC}	0.58	0.66
R_A	0.08	0.16
k_{EC}	0.11	0.15
k_{EM}	0.08	0.10
k_{CS}	0.07	0.07

Considering the internal flow dynamics of a karst aquifer is important to quantify potential pollution but also to predict and manage spring discharge scenarios regarding climate change. Figure 7b gives an overview of the internal flows between the different compartments of the KarstMod model.

The flow from compartment E (epikarst) to compartment C (conduit) is highly variable, depending on the input signal (rainfall). The highest internal flow with the highest variability (also depending on the input signal) occurs between E and M (matrix). Internal flow from M to C is more or less constant for the whole investigation period with only slight increases directly after rainfall events, when the whole water level in the system rises. The matrix acts as a buffer and a storage for water and slowly releases the water into the conduits and thence to the spring (Fig 31b). Matrix storage is therefore particularly important for the discharge of the spring during low-flow periods (baseflow).

This modelling result also matches the geological setting in the investigated system, where the Main Dolomite-Limestone formation is several hundred meters thick and outlines the importance of the matrix-storage for the whole aquifer.

A conceptual model of the internal flow dynamics inside the investigated system is given in Figure 33.

Other models of karst aquifers (e.g. Chen and Goldscheider, 2014; Baudement et al., 2017; Lončar et al., 2018) also show that the resulting hydrographs are composed of rapid-flow and slow-flow components (baseflow, M→C) as described by, for example, Ford and Williams (2007). Different amounts of internal flows in other studies are presumably the result of different structures (lithology, thickness etc.) of the respective aquifers.
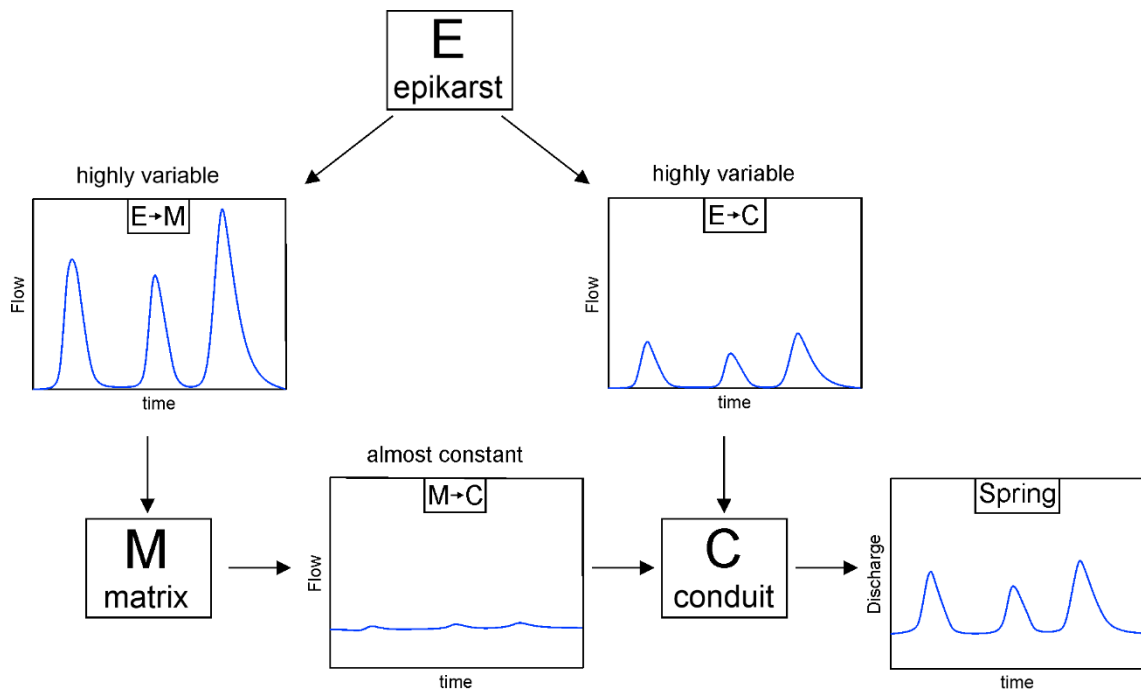
Figure 33: Conceptual model of the flow dynamics inside the investigated karst aquifer. E→C = flow from compartment E to C, E→M = flow from compartment E to M and M→C = flow from compartment M to C and spring discharge.

5.4   Conclusion

With these investigations in a high alpine karst system with a clearly defined catchment, we obtained new and improved knowledge about the dynamic water and mass balances of alpine karst systems.

Tracer tests show that the investigated karst plateau has only one major spring as outlet. The surface catchment area of this spring is about 6.8 km² which was also confirmed by the KarstMod model (6.9 km²).

While the observed discharge values show a rapid and marked increase after rainfall events, the recorded specific electrical conductivity values decrease accordingly. Measured and calculated bicarbonate values react the same way to rainfall events as EC. The bicarbonate-EC relation illustrates that bicarbonate is the major anion as the karst system consists of a mixture of limestone and dolomite. The calculated bicarbonate flux at the investigated spring QGA varies between 1 and over 210 g/s.

The calculated value for the atmospheric CO_2 sink for the Disnergschroef area is 39.7 t a^{-1} km^{-2} (mean value for the whole investigation period). This value is lower compared to areas with pure limestone outcrops e.g. in southern and northern China. However, there is still a significant contribution of carbonate rock weathering to the transient atmospheric CO_2 sink in the study area. Results of this study also show that the melting period contributes more to the CO_2 sink then low-flow conditions, because the higher discharge overrides the lower bicarbonate concentrations as

also shown by Zeng et al. (2012). Nevertheless, future research is needed to evaluate the effect of the CO_2 sink in longer time scales (e.g. CO_2 degassing again from the river back to the atmosphere) or if this effect permanently removes CO_2 from the atmosphere.

The calculated denudation rate for carbonate rocks in our study site is between 23.1 mm/1000 a and 47.1 mm/1000 a, which is slightly lower compared to other studies of karst areas in Europe (e.g. Plan, 2005). The reason for this might be different climatic and geological conditions.

Within this study, a reservoir model, based on KarstMod, has been applied to the Disnergschroef karst system. Based on this model, the internal flow dynamics of the karst system and the reaction of the system to rainfall events could be described. The simulated discharge curve shows a good fit to the measured discharge curve. Furthermore, the performance criteria of the model compared to the measured discharge values show that KarstMod is a valuable tool to simulate the discharge behavior of the investigated spring in response to rainfall events. The model also gives information about the internal flows between the different model compartments. The highest variability of the internal flow was observed between Epikarst and Matrix, while the flow from Matrix to Conduits is almost constant and is responsible for the observed baseflow at the spring. This demonstrates the importance of the matrix as water storage especially during dry conditions.

Future KarstMod model applications in alpine regions should consider snowmelt periods and should couple runoff models with mass transport models, e.g. to simulate the CO_2 sink of karst areas. These kinds of models and the information obtained can be of major interest for the management of karst springs, especially in regard to flood events occurring after heavy rainfall events, and also to assess the effects of climate change in alpine areas.

Acknowledgments

Chapter 6

6   Conclusion and Outlook

6.1   General Overview

A profound understanding of karst aquifer systems is of special importance especially regarding the sustainable management of karst water resources. High alpine karst areas offer an enormous potential for future water supply, but because of the remoteness and special climatic effects, the understanding of the functioning of these high alpine karst aquifers is even more important for a proper and sustainable management.

In this thesis, new innovative methods and approaches were applied, to characterize different high alpine karst systems in the Lechquellengebirge in Vorarlberg, Austria.

In order to study and to quantify conduit-matrix interaction, which is an often described process in karst systems, a high resolution hydrochemical monitoring was used. A quantitative description of this process was possible in the investigated system because of its special geological situation. By applying mixing calculations the results of this study show the importance of the matrix as a water storage, especially during low-flow periods. The results allow a better description of the aquifer behaviour during low-flow and high-flow conditions.

A typical challenge in karst systems are the strong water quality fluctuations, especially after rain events. Contamination events occur because of the special characteristics of karst aquifers (high variability of flow and transport) as described in chapter 1. To examine the correlations between physicochemical parameters, particles, faecal bacteria and natural fluorescence, a high-resolution monitoring was conducted at two karst springs. After rainfall events two turbidity peaks and at the same time two peaks of the small particle fractions were observed. At the time of the secondary peak, a high correlation between small particles, conventional cultivation based determinations of faecal bacteria and tryptophan-like fluorescence was found. As a result, tryptophan-like fluorescence can act as a real-time indicator of *E. coli* and together with the analysis of the particle-size distribution can act as an early warning system for faecal contamination.

In study two, tryptophan showed a good correlation to coliform and faecal bacteria, but the transport behaviour and transport properties were still insufficiently known. An artificial tracer test was conducted in a small epikarst system to compare the transport behaviour of tryptophan and humic acid with an almost ideal conservative tracer uranine. The breakthrough curves and the determined results indicate an almost identical behaviour of uranine and tryptophan, while the humic acid tracer showed retardation processes.

In chapter 5, a karst system, which has a clearly defined catchment and only one spring as major outlet of the whole system, was investigated. We used the software package KarstMod to simulated the rainfall-discharge behaviour of the investigated spring and to simulate and calculate the respective contributions of the conduits and of the matrix to the spring discharge. The modelling results indicate the importance of the matrix as a water storage, especially during low-flow conditions. For this karst system, the hydrochem-discharge method (Liu & Zhao, 2000) was used, to calculate the contribution of the investigated karst system to the atmospheric CO_2 sink. The results and the comparison to other karst areas show, that the investigated system contributes to the transient atmospheric CO_2 sink, which is an important aspect regarding climate change.

6.2   Perspective and Outlook

- **Refining of the hydrogeological conceptual models**

The development of hydrogeological conceptual models was necessary for all investigated karst aquifers in this study, to gain a proper understanding of the functioning. In all systems, natural tracers (e.g. stable isotopes, natural fluorescence) but also artificial tracers could help to assess the groundwater transit-time distribution and flow components in the respective system. The results could help to refine the previous developed hydrogeological conceptual models and also to check the results obtained from modelling.

- **Improved hydrological and hydrochemical monitoring**

The hydrochemical sampling for all investigated karst systems could be extended to longer time periods and especially to time periods where snow-melt occurs in order to assess and better understand the influence of snow melt water, especially for the matrix storage. Moreover, more detailed rainfall data, directly from the investigated catchments would deliver more precise input data, especially for the modelling procedures. Radar data of the precipitation could also be used after a calibration and validation with ground based weather stations. Another important factor, especially for modelling is the evapotranspiration, where more detailed data might especially improve the modelling results.

- **Improved fluorescence monitoring of natural compounds**

Current instruments allow the online monitoring of the most important natural fluorescence compounds at springs (e.g. GGUN-FL30, Albillia Co) which can be equipped with special optics e.g. for tryptophan-like fluorescence measurements. Artificial tracers (e.g. uranine) can also be measured in real-time with these devices. Until now, especially the sources of these natural fluorescence compounds in the catchments are not fully clear. A monitoring of the input water

e.g. at sinking streams could help to understand the development of the fluorescence compounds in the aquifer.

- **Using distributed karst catchment models (together with regional climate models)**

More complex, distributed karst models, could be used in the investigated systems to obtain more detailed spatially distributed information about the karst systems. The model, developed by Chen & Goldscheider (2014) which was applied to a complex folded alpine karst system in Austria could also be applied to the investigated karst systems in the Lechquellengebirge. For the prediction of the behaviour of the karst systems in the future with respect to climate change, the climatic input data are of special importance. As also advised by Chen (2017) precipitation and temperature time series should be downscaled from regional climate models to study and predict the dynamics of water fluxes and storages within the studied catchments.

6.3   Transferability aspects

The section of the World Karst Aquifer Map (WOKAM, Fig. 31) shows the high proportion of carbonate rocks, especially in the northern calcareous Alps. These wide areas, dominated by karst with similar characteristics to those investigated in this thesis, offer an enormous potential for future water supply but face similar challenges in terms of water quantity and quality.

Figure 34: Extract of the World Karst Aquifer Map (WOKAM, Chen et al., 2017) to illustrate the appearance of karst areas in the European Alps.

The applied approaches and methods used in this thesis, including tracer tests, hydrochemical investigations, on-site monitoring of water quality by using parameters like natural fluorescence, particle-size distribution and analysis of faecal indicator bacteria by using standard cultivation-

based methods (e.g. Idexx Colisure) are valuable tools to study such alpine karst aquifers, even in remote areas with restricted infrastructure.

In view of climate change and the increasing water demand in many areas, the sustainable use and management of karst water resources will become more important and will require more specific and more detailed investigations of karst aquifers.

Some useable investigation approaches for mountaineous karst aquifers were presented in this thesis and are easily transferable to other mountaineous karst aquifers. The obtained information are valuable in order to improve the understanding of the functioning of alpine karst aquifers and also to improve the usage and management of these aquifers.

Acknowledgments

Declaration of authorship

Study 1

Citation: Frank S, Goeppert N, Ohmer M, Goldscheider N (2019) Sulfate variations as a natural tracer for conduit-matrix interaction in a complex karst aquifer, Hydrological Processes, 33, 1292-1303, doi 10.1002/hyp.13400.

Declaration of authorship: Simon Frank (SF) and Marc Ohmer gathered the data, which were evaluated in consultation with Nadine Goeppert and Nico Goldscheider. SF wrote the manuscript. The manuscript was reviewed and edited by all authors.

Study 2

Citation: Frank S, Goeppert N, Goldscheider, N (2018) Fluorescence-based multi-parameter approach to characterize dynamics of organic carbon, faecal bacteria and particles at alpine karst springs, Science of the Total Environment, 615, 1446-1459, doi 10.10.16/j.scitotenv.2017.09.095.

Declaration of authorship: Simon Frank (SF) conducted the monitoring at the three springs and evaluated the data in consultation with Nadine Goeppert and Nico Goldscheider. SF wrote the manuscript which was reviewed and edited by all authors.

Study 3
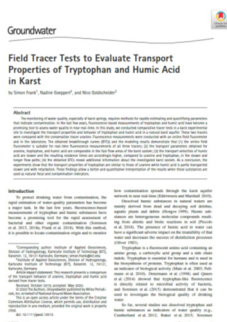
Citation: Frank S, Goeppert N, Goldscheider N (2020) Field Tracer Tests to Evaluate Transport Properties of Tryptophan and Humic Acid in Karst, Groundwater.
doi: 10.1111/gwat.13015

Declaration of authorship: Simon Frank (SF) performed the tracer tests and evaluated the data in consultation with Nadine Goeppert and Nico Goldscheider. SF wrote the manuscript. The manuscript was reviewed and edited by all authors.

Study 4

Citation: Frank S, Goeppert N, Goldscheider N (2019) Dynamic water and mass budget of an alpine karst catchment, Hydrogeology Journal, (submitted).

Declaration of authorship: Simon Frank (SF) gathered the data, which were evaluated together with Nadine Goeppert and Nico Goldscheider. SF wrote the manuscript. All authors reviewed and edited the manuscript.

References

Aklujkar, M., Risso, C., Smith, J., Beaulieu, D., Dubay, R., Giloteaux, L., DiBurro, K., Holmes, D., 2014. Anaerobic degradation of aromatic amino acids by the hyperthermophilic archaeon Ferroglobus placidus. Microbiology 160, 2694–2709. https://doi.org/10.1099/mic.0.083261-0

Andreo, B., Gil-Márquez, J.M., Mudarra, M., Linares, L., Carrasco, F., 2016. Hypothesis on the hydrogeological context of wetland areas and springs related to evaporitic karst aquifers (Málaga, Córdoba and Jaén provinces, Southern Spain). Environmental Earth Sciences 75, 759. https://doi.org/10.1007/s12665-016-5545-1

Appelo, C.A.J., Postma, D., 2005. Geochemistry, groundwater and pollution. A.A. Balkema, Amsterdam.

Ashton, K., 1966. The Analysis of Flow Data from Karst Drainage Systems, Transactions of the Cave Research Group of Great Britain.

Atkinson, T.C., 1977. Diffuse flow and conduit flow in limestone terrain in the Mendip Hills, Somerset (Great Britain). Journal of Hydrology 35, 93–110. https://doi.org/10.1016/0022-1694(77)90079-8

Bakalowicz, M., 2005. Karst groundwater: a challenge for new resources. Hydrogeology Journal 13, 148–160. https://doi.org/10.1007/s10040-004-0402-9

Bakalowicz, M., 1979. Contribution de la géochimie des eaux à la connaissance de l'aquifère karstique et de la karstification. Univ. P. et M. Curie, Paris V, 269p.

Baker, A., 2005. Thermal fluorescence quenching properties of dissolved organic matter. Water Research 39, 4405–4412. https://doi.org/10.1016/j.watres.2005.08.023

Baker, A., Cumberland, S.A., Bradley, C., Buckley, C., Bridgeman, J., 2015. To what extent can portable fluorescence spectroscopy be used in the real-time assessment of microbial water quality? Science of The Total Environment 532, 14–19. https://doi.org/10.1016/j.scitotenv.2015.05.114

Baker, A., Genty, D., 1999. Fluorescence wavelength and intensity variations of cave waters. Journal of Hydrology 217, 19–34. https://doi.org/10.1016/S0022-1694(99)00010-4

Baker, A., Lamont-Black, J., 2001. Fluorescence of dissolved organic matter as a natural tracer of ground water. Ground Water 39, 745–750.

Ban, F., Pan, G., Zhu, J., Cai, B., Tan, M., 2008. Temporal and spatial variations in the discharge and dissolved organic carbon of drip waters in Beijing Shihua Cave, China. Hydrological Processes 22, 3749–3758. https://doi.org/10.1002/hyp.6979

Barberá, J.A., Andreo, B., 2015. Hydrogeological processes in a fluviokarstic area inferred from the analysis of natural hydrochemical tracers. The case study of eastern Serranía de Ronda (S Spain). Journal of Hydrology 523, 500–514. https://doi.org/10.1016/j.jhydrol.2015.01.080

Barbieri, M., Nigro, A., Petitta, M., 2017. Groundwater mixing in the discharge area of San Vittorino Plain (Central Italy): geochemical characterization and implication for drinking uses. Environmental Earth Sciences 76, 393. https://doi.org/10.1007/s12665-017-6719-1

Batiot, C., Liñán, C., Andreo, B., Emblanch, C., Carrasco, F., Blavoux, B., 2003. Use of Total Organic Carbon (TOC) as tracer of diffuse infiltration in a dolomitic karstic system: The Nerja Cave (Andalusia, southern Spain): TOC as a tracer of diffuse infiltration. Geophysical Research Letters 30. https://doi.org/10.1029/2003GL018546

Baudement, C., Arfib, B., Mazzilli, N., Jouves, J., Lamarque, T., Guglielmi, Y., 2017. Groundwater management of a highly dynamic karst by assessing baseflow and quickflow with a rainfall-discharge model (Dardennes springs, SE France). Bulletin de la Société géologique de France 188, 40. https://doi.org/10.1051/bsgf/2017203

Behrens, H., Beims, U., Dieter, H., Dietze, G., Eikmann, T., Grummt, T., Hanisch, H., Henseling, H., Käß, W., Kerndorff, H., Leibundgut, C., Müller-Wegener, U., Rönnefahrt, I., Scharenberg, B., Schleyer, R., Schloz, W., Tilkes, F., 2001. Toxicological and ecotoxicological assessment of water tracers. Hydrogeology Journal 9, 321–325. https://doi.org/10.1007/s100400100126

Berkowitz, B., Cortis, A., Dentz, M., Scher, H., 2006. Modeling non-Fickian transport in geological formations as a continuous time random walk. Reviews of Geophysics 44, RG2003. https://doi.org/10.1029/2005RG000178

Beven, K., Binley, A., 1992. The future of distributed models: Model calibration and uncertainty prediction. Hydrological Processes 6, 279–298. https://doi.org/10.1002/hyp.3360060305

Birdwell, J.E., Engel, A.S., 2009. Variability in Terrestrial and Microbial Contributions to Dissolved Organic Matter Fluorescence in the Edwards Aquifer, Central Texas. Journal of Cave and Karst Studies 71, 2, 144-156.

Birk, S., Liedl, R., Sauter, M., 2004. Identification of localised recharge and conduit flow by combined analysis of hydraulic and physico-chemical spring responses (Urenbrunnen, SW-Germany). Journal of Hydrology 286, 179–193. https://doi.org/10.1016/j.jhydrol.2003.09.007

Boulton, A.J., Datry, T., Kasahara, T., Mutz, M., Stanford, J.A., 2010. Ecology and management of the hyporheic zone: stream–groundwater interactions of running waters and their floodplains. Journal of the North American Benthological Society 29, 26–40. https://doi.org/10.1899/08-017.1

Butscher, C., Huggenberger, P., 2008. Intrinsic vulnerability assessment in karst areas: A numerical modeling approach: Vulnerability. Water Resources Research 44. https://doi.org/10.1029/2007WR006277

Butturini, A., Ejarque, E., 2013. Technical Note: Dissolved organic matter fluorescence – a finite mixture approach to deconvolve excitation-emission matrices. Biogeosciences 10, 5875–5887. https://doi.org/10.5194/bg-10-5875-2013

Carucci, V., Petitta, M., Aravena, R., 2012. Interaction between shallow and deep aquifers in the Tivoli Plain (Central Italy) enhanced by groundwater extraction: A multi-isotope approach and geochemical modeling. Applied Geochemistry 27, 266–280. https://doi.org/10.1016/j.apgeochem.2011.11.007

Chen, H., Kenny, J.E., 2007. A Study of pH Effects on Humic Substances Using Chemometric Analysis of Excitation-Emission Matrices. Annals of Environmental Science 1, 1-9.

Chen, W., Westerhoff, P., Leenheer, J.A., Booksh, K., 2003. Fluorescence Excitation−Emission Matrix Regional Integration to Quantify Spectra for Dissolved Organic Matter.

Environmental Science and Technology 37, 5701–5710. https://doi.org/10.1021/es034354c

Chen, Z., 2017. Modeling a geologically complex karst aquifer system, Hochifen-Gottesacker, Alps, Karlsruhe Institute of Technology, Dissertation, 138p.

Chen, Z., Auler, A.S., Bakalowicz, M., Drew, D., Griger, F., Hartmann, J., Jiang, G., Moosdorf, N., Richts, A., Stevanovic, Z., Veni, G., Goldscheider, N., 2017. The World Karst Aquifer Mapping project: concept, mapping procedure and map of Europe. Hydrogeology Journal 25, 771–785. https://doi.org/10.1007/s10040-016-1519-3

Chen, Z., Goldscheider, N., 2014. Modeling spatially and temporally varied hydraulic behavior of a folded karst system with dominant conduit drainage at catchment scale, Hochifen–Gottesacker, Alps. Journal of Hydrology 514, 41–52. https://doi.org/10.1016/j.jhydrol.2014.04.005

Coble, P.G., 1996. Characterization of marine and terrestrial DOM in seawater using excitation-emission matrix spectroscopy. Marine Chemistry 51, 325–346. https://doi.org/10.1016/0304-4203(95)00062-3

Coble, P.G., Green, S.A., Blough, N.V., Gagosian, R.B., 1990. Characterization of dissolved organic-matter in the Black-Sea by fluorescence spectroscopy. Nature 432–435.

Coble, P.G., Lead, J., Baker, A., Reynolds, D.M., Spencer, R.G.M., 2014. Aquatic Organic Matter Fluorescence 408.

Cornaton, F., Perrochet, P., 2002. Analytical 1D dual-porosity equivalent solutions to 3D discrete single-continuum models. Application to karstic spring hydrograph modelling. Journal of Hydrology 262, 165–176. https://doi.org/10.1016/S0022-1694(02)00033-1

Cumberland, S., Bridgeman, J., Baker, A., Sterling, M., Ward, D., 2012. Fluorescence spectroscopy as a tool for determining microbial quality in potable water applications. Environmental Technology 33, 687–693. https://doi.org/10.1080/09593330.2011.588401

Determann, S., Lobbes, J.M., Reuter, R., Rullkötter, J., 1998. Ultraviolet fluorescence excitation and emission spectroscopy of marine algae and bacteria. Marine Chemistry 62, 137–156. https://doi.org/10.1016/S0304-4203(98)00026-7

DIN 38402-61, 2014. Deutsche Einheitsverfahren zur Wasser-, Abwasser- und Schlammuntersuchung – Allgemeine Angaben (Gruppe A) – Teil 62: Plausibilitätskontrolle von Analysendaten durch Ionenbilanzierung (A 62); German standard methods for the examination of water, waste water and sludge – General information (group A) – Part 62: Plausibility check of analytical data by performing an ion balance (A 62).

Dobler, C., Bürger, G., Stötter, J., 2013. Simulating future precipitation extremes in a complex Alpine catchment. Natural Hazards and Earth System Sciences 13, 263–277. https://doi.org/10.5194/nhess-13-263-2013

Dreybrodt, W., 1990. The Role of Dissolution Kinetics in the Development of Karst Aquifers in Limestone: A Model Simulation of Karst Evolution. The Journal of Geology 98, 639–655. https://doi.org/10.1086/629431

Dreybrodt, W., 1988. Processes in karst systems: physics, chemistry and geology. Springer, Berlin, New York.

DVWK, 1996. Ermittlung der Verdunstung von Land- und Wasserflächen.

Ediriweera, D.D., Marshall, I.W., 2010. Monitoring water distribution systems: understanding and managing sensor networks. Drinking Water Engineering and Science 3, 107–113. https://doi.org/10.5194/dwes-3-107-2010

Elliott, S., Lead, J.R., Baker, A., 2006. Characterisation of the fluorescence from freshwater, planktonic bacteria. Water Research 40, 2075–2083. https://doi.org/10.1016/j.watres.2006.03.017

Ender, A., Goeppert, N., Goldscheider, N., 2018. Spatial resolution of transport parameters in a subtropical karst conduit system during dry and wet seasons. Hydrogeology Journal 26, 2241–2255. https://doi.org/10.1007/s10040-018-1746-x

Ender, A., Goeppert, N., Grimmeisen, F., Goldscheider, N., 2017. Evaluation of β- d-glucuronidase and particle-size distribution for microbiological water quality monitoring in Northern Vietnam. Science of The Total Environment 580, 996–1006. https://doi.org/10.1016/j.scitotenv.2016.12.054

Fellman, J.B., Hood, E., D'Amore, D.V., Edwards, R.T., White, D., 2009. Seasonal changes in the chemical quality and biodegradability of dissolved organic matter exported from soils to streams in coastal temperate rainforest watersheds. Biogeochemistry 95, 277–293. https://doi.org/10.1007/s10533-009-9336-6

Fellman, J.B., Hood, E., Spencer, R.G.M., 2010. Fluorescence spectroscopy opens new windows into dissolved organic matter dynamics in freshwater ecosystems: A review. Limnology and Oceanography 55, 2452–2462. https://doi.org/10.4319/lo.2010.55.6.2452

Field, M.S., 1988. The vulnerability of karst aquifers to chemical contamination. U.S. Environmental Protection Agency.

Field, M.S., Pinsky, P.F., 2000. A two-region nonequilibrium model for solute transport in solution conduits in karstic aquifers. Journal of Contaminant Hydrology 44, 3-4, 329-351. https://doi.org/10.1016/S0169-7722(00)00099-1

Filippini, M., Squarzoni, G., De Waele, J., Fiorucci, A., Vigna, B., Grillo, B., Riva, A., Rossetti, S., Zini, L., Casagrande, G., Stumpp, C., Gargini, A., 2018. Differentiated spring behavior under changing hydrological conditions in an alpine karst aquifer. Journal of Hydrology 556, 572-584. https://doi.org/10.1016/j.jhydrol.2017.11.040

Finger, D., Heinrich, G., Gobiet, A., Bauder, A., 2012. Projections of future water resources and their uncertainty in a glacierized catchment in the Swiss Alps and the subsequent effects on hydropower production during the 21st century: Pprojections of Future Water Resources. Water Resources Research 48. https://doi.org/10.1029/2011WR010733

Finger, D., Hugentobler, A., Huss, M., Voinesco, A., Wernli, H., Fischer, D., Weber, E., Jeannin, P.-Y., Kauzlaric, M., Wirz, A., Vennemann, T., Hüsler, F., Schädler, B., Weingartner, R., 2013. Identification of glacial meltwater runoff in a karstic environment and its implication for present and future water availability. Hydrology and Earth System Sciences 17, 3261–3277. https://doi.org/10.5194/hess-17-3261-2013

Fleury, P., Plagnes, V., Bakalowicz, M., 2007. Modelling of the functioning of karst aquifers with a reservoir model: Application to Fontaine de Vaucluse (South of France). Journal of Hydrology 345, 38–49. https://doi.org/10.1016/j.jhydrol.2007.07.014

Ford, D., Williams, P., 2007. Karst Hydrogeology and Geomorphology. John Wiley & Sons, Chichester, 578p.

Frank, S., Goeppert, N., Goldscheider, N., 2018. Fluorescence-based multi-parameter approach to characterize dynamics of organic carbon, faecal bacteria and particles at alpine karst springs. Science of The Total Environment 615, 1446–1459. https://doi.org/10.1016/j.scitotenv.2017.09.095

Frank, S., Goeppert, N., Ohmer, M., Goldscheider, N., 2019. Sulfate variations as a natural tracer for conduit-matrix interaction in a complex karst aquifer. Hydrological Processes 33, 1292–1303. https://doi.org/10.1002/hyp.13400

Friebe, J.G., 2004. Zur Geologie Vorarlbergs - eine Einführung unter besonderer Berücksichtigung verkarstungsfähiger Gesteine. Vorarlberger Naturschau 15, 19–40.

Gabrovšek, F., 2009. On concepts and methods for the estimation of dissolutional denudation rates in karst areas. Geomorphology 106, 9–14. https://doi.org/10.1016/j.geomorph.2008.09.008

Gams, I., 2004. Kras v Sloveniji v prostoru in casu, 515, ZRC Publishing, Ljubljana

Geologische Bundesanstalt, 2007. Geologische Karte von Vorarlberg 1:100000.

Geyer, T., Birk, S., Licha, T., Liedl, R., Sauter, M., 2007. Multitracer Test Approach to Characterize Reactive Transport in Karst Aquifers. Ground Water 45, 36–45. https://doi.org/10.1111/j.1745-6584.2006.00261.x

Ghisaidoobe, A., Chung, S., 2014. Intrinsic Tryptophan Fluorescence in the Detection and Analysis of Proteins: A Focus on Förster Resonance Energy Transfer Techniques. International Journal of Molecular Sciences 15, 22518–22538. https://doi.org/10.3390/ijms151222518

Gilmore, A.M., 2011. Water Quality Measurements with HORIBA Jobin Yvon Fluorescence Instrumentation 8.

Glynn, P.D., Plummer, L.N., 2005. Geochemistry and the understanding of ground-water systems. Hydrogeology Journal 13, 263–287. https://doi.org/10.1007/s10040-004-0429

Goeppert, N., Goldscheider, N., 2019. Improved understanding of particle transport in karst groundwater using natural sediments as tracers. Water Research 166, 115045. https://doi.org/10.1016/j.watres.2019.115045

Goeppert, N., Goldscheider, N., Scholz, H., 2011. Karst geomorphology of carbonatic conglomerates in the Folded Molasse zone of the Northern Alps (Austria/Germany). Geomorphology 130, 289–298. https://doi.org/10.1016/j.geomorph.2011.04.011

Goldscheider, N., 2011. Alpine Hydrogeologie. Grundwasser 16, 1–1. https://doi.org/10.1007/s00767-010-0157-2

Goldscheider, N., 2008. A new quantitative interpretation of the long-tail and plateau-like breakthrough curves from tracer tests in the artesian karst aquifer of Stuttgart, Germany. Hydrogeology Journal 16, 1311–1317. https://doi.org/10.1007/s10040-008-0307-0

Goldscheider, N., 2005a. Fold structure and underground drainage pattern in the alpine karst system Hochifen-Gottesacker. Eclogae Geologicae Helvetiae 98, 1–17. https://doi.org/10.1007/s00015-005-1143-z

Goldscheider, N., 2005b. Karst groundwater vulnerability mapping: application of a new method in the Swabian Alb, Germany. Hydrogeology Journal 13, 555–564. https://doi.org/10.1007/s10040-003-0291-3

Goldscheider, N., Chen, Z., Auler, A.S., Bakalowicz, M., Broda, S., Drew, D., Hartmann, J., Jiang, G., Moosdorf, N., Stevanovic, Z., Veni, G., 2020. Global distribution of carbonate rocks and karst water resources. Hydrogeology Journal 28, 1661–1677. https://doi.org/10.1007/s10040-020-02139-5

Goldscheider, N., Drew, D. (Eds.), 2007. Methods in karst hydrogeology. Taylor & Francis, Leiden ; New York.

Goldscheider, N., Goeppert, N., 2004. Hydrogeologie der alpinen Karstlandschaften Vorarlbergs. Vorarlberger Naturschau 15, 41–62.

Goldscheider, N., Meiman, J., Pronk, M., Smart, C., 2008. Tracer tests in karst hydrogeology and speleology. International Journal of Speleology 37, 27–40. https://doi.org/10.5038/1827-806X.37.1.3

Goldscheider, N., Pronk, M., Zopfi, J., 2010. New insights into the transport of sediments and microorganisms in karst groundwater by continuous monitoring of particle-size distribution. Geologia Croatica 63, 137–142. https://doi.org/10.4154/gc.2010.10

Göppert, N., Goldscheider, N., 2007. Solute and Colloid Transport in Karst Conduits under Low- and High-Flow Conditions. Ground Water 46. https://doi.org/10.1111/j.1745-6584.2007.00373.x

Green, E.A., 1997. Tracing recharge from sinking streams over spatial dimensions of kilometers in a karst aquifer. Groundwater 35, 898–904. https://doi.org/10.1111/j.1745-584.1997.tb00159.x

Gremaud, V., Goldscheider, N., Savoy, L., Favre, G., Masson, H., 2009. Geological structure, recharge processes and underground drainage of a glacierised karst aquifer system, Tsanfleuron-Sanetsch, Swiss Alps. Hydrogeology Journal 17, 1833–1848. https://doi.org/10.1007/s10040-009-0485-4

Gunn, J., 1981. Limestone solution rates and processes in the Waitomo district, New Zealand, Earth Surface Processes and Landforms, 6, 427-445.

Hartmann, A., Barberá, J.A., Lange, J., Andreo, B., Weiler, M., 2013. Progress in the hydrologic simulation of time variant recharge areas of karst systems – Exemplified at a karst spring in Southern Spain. Advances in Water Resources 54, 149–160. https://doi.org/10.1016/j.advwatres.2013.01.010

Hartmann, A., Goldscheider, N., Wagener, T., Lange, J., Weiler, M., 2014. Karst water resources in a changing world: Review of hydrological modeling approaches: Karst Water Resources Prediction. Reviews of Geophysics 52, 218–242. https://doi.org/10.1002/2013RG000443

Hartmann, A., Kralik, M., Humer, F., Lange, J., Weiler, M., 2012. Identification of a karst system's intrinsic hydrodynamic parameters: upscaling from single springs to the whole

aquifer. Environmental Earth Sciences 65, 2377–2389. https://doi.org/10.1007/s12665-011-1033-9

Hartmann, J., 2009. Bicarbonate-fluxes and CO_2-consumption by chemical weathering on the Japanese Archipelago — Application of a multi-lithological model framework. Chemical Geology 265, 237–271. https://doi.org/10.1016/j.chemgeo.2009.03.024

Hilberg, S., Kreuzer, M., 2013. Identification of a deep flow system in a dolomitic alpine aquifer – case study Wimmerbauern spring, Bad Ischl. Austrian Journal of Earth Sciences 106, 16-25.

Hongve, D., 1999. Production of dissolved organic carbon in forested catchments. Journal of Hydrology 224, 91–99. https://doi.org/10.1016/S0022-1694(99)00132-8

Hornberger, G.M., Spear, R.C., 1981. Approach to the preliminary analysis of environmental systems. Journal of Environmental Management 12, 7–18.

Hudson, N., Baker, A., Ward, D., Reynolds, D.M., Brunsdon, C., Carliell-Marquet, C., Browning, S., 2008. Can fluorescence spectrometry be used as a surrogate for the Biochemical Oxygen Demand (BOD) test in water quality assessment? An example from South West England. Science of The Total Environment 391, 149–158. https://doi.org/10.1016/j.scitotenv.2007.10.054

Janke, A., 1951. Der mikrobielle Abbau der Aminosäuren. Archiv für Mikrobiologie 15. 472-499.

Käss, W., 2004. Geohydrologische Markierungstechnik, Lehrbuch der Hydrogeologie. Gebrüder Bornträger, Berlin, Stuttgart.

Katz, B.G., Hornsby, H.D., Bohlke, J.F., Mokray, M.F., 1999. Sources and chronology of nitrate contamination in spring waters, Suwannee River basin, Florida. USGS, Water-Resources Investigation Report 99-4252. https://doi.org/10.3133/wri994252

Kaufmann, G., Braun, J., 2002. Modelling karst denudation on a synthetic landscape: Modelling karst denudation. Terra Nova 13, 313–320. https://doi.org/10.1046/j.1365-3121.2001.00345.x

Khamis, K., Sorensen, J.P.R., Bradley, C., Hannah, D.M., Lapworth, D.J., Stevens, R., 2015. In situ tryptophan-like fluorometers: assessing turbidity and temperature effects for freshwater applications. Environmental Science: Processes Impacts 17, 740–752. https://doi.org/10.1039/C5EM00030K

Kralik, M., 2001. Strategie zum Schutz der Karstwassergebiete in Österreich. Umweltbundesamt, Wien.

Kreft, A., Zuber, A., 1978. On the physical meaning of the dispersion equation and its solution for different initial and boundary conditions. Chemical Engineering Science 33, 1471–1480.

Kunaver, J., 1979. Some xperiences in measuring the surface karst denudation in high alpine environment, Actes du symposium international sur l'erosion karstique, UIS, Commision de erosion du karst, Aix-en-Provence-Marseille-Nimes, 75-85.

Lakey, B., Krothe, N.C., 1996. Stable Isotopic Variation of Storm Discharge from a Perennial Karst Spring, Indiana. Water Resources Research 32, 721–731. https://doi.org/10.1029/95WR01951

Lakowicz, J.R., 2006. Principles of Fluorescence Spectroscopy, 3rd ed., New York, Springer Science+Business Media.

Land Vorarlberg, 2018. Wasser Wirtschaft, Informationswirtschaft und Hydrographie.

Lang, Y.-C., Liu, C.-Q., Zhao, Z.-Q., Li, S.-L., Han, G.-L., 2006. Geochemistry of surface and ground water in Guiyang, China: Water/rock interaction and pollution in a karst hydrological system. Applied Geochemistry 21, 887–903. https://doi.org/10.1016/j.apgeochem.2006.03.005

Lapworth, D.J., Gooddy, D.C., Allen, D., Old, G.H., 2009. Understanding groundwater, surface water, and hyporheic zone biogeochemical processes in a Chalk catchment using fluorescence properties of dissolved and colloidal organic matter. Journal of Geophysical Research 114. https://doi.org/10.1029/2009JG000921

Lauber, U., Ufrecht, W., Goldscheider, N., 2014. Spatially resolved information on karst conduit flow from in-cave dye tracing. Hydrology and Earth System Sciences 18, 435–445. https://doi.org/10.5194/hess-18-435-2014

Lawaetz, A.J., Stedmon, C.A., 2009. Fluorescence Intensity Calibration Using the Raman Scatter Peak of Water. Applied Spectroscopy 63, 936–940. https://doi.org/10.1366/000370209788964548

Leibundgut, C., 1998. Vulnerability of karst aquifers. Karst Hydrology, Proceedings of Workshop W2.

Lemke, D., Schnegg, P.-A., Schwientek, M., Osenbrück, K., Cirpka, O.A., 2013. On-line fluorometry of multiple reactive and conservative tracers in streams. Environmental Earth Sciences 69, 349–358. https://doi.org/10.1007/s12665-013-2305-3

Liñán Baena, C., Andreo, B., Mudry, J., Carrasco Cantos, F., 2009. Groundwater temperature and electrical conductivity as tools to characterize flow patterns in carbonate aquifers: The Sierra de las Nieves karst aquifer, southern Spain. Hydrogeology Journal 17, 843–853. https://doi.org/10.1007/s10040-008-0395-x

Liu, Z., Zhao, J., 1999. Contribution of carbonate rock weathering to the atmospheric CO_2 sink. Environmental Geology 39, 1053–1058. https://doi.org/10.1007/s002549900072

Lončar, G., Šreng, Ž., Bekić, D., Kunštek, D., 2018. Hydraulic-Hydrology Analysis of the Turbulent Seepage Flow within Karst Aquifer of the Golubinka Spring Catchment. Geofluids 2018, 1–12. https://doi.org/10.1155/2018/6424702

López-Chicano, M., Bouamama, M., Vallejos, A., Pulido-Bosch, A., 2001. Factors which determine the hydrogeochemical behaviour of karstic springs. A case study from the Betic Cordilleras, Spain. Applied Geochemistry 16, 1179–1192. https://doi.org/10.1016/S0883-2927(01)00012-9

Mahler, B.J., Lynch, F.L., 1999. Muddy waters: temporal variation in sediment discharging from a karst spring. Journal of Hydrology 214, 165–178. https://doi.org/10.1016/S0022-1694(98)00287-X

Mahler, B.J., Personné, J.-C., Lods, G.F., Drogue, C., 2000. Transport of free and particulate-associated bacteria in karst. Journal of Hydrology 238, 179–193. https://doi.org/10.1016/S0022-1694(00)00324-3

Maie, N., Scully, N.M., Pisani, O., Jaffé, R., 2007. Composition of a protein-like fluorophore of dissolved organic matter in coastal wetland and estuarine ecosystems. Water Research 41, 563–570. https://doi.org/10.1016/j.watres.2006.11.006

Maliva, R.G., 2016. Aquifer Characterization Techniques, Springer Hydrogeology. Springer International Publishing, Cham. https://doi.org/10.1007/978-3-319-32137-0

Maloszewski, P., Benischke, R., Harum, T., 1992. Mathematical modelling of tracer experiments in the karst of Lurbach-System. Beiträge zur Hydrogeologie 43, 116–136.

Martin, J.B., Dean, R.W., 2001. Exchange of water between conduits and matrix in the Floridan aquifer. Chemical Geology 179, 145–165. https://doi.org/10.1016/S0009-2541(01)00320-5

Martin, J.B., Screaton, E.J., 2001. Exchange of Matrix and Conduit Water with Examples from the Floridan Aquifer, U.S. Geological Survey Karst Interest Group Proceedings.

Massei, N., Dupont, J.P., Mahler, B.J., Laignel, B., Fournier, M., Valdes, D., Ogier, S., 2006. Investigating transport properties and turbidity dynamics of a karst aquifer using correlation, spectral, and wavelet analyses. Journal of Hydrology 329, 244–257. https://doi.org/10.1016/j.jhydrol.2006.02.021

Massei, N., Wang, H.Q., Dupont, J.P., Rodet, J., Laignel, B., 2003. Assessment of direct transfer and resuspension of particles during turbid floods at a karstic spring. Journal of Hydrology 275, 109–121. https://doi.org/10.1016/S0022-1694(03)00020-9

Mazzilli, N., Guinot, V., Jourde, H., Lecoq, N., Labat, D., Arfib, B., Baudement, C., Danquigny, C., Dal Soglio, L., Bertin, D., 2017. KarstMod: A modelling platform for rainfall - discharge analysis and modelling dedicated to karst systems. Environmental Modelling & Software 122. https://doi.org/10.1016/j.envsoft.2017.03.015

Meiman, J., Ewers, R.O., Quinlan, J.F., 1988. Investigation of flood pulse movement through a maturely karstified aquifer at Mammoth Cave National Park: A new approach, in: National Water Well Association. Presented at the Second conference on environmental problems in karst terranes and their solutions conference, Dublin OH, pp. 227–263.

Mitrofan, H., Marin, C., Povară, I., 2015. Possible Conduit-Matrix Water Exchange Signatures Outlined at a Karst Spring. Groundwater 53, 113–122. https://doi.org/10.1111/gwat.12292

Mobed, J.J., Hemmingsen, S.L., Autry, J.L., McGown, L.B., 1996. Fluorescence Characterization of IHSS Humic Substances: Total Luminescence Spectra with Absorbance Correction. Environmental Science and Technology. 30, 3061–3065. https://doi.org/10.1021/es960132l

Mudarra, M., Andreo, B., 2010. Hydrogeological functioning of a karst aquifer deduced from hydrochemical components and natural organic tracers present in spring waters. The case of Yedra Spring (Southern Spain). Acta Carsologica 39. https://doi.org/10.3986/ac.v39i2.98

Mudarra, M., Andreo, B., Baker, A., 2011. Characterisation of dissolved organic matter in karst spring waters using intrinsic fluorescence: Relationship with infiltration processes. Science of The Total Environment 409, 3448–3462. https://doi.org/10.1016/j.scitotenv.2011.05.026

Nash, J.E., Sutcliffe, J.V., 1970. River flow forecasting through conceptual models part I - A discussion of principles. Journal of Hydrology 10, 282–290. https://doi.org/10.1016/0022-1694(70)90255-6

Oliver, B.G., Thurman, E.M., Malcolm, R.L., 1983. The contribution of humic substances to the acidity of colored natural waters. Geochimica et Cosmochimica Acta 47, 2031–2035. https://doi.org/10.1016/0016-7037(83)90218-1

Parlanti, E., 2000. Dissolved organic matter Fuorescence spectroscopy as a tool to estimate biological activity in a coastal zone submitted to anthropogenic inputs. Organic Geochemistry 31, 1765-1781. https://doi.org/10.1016/S0146-6380(00)00124-8

Petalas, C.P., Akratos, C.S., Tsihrintzis, V.A., 2018. Hydrogeological Investigation of a Karst Aquifer System. Environmental Processes 5, 155–181. https://doi.org/10.1007/s40710-017-0277-0

Piccolo, A., 2018. Chapter 4 - The Molecular Composition of Humus Carbon: Recalcitrance and Reactivity in Soils. The Future of Soil Carbon, 87-124. https://doi.org/10.1016/B978-0-12-811687-6.00004-3

Plan, L., 2005. Factors controlling carbonate dissolution rates quantified in a field test in the Austrian alps. Geomorphology 68, 201–212. https://doi.org/10.1016/j.geomorph.2004.11.014

Plan, L., Decker, K., Faber, R., Wagreich, M., Grasemann, B., 2009. Karst morphology and groundwater vulnerability of high alpine karst plateaus. Environmental Geology 58, 285–297. https://doi.org/10.1007/s00254-008-1605-5

Poulain, A., Watlet, A., Kaufmann, O., Van Camp, M., Jourde, H., Mazzilli, N., Rochez, G., Deleu, R., Quinif, Y., Hallet, V., 2018. Assessment of groundwater recharge processes through karst vadose zone by cave percolation monitoring. Hydrological Processes 32, 2069–2083. https://doi.org/10.1002/hyp.13138

Press, W.H., Teukolsky, S.A., Vetterling, W.T., Flannery, B.P., 1992. Numerical Recipes in C. Cambridge University, New York.

Pronk, M., Goldscheider, N., Zopfi, J., 2007. Particle-Size Distribution As Indicator for Fecal Bacteria Contamination of Drinking Water from Karst Springs. Environmental Science and Technology 41, 8400–8405. https://doi.org/10.1021/es071976f

Quiers, M., Batiot-Guilhe, C., Bicalho, C.C., Perrette, Y., Seidel, J.-L., Van Exter, S., 2014. Characterisation of rapid infiltration flows and vulnerability in a karst aquifer using a decomposed fluorescence signal of dissolved organic matter. Environmental Earth Sciences 71, 553–561. https://doi.org/10.1007/s12665-013-2731-2

Raeisi, E., Groves, C., Meiman, J., 2007. Effects of partial and full pipe flow on hydrochemographs of Logsdon river, Mammoth Cave Kentucky USA. Journal of Hydrology 337, 1–10. https://doi.org/10.1016/j.jhydrol.2006.11.015

Ravbar, N., Engelhardt, I., Goldscheider, N., 2011. Anomalous behaviour of specific electrical conductivity at a karst spring induced by variable catchment boundaries: the case of the Podstenjšek spring, Slovenia. Hydrological Processes 25, 2130–2140. https://doi.org/10.1002/hyp.7966

Reshes, G., Vanounou, S., Fishov, I., Feingold, M., 2008. Cell Shape Dynamics in Escherichia coli. Biophysical Journal 94, 251–264. https://doi.org/10.1529/biophysj.107.104398

Ryzinska-Paier, G., Lendenfeld, T., Correa, K., Stadler, P., Blaschke, A.P., Mach, R.L., Stadler, H., Kirschner, A.K.T., Farnleitner, A.H., 2014. A sensitive and robust method for automated on-line monitoring of enzymatic activities in water and water resources. Water Science and Technology 69, 1349–1358. https://doi.org/10.2166/wst.2014.032

Saltelli, A., 2002. Making best use of model evaluations to compute sensitivity indices. Computer Physics Communications 145, 280–297 https://doi.org/10.1016/S0010-4655(02)00280-1

Saltelli, A., Ratto, M., Andres, T., Campolongo, F., Cariboni, J., Gatelli, D., Saisana, M., Tarantola, S., 2007. Global Sensitivity Analysis. The Primer. John Wiley & Sons, Ltd.

Seaman, J.C., Bertsch, P.M., Wilson, M., Singer, J., Majs, F., Aburime, S.A., 2007. Tracer Migration in a Radially Divergent Flow Field: Longitudinal Dispersivity and Anionic Tracer Retardation. Vadose Zone Journal 6, 373–386. https://doi.org/10.2136/vzj2006.0109

Senesi, N., Miano, T.M., Provenzano, M.R., Brunetti, G., 1991. Characterization, differentiation and classification of humic substances by fluorescence spectroscopy. Soil Science 259–271.

Sinreich, M., Pronk, M., Kozel, R., 2014. Microbiological monitoring and classification of karst springs. Environmental Earth Sciences 71, 563–572. https://doi.org/10.1007/s12665-013-2508-7

Sivelle, V., Labat, D., Mazzilli, N., Massei, N., Jourde, H., 2019. Dynamics of the Flow Exchanges between Matrix and Conduits in Karstified Watersheds at Multiple Temporal Scales. Water 11, 569. https://doi.org/10.3390/w11030569

Skoglund, R., Lauritzen, S.-E., 2011. Subglacial Maze Origin in Low-Dip Marble Stripe Karst: Examples from Norway. Journal of Cave and Karst Studies 73, 31–43. https://doi.org/10.4311/jcks2009ES0108

Smart, P.L., Hobbs, S.L., 1986. Characterisation of carbonate aquifers: a conceptual base, in: Proceedings of the Environmental Problems in Karst Terranes and Their Solutions Conference. Presented at the National Water Well Association, Dublin OH, pp. 1–14.

Sobol, I.M., 1977. Uniformly distributed sequences with an additional uniform property. USSR Computational Mathematics and Mathematical Physics 16, 236–242.

Sorensen, J.P.R., Baker, A., Cumberland, S.A., Lapworth, D.J., MacDonald, A.M., Pedley, S., Taylor, R.G., Ward, J.S.T., 2018. Real-time detection of faecally contaminated drinking water with tryptophan-like fluorescence: defining threshold values. Science of The Total Environment 622–623, 1250–1257. https://doi.org/10.1016/j.scitotenv.2017.11.162

Sorensen, J.P.R., Lapworth, D.J., Marchant, B.P., Nkhuwa, D.C.W., Pedley, S., Stuart, M.E., Bell, R.A., Chirwa, M., Kabika, J., Liemisa, M., Chibesa, M., 2015. In-situ tryptophan-like fluorescence: A real-time indicator of faecal contamination in drinking water supplies. Water Research 81, 38–46. https://doi.org/10.1016/j.watres.2015.05.035

Sorensen, J.P.R., Sadhu, A., Sampath, G., Sugden, S., Dutta Gupta, S., Lapworth, D.J., Marchant, B.P., Pedley, S., 2016. Are sanitation interventions a threat to drinking water supplies in rural India? An application of tryptophan-like fluorescence. Water Research 88, 923–932. https://doi.org/10.1016/j.watres.2015.11.006

Sorensen, J.P.R., Vivanco, A., Ascott, M.J., Gooddy, D.C., Lapworth, D.J., Read, D.S., Rushworth, C.M., Bucknall, J., Herbert, K., Karapanos, I., Gumm, L.P., Taylor, R.G.,

2018. Online fluorescence spectroscopy for the real-time evaluation of the microbial quality of drinking water. Water Research 137, 301–309. https://doi.org/10.1016/j.watres.2018.03.001

Stadler, H., Klock, E., Skritek, P., Mach, R.L., Zerobin, W., Farnleitner, A.H., 2010. The spectral absorption coefficient at 254 nm as a real-time early warning proxy for detecting faecal pollution events at alpine karst water resources. Water Science and Technology 62, 1898–1906. https://doi.org/10.2166/wst.2010.500

Stedmon, C.A., Markager, S., 2005. Tracing the production and degradation of autochthonous fractions of dissolved organic matter by fluorescence analysis. Limnology and Oceanography 50, 1415–1426. https://doi.org/10.4319/lo.2005.50.5.1415

Stevanović, Z., 2018. Global distribution and use of water from karst aquifers. Geological Society, London, Special Publications 466, 217–236. https://doi.org/10.1144/SP466.17

Sun, F., Zong, W., Liu, R., Chai, J., Liu, Y., 2010. Micro-environmental influences on the fluorescence of tryptophan. Spectrochimica Acta Part A: Molecular and Biomolecular Spectroscopy 76, 142–145. https://doi.org/10.1016/j.saa.2010.03.002

Tissier, G., Perrette, Y., Dzikowski, M., Poulenard, J., Hobléa, F., Malet, E., Fanget, B., 2013. Seasonal changes of organic matter quality and quantity at the outlet of a forested karst system (La Roche Saint Alban, French Alps). Journal of Hydrology 482, 139–148. https://doi.org/10.1016/j.jhydrol.2012.12.045

Toride, N., Leij, F., van Genuchten, M., 1999. The CXTFIT code for estimating transport parameters from laboratory or field tracer experiments (Research Report No. 137). US Salinity Laboratory, Agricultural Research Service, Riverside CA.

Vesper, D.J., White, W.B., 2004. Storm pulse chemographs of saturation index and carbon dioxide pressure: implications for shifting recharge sources during storm events in the karst aquifer at Fort Campbell, Kentucky/Tennessee, USA. Hydrogeology Journal 12. https://doi.org/10.1007/s10040-003-0299-8

Vigna, B., Banzato, C., 2015. The hydrogeology of high-mountain carbonate areas: an example of some Alpine systems in southern Piedmont (Italy). Environmental Earth Sciences 74, 267–280. https://doi.org/10.1007/s12665-015-4308-8

Wagner, M., 2014. DOC-Analytik mittels 2D-Fluoreszenz-Spektroskopie, Charakterisierung und Quantifizierung natürlicher organischer Wasserinhaltsstoffe mittels Fluoreszenzspektroskopie. DVGW-Technologiezentrum Wasser, Karlsruhe.

Werner, R., 2007. Klima von Vorarlberg. Amt der Vorarlberger Landesregierung, Bregenz.

White, W.B., 2003. Conceptual models for karstic aquifers. Speleogenesis and Evolution of Karst Aquifers 1.

White, W.B., 1984. Rate processes: chemical kinetics and karst landform development: La Fleur (ed.), Groundwater as a geomorphic agent, Allen and Unwin, London, Boston, Sydney.

White, W.B., Culver, D.C., Herman, J.S., Kane, T.C., Mylroie, J.E., 1995. The dissolution of carbonate rock produces unique landscapes and poses significant hydrological and environmental concerns. American Scientist 83, 11.

WHO, 2011. Guidelines for Drinking-water Quality.

Wu, P., Tang, C., Zhu, L., Liu, C., Cha, X., Tao, X., 2009. Hydrogeochemical characteristics of surface water and groundwater in the karst basin, southwest China. Hydrological Processes 23, 2012–2022. https://doi.org/10.1002/hyp.7332

Yoshimura, K., Inukura, Y., 1997. The geochemical cycle of carbon dioxide in a carbonate rock area, Akiyoshi-dai Plateau, Yamaguchi, Southwestern Japan, proc. 30th Intl. Geol. 24, 114-126.

Yuan, J., Xu, F., Deng, G., Tang, Y., Li, P., 2017. Hydrogeochemistry of Shallow Groundwater in a Karst Aquifer System of Bijie City, Guizhou Province. Water 9, 625. https://doi.org/10.3390/w9080625

Zeng, C., Gremaud, V., Zeng, H., Liu, Z., Goldscheider, N., 2012. Temperature-driven meltwater production and hydrochemical variations at a glaciated alpine karst aquifer: implication for the atmospheric CO2 sink under global warming. Environmental Earth Sciences 65, 2285–2297. https://doi.org/10.1007/s12665-011-1160-3

Zwahlen, F., 2004. Vulnerability and Risk Mapping for the Protection of Carbonate (Karst) Aquifers. European Commission COST-Action 620.
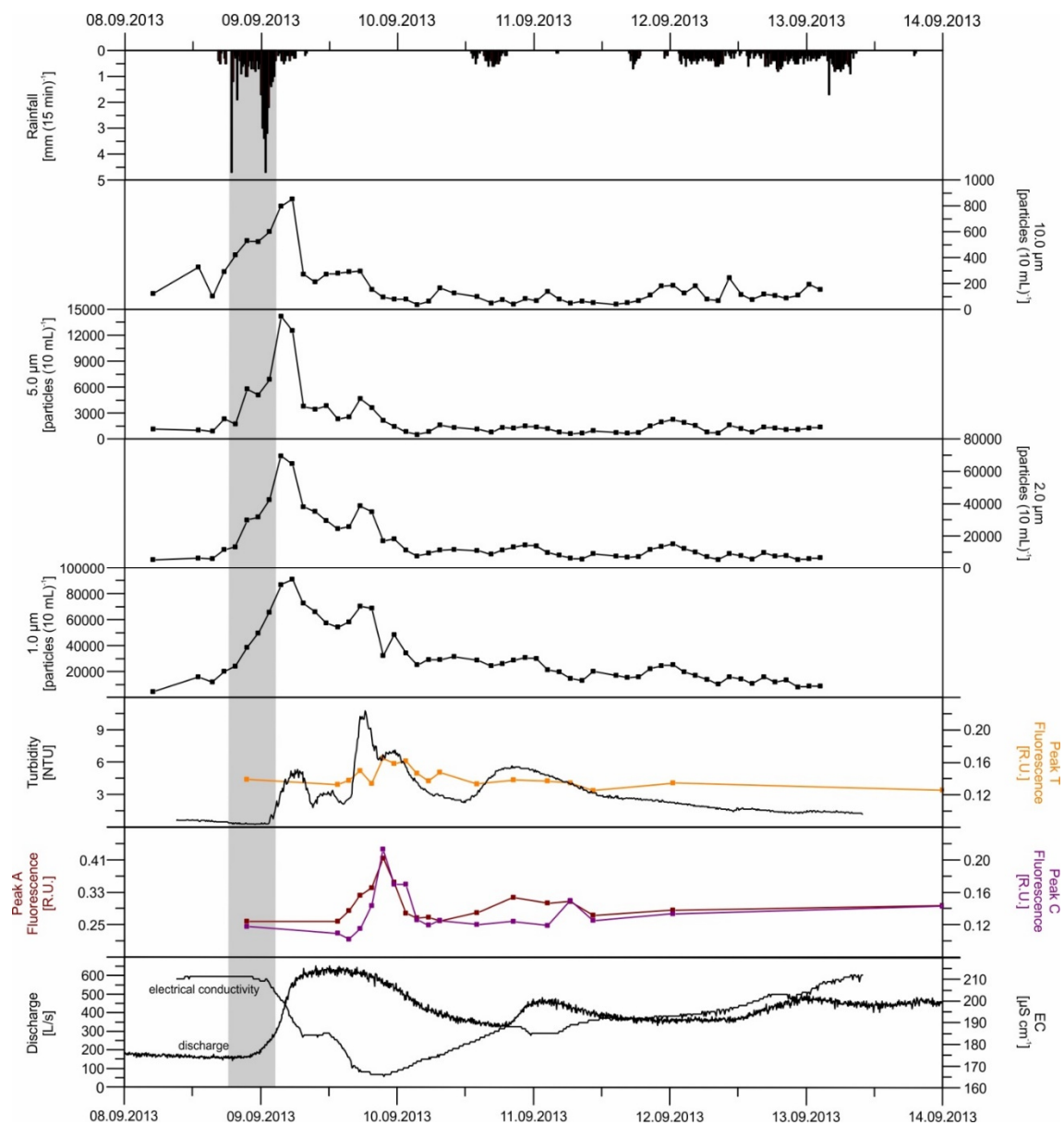
Supplementary Information

Supplementary Material – Chapter 3

Supplementary 1: Minimum and maximum values of TOC and peaks A, C, and T fluorescence obtained of 11 other karst springs in the Großes Walsertal Valley during the dry period in the sampling campaign 2015.
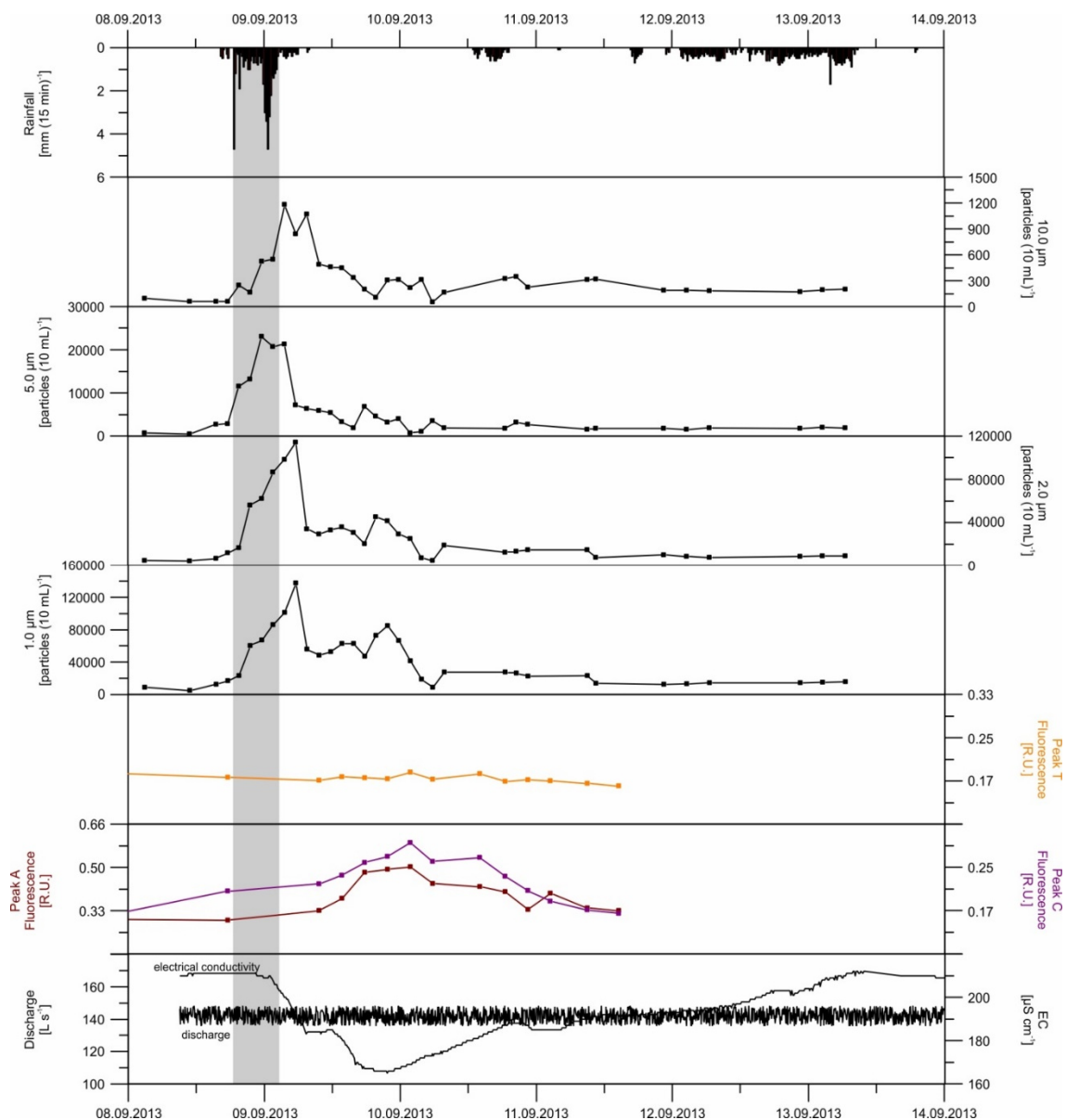
| Sampling Site	TOC		Peak A		Peak C		Peak T	
	Min. [mg L^{-1}]	Max. [mg L^{-1}]	Min. [R.U.]	Max. [R.U.]	Min. [R.U.]	Max. [R.U.]	Min. [R.U.]	Max. [R.U.]
FQ0	0.32	0.41	0.74	0.75	0.43	0.48	0.37	0.41
FQ1	0.40	0.46	0.74	0.80	0.46	0.48	0.41	0.45
FQ2	0.59	0.68	0.85	0.91	0.51	0.55	0.44	0.47
FQ3	0.62	0.70	0.88	0.89	0.53	0.54	0.43	0.45
FBM	0.66	0.69	0.93	0.98	0.59	0.62	0.48	0.49
FBG	0.73	0.73	0.98	1.04	0.57	0.60	0.52	0.52
LAQ1	0.56	0.57	0.79	0.82	0.48	0.49	0.51	0.54
LAQ2	0.47	0.57	0.84	0.88	0.49	0.56	0.46	0.48
GA1	0.61	0.72	0.92	0.95	0.51	0.52	0.45	0.46
GA2	0.58	0.71	0.94	1.01	0.58	0.60	0.42	0.43
ASQ	0.45	0.47	0.80	0.82	0.44	0.48	0.39	0.40

Supplementary 2: Temporal evolution of Peak A, C and T fluorescence intensities of WBQ together with EC, discharge, turbidity and rainfall during the investigation period September 2013. The figure also shows the particle-size distribution of 4 different particle fractions. The particle-size distribution showed two distinct peaks for the 1.0 and 2.0 μm fractions around 9 h and 25 h after the start of the rainfall, at the same time when two peaks for turbidity were observed. The fluorescence peaks A and C also correlated with the second particle peak but show a slight time shift of 1 to 2 h.

Supplementary 3: Temporal evolution of Peak A, C and T fluorescence intensities of SBQ together with EC, discharge and rainfall during the investigation period September 2013. The figure also shows the particle-size distribution of 4 different particle fractions. The slightly higher discharge in 2013 compared to 2015 is most probably the result of construction works at the overflow outlet of SBQ during spring and summer 2015. The fluorescence intensities were in the same range as 2015 but show a slightly slower increase after the rainfall resulting from a different sampling location.

Supplementary Material – Chapter 4
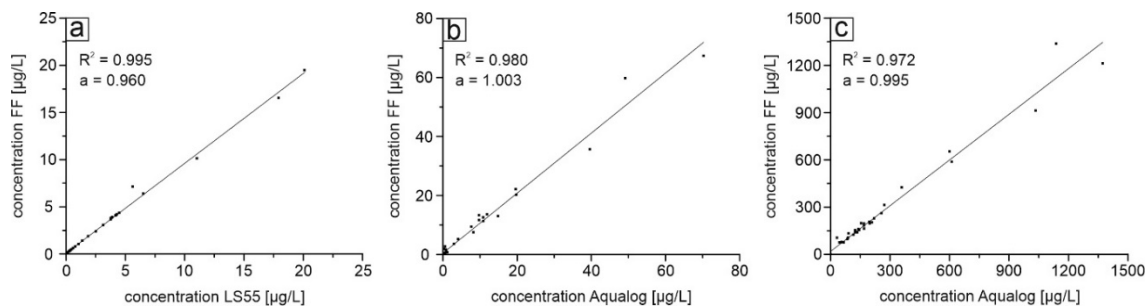
Supplementary 5: a) Measured uranine concentration with the field fluorometer (FF), compared to the measured concentration with the LS55 in the laboratory, 1b) comparison of the measured tryptophan concentration of the FF and the Aqualog, 1c) comparison of the measured humic acid concentration of the FF and the Aqualog.
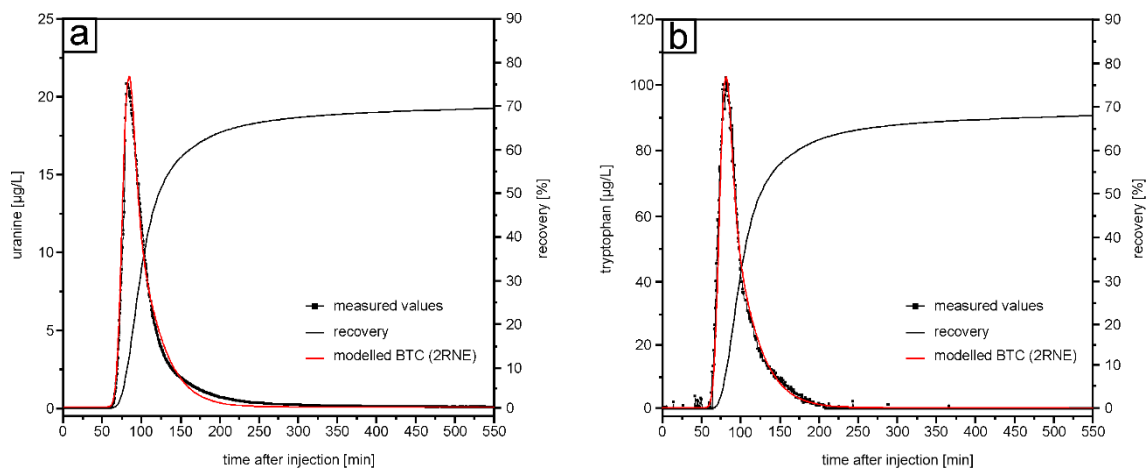
Supplementary 6: a) Break through curve (BTC) of uranine and the corresponding recovery (discharge 8.5 L/s), b) BTC of tryptophan and the corresponding recovery (discharge 7.5 L/s).